Western Graduate&PostdoctoralStudies

4-16-2015 12:00 AM

Solar Photocatalytic Reduction of Zn2+ Using Graphene-Based TiO2 Composite Catalyst for Application to CSO Treatment

Gloria Kumordzi, *The University of Western Ontario*

Supervisor: Dr. Ajay K. Ray, *The University of Western Ontario*
Joint Supervisor: Dr. Ernest K. Yanful, *The University of Western Ontario*
A thesis submitted in partial fulfillment of the requirements for the Master of Engineering Science degree in Chemical and Biochemical Engineering
© Gloria Kumordzi 2015

Follow this and additional works at: https://ir.lib.uwo.ca/etd

Part of the Catalysis and Reaction Engineering Commons

SOLAR PHOTOCATALYTIC REDUCTION OF Zn^{2+} USING GRAPHENE-BASED TiO_2 COMPOSITE CATALYST FOR APPLICATION TO CSO TREATMENT

(Thesis Format: Monograph)

By

Gloria Kumordzi

Graduate program in Chemical and Biochemical Engineering

A thesis submitted in partial fulfilment

of the requirements for the degree of

Master of Engineering Science

School of Graduate and Postdoctoral Studies

Western University

London, Ontario, Canada

ABSTRACT

The improvement of photocatalyst efficiency in utilizing the majority of wavelengths in the solar spectrum, an abundant natural resource, presents the next step in the large scale application of photocatalysis for the treatment of dissolved organic and inorganic pollutants in wastewater. In this study, a composite catalyst of TiO_2 and Graphene synthesized by a hydrothermal treatment method is used to photo-reduce Zn^{2+}, the most abundant heavy metal found in combined sewer overflows (CSOs). The performance of this composite catalyst was assessed under various process conditions such as pH, light intensity, catalyst loading and light source. The TiO_2-Graphene composite catalyst showed a 14.0 ± 1.0 % increase in adsorption capacity of the model compound as compared to pure TiO_2 at neutral pH. Also, a 19.2 ± 0.04 % increase in the photoactivity for the reduction of Zn^{2+} was recorded under solar light conditions using TiO_2-G photocatalyst as compared to bare TiO_2 when reaction rate constants are compared. This enhancement is a result of the availability of more sorption sites, decrease in bandgap of the TiO_2, and effectiveness of the charge separation in the TiO_2-G composite catalyst.

Keywords: Adsorption, Photocatalysis, Photo-reduction, solar light, Ultra violet light, Visible light, Graphene- Based TiO_2, TiO_2,

ACKNOWLEDGEMENTS

I would like to first of all express my sincere gratitude to my supervisors Dr. Ajay K. Ray and Dr. Ernest K. Yanful for the opportunity to pursue this project. Your continuous guidance and support is highly appreciated and I am extremely privileged to have worked with you.

To all members of the Clean Technologies for Water Refining and Nutrient and Energy Recovery (TWNER) project, I am grateful for all the training and useful feedback and support. This has indeed been a great learning experience.

I am also especially grateful to Ghodsieh Malekshoar for all her help and guidance throughout my research.

I am especially grateful to Fate Hashemi for all her service. Also, I am extremely grateful to Tim Stephens and Caitlin Marshall from the Department of Civil and Environmental Engineering for their training and assistance in the analytical equipment used for this project.

Also to my lab mates: Kyriakos Manoli, Noshin Hashim, Naeimeh Faraji and others for all your help and support in diverse areas throughout my journey.

To my Family; Anthony Kumordzi, Felicia Kumordzi, Rebecca, Millicent, Enoch, Dr. Kenneth Asamoah-Boateng and William Kofi Oblawu for all your support and encouragement during some stressful times during this period.

To my friends; Asare-Badiako family, Lucia Kafui Hussey and Lydia Osei for your support and encouragement.

And most of all to God without whom nothing is possible.

TABLE OF CONTENTS

LIST OF TABLES

LIST OF FIGURES

LIST OF SCHEMES

NOMENCLATURE

C   concentration (ppm)

C_o Initial concentration (ppm)

C_{cat} Catalyst concentration (g/L)

e^- Electron

h^+ Hole

I   Light intensity (mW/cm^2)

K_{ads} Adsorption rate constant (ppm^{-1})

k_1 pseudo-first-order rate constant (min^{-1})

k_2 pseudo-second-order rate constant (g/mg.min)

K_{app} Apparent reaction rate constant (min^{-1})

r_o Initial rection rate, (mg/L.min)

Q_m Maximum adsorption capacity (mg/g)

A_{sp} Specific surface area of catalyst

A_{spc} Specific surface area of composite catalyst

NHE   Normal hydrogen electrode

SHE   Standard hydrogen electrode

q_e Adsorption capacity at adsorption/desorption equilibrium   (mg/g)

T   Temperature (K)

t   Time (min)

V_r Volume of liquid (L)

OH^* Hydroxyl radical

λ Light   wavelength   (nm)

1 INTRODUCTION

1.1 Background on Research

Since the beginning of the 20th century, various forms of infrastructure had been put in place to collect and treat wastewater. Drains were developed especially in the cities to transport both sanitary and storm run-off to pollution reduction facilities. These types of drains are known as combined sewers. Combined sewers are found in old cities such as New York, Ottawa, London Ontario, Kingston and Toronto but to mention a few and most of them are currently in use (U.S. Environmental Protection Agency, 2001).

During some wet weather events, the total wastewater flow rate might exceed the peak design capacity of the wastewater treatment facilities available or the sewage transportation systems. Prominent contributing factors include increase in population, increased infiltration resulting from cracks in sewers caused by ageing or the lack of maintenance and or repair, blockages as well as some system failures which can be structural, mechanical or electrical, which in turn causes overloads in the combined sewers.

When this overload occurs, some of the wastewater from the combined sewers is discharged directly into a receiving surface water body without reaching the treatment facility. These overflow occurrences which are mainly recorded in older parts of cities are known as combined sewer overflows (CSOs)(Holeton, et al., 2011; Tchobanoglous, et al., 2003).
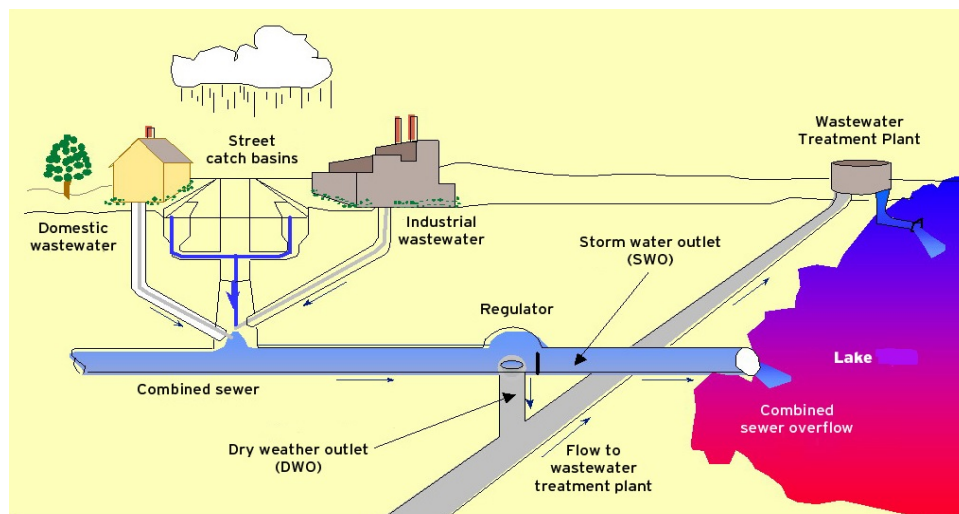
Scheme 1.1 Representation of a combined sewer overflow (source Northeast Ohio Regional sewer district. Online www.neorsd.org/CSO_edu.php retrieved online on 09/09/2014)

Recently, there has been increased concern over these occurrences because the contents of these large overflows are harmful to the quality of the receiving surface water (Muliss, et al., 1996; Tchobanoglous, et al., 2003) and this is even more so critical when the same water body is the source of drinking water (Marsalek and Rochfort, 2004). Storm water run-off pollutant concentration is greatly influenced by the land use in a particular area (Clark and Pitt, 2012).

During a wet weather event, particulate materials are washed away from impermeable surfaces, such as roofs, streets, and pavements in residential areas and industrial sites, into the combined sewers.

The constituents of theses overflows might vary from one municipality to the other depending on the kinds of industries, commercial properties and activities located there

(Holeton, et al., 2011). Normally, CSOs comprise domestic sewage, storm water run-off washed from impermeable surfaces and or industrial wastewaters. These mixtures may contain substantial levels of suspended solids (SS), heavy metals, nutrients, oxygen demanding organic material (BOD), pathogens, oil and grease (Flores-Rodriguez, et al., 1994; Jeon, et al., 2013). In addition to these, endocrine disruptors, legacy contaminants such as surfactants, and polycyclic aromatic hydrocarbons may be included (PAHs) (Holeton, et al., 2011; Zukovs, 2005).

It's estimated that the cities around the Great Lakes contribute more than approximately 90 billion liters to the lakes annually (Podolsky, et al., 2008). For this reason strategies had been adopted by various provinces and states surrounding the Great Lakes to protect them. These include the US EPA CSO control policy (US Environmental Protection Agency, 1994) and the ministry of environment (MOE) Procedure F-5-5 (Ontario pollution prevention control plan, 1997).

1.1.1 The Ontario Pollution Prevention and Control Plan (PPCP)

Procedure F-5-5 is the policy in Ontario that provides guidelines for CSO management. Under PPCP, municipalities are required to draw a plan that comprises the following; *(i)* categorisation of the combined sewer system, *(ii)* investigation of structural and non-structural CSO control alternatives, *(iii)* the provision of actionable plans together with cost estimates to eliminate dry weather overflow and drastically reduce wet weather flows *(iv)* continuous monitoring of sewer system for future upgrades and ensuring compliance with provincial requirement.

Currently in Ontario, the minimum level of treatment of CSO is primary treatment or equivalent which corresponds to the removal of grit and settleable solids.

Table 1.1 Regulations for CSO discharge in Ontario

Parameter	Regulation
Carbonaceous biochemical oxygen demand (CBOD$_5$)	30% removal
Total suspended solids (TSS)	50% removal
Disinfection	< 1,000 E.coli CFU/100 mL

Source; (Ministry of Environment, Zukovs, 2005)

1.1.2 Current CSO Control Technologies

There has been a lot of control technologies proposed and implemented by some municipalities to combat overflows. These can be grouped into four main categories namely; operation and maintenance practices, collection system controls, storage facilities and treatment technologies (US Environmental Protection Agency, 2014). Chief amongst them is storage (Field, 1982; Field, et al., 1994; Field, et al., 1995). Storage facilities are put up to keep the excess wastewater until such a time when flow levels go down and then they are pumped back into the treatment facilities. High-rate treatment at outfall points have also been considered such as the vortex solids separators and retention treatment basins (Wardrop Engineering Inc. and TetrES consultants Ic, 2002).

One other option that is being explored is in-line treatment of wastewater constituent during wet-weather conditions. In this system, the removal of particulate and colloidal

matter is achieved by chemical coagulation and settling before discharging the CSO at the outfall location (El Samrani, et al., 2008).

There are also technologies addressing the total suspended solids (TSS), biochemical oxygen demand (BOD) and pathogen levels (Field, et al., 2004). But there has been very little work looking at treating the dissolved pollutants in CSOs (El Samrani, et al., 2008).

Other physico-chemical treatment technologies such as Actiflo® process developed by US Filter Kruger which offers an 80- 90% removal of TSS, 65- 90 % organic matter (Plum, et al., 1998), and DensaDeg® process are high-rate clarification or ballasted flocculation treatment processes.

Though these technologies have established the removal of greater portions of total suspended solids, the need to investigate some other high-rate technologies to address the dissolved pollutants in combined sewer overflows is much needed in anticipation of more stringent release requirements in the future.

The first flush from the beginning of the wet weather season has pollutant concentrations ranging from 1.2 to 20 times more than towards the end of the season (Clark, et al., 2005). Heavy metals are a major constituent of overflows; they find their way into wastewater streams by a number of means including domestic activities, industrial wastewater and storm water runoff (Holeton, et al., 2011). The usual suspect metals present in wastewater are Cu, Zn, Pb, Cr, Al, Cd, Cr, Fe, Mn, Ni (El Samrani, et al., 2008).

Reemtsma et al. (2000) presented the results of a study of the heavy metal load of combined sewer overflows over a two-year period and reported Al, Cr, Cu, Fe, Mn, and

Zn, concentrations that exceeded those for tertiary treated wastewater. Surface run-off has high concentrations of Cu (120 µg/L) and Zn (460 µg/L). Fe and Al were also present in significant quantities. Al, Cu, Pb and Zn are the four most abundant metals found in different surface run-offs (Reemtsma, et al., 2000).

At present, heavy metal concentration in CSO is not a regulated parameter but there will definitely be increased industrial development and domestic demand for metals (Chen and Ray, 2001). For this reason there is a need to develop high-rate technologies focused on their removal together with currently regulated parameters.

The present work focuses on the removal of a dissolved inorganic heavy metal ion from water. Several technologies have been used over the years to treat water contaminated with heavy metals of which the most widely used is adsorption. However, this technique has the disadvantage of only transferring pollutant from one phase to another.

Heterogeneous photocatalysis is a technology which has found application in water and wastewater treatment for the degradation of undesirable dissolved organic and inorganic constituents of wastewater (Chong, et al., 2010a). This treatment method makes use of light to activate a semiconductor catalyst which then generates electron/hole pairs (e/h^+) capable of reducing and or oxidizing pollutants adsorbed on the surface of the catalyst. This method provides a huge advantage over adsorption only as a treatment method in that it reduces metal ions to their elemental state (Li, et al., 2012).

Presently, the photocatalytic oxidation of organic compounds to destroy hazardous waste has been exhaustively studied. Dyes, surfactants, aromatics aliphatic alcohols, halo

aromatics, and other compounds have been successfully photo oxidized under various conditions (Chong, et al., 2010b).

In addition to these there are currently a few commercially applied technologies based on the photocatalytic process. These include indoor and automobile air cleaning, self-cleaning tiles, window blinds, and lamp shades and so on (Fujishima, et al., 2000; Ibhadon A., O., Fitzpatrick, P., 2013; Sellappan, 2013).

Though photocatalysis is a promising technology, its major shortcoming is the inefficiency of the majority of the most suitable semiconductor catalyst in use today. For this method to be successfully considered for application as a high-rate treatment method the present thesis investigated how semiconductor catalyst modification by compositing with graphene impacts the efficiency of the semiconductor.

1.2 Scope of Research and Objectives

The study explores the conditions under which a metal with relatively unfavourable redox potential and of great environmental importance can be treated with heterogeneous photocatalysis and the impact of graphene-based TiO_2 composite catalyst, for the purpose of its application in the treatment of CSOs. It investigates the removal of Zn^{2+} in suspended TiO_2 and TiO_2-graphene catalyst by adsorption followed by photo-reduction.

This thesis is composed of 5 Chapters. Chapter 1 covers the background to the problems associated with CSOs, current treatment technologies and regulations. Chapter 2 delves into existing literature on dissolved metal ions found in CSOs, treatment methods for metal ions, heterogonous photocatalysis and graphene. The experimental details are covered in Chapter 3 after which Chapter 4 addresses the results and discussion. In Chapter 4, detailed experiments were conducted to ascertain the effects of various process parameters on the system, and the chapter also assesses the performance of the modified composite catalyst as compared to pure Degussa P25 TiO_2. Chapter 5 gives the summarized conclusions of the study and provides recommendations for future studies.

2 LITERATURE REVIEW

2.1 Heavy Metal Ions in CSOs- Sources and Impact

Heavy metals are a subset of elements that exhibit metallic properties with atomic densities greater than 6 gcm^{-3}(Chowdhury, et al., 2014). Among these, metals such as zinc, nickel, lead, copper, mercury, chromium, and arsenic are of great environmental importance. These include transition metals, metalloids lanthanide and actinides. Several domestic activities such as incineration of waste materials, automobile exhaust, the use of aerosols and industrial activities such as metal plating, paints and pigments, battery manufacturing, mining, dying and tanning, viscose rayon, yarn and fibre production, ground wood pulp production, fertilizer production and land application, and newsprint paper production, to mention a few, make use of and generate significant amounts of heavy metals (Chowdhury, et al., 2014; Reemtsma, et al., 2000; Turan, et al., 2011). Whether or not a metal is of environmental importance, is influenced by the degree of toxicity it contributes at low concentrations. Heavy metals ions are of interest because they do not degrade into less harmful substances; instead, they accumulate over time and their effect on living organisms increases (Moreno-Barbosa, et al., 2013).

Metals such as mercury, cadmium and lead and chromium are dangerous to living organisms. They may be carcinogenic or affect internal organs, skin and bones. Others such as zinc and lead can cause corrosion (Lennetech water treatment solutions, Accessed 9/15/2014). Although some metals are important to maintain proper functioning of the body, excess amounts can cause some detrimental effects.

Over the years, several methods and technologies have been developed to rid wastewater streams of harmful metal constituents. The removal methods include (i) coagulation and precipitation; the sludge produced from the precipitation is either disposed off or recovered (ii) membrane process such as reverse osmosis (iii) ion exchange (iv) adsorption; the adhesion of substances in solution to the surface of a suitable solid (Canterino, et al., 2008; Tchobanoglous, et al., 2003; Yeber, et al., 2009b).

So far, the most commonly used method for metal removal is adsorption because it is less expensive and relatively easy and effective (Wang, et al., 2013). Also, methods such as electro-dialysis and ultrafiltration have been explored (Liu, et al., 2011). These methods on the other hand can be expensive and ineffective when the concentrations of target pollutants are low (Deliyanni, et al., 2007).

In adsorptive removal, adsorbents such as biomass, carbon nano-materials, activated carbon, bentonite and resins have been used (Wang, et al., 2013). Adsorption so far has been proposed as the best method for removing metal ions when the concentrations are very low. Choice of adsorbent depends on cost, availability and the adsorptive capacity (Deliyanni, et al., 2007).

However, the limitation of using adsorption as a method of treatment is that after the removal, the pollutant particles or ions are lodged onto the surface of the adsorbent. Other processes have to be effected to safely dispose off the saturated materials, otherwise the potential environmental concerns of pollution by these metals would not have been addressed at all. Hence the need to investigate material that has the ability to adsorb metal ions and simultaneously reduce them into their non-toxic form for safe disposal or recovery.

Photocatalyst nano particles have been proved to possess a high adsorption capacity for metals ions while providing the added advantage of reducing the more frequently positively charged metal ions to their nontoxic elementary forms when exposed to light energy. A lot of work has been done in the area of ultraviolet light (UV) and solar active catalyst for the reduction of several metal ion (Chen and Ray, 2001; Chenthamarakshan and Rajeshwar, 2000a; Litter, 1999; Ming, 2002a; Wang, et al., 2010).

2.2 Heterogeneous Photocatalysis

2.2.1 Fundamental concepts

Once a semiconductor photocatalyst is illuminated with and absorbs photons of energy derived from solar radiation (UV and Visible light) which is equal to or greater than the band gap energy of the particular semiconductor, electron- hole pairs (e^-/h^+) are generated as a result of electrons being promoted (excited) from the valence band to the conduction band. When this occurs, the catalyst surface is said to have been activated. The light intensity and the type of semiconductor particles determine the concentration of (e^-/h^+) available for reaction (Chen et al., 2000).

These photo-generated electrons are attracted by electron acceptors such as oxygen and metal cations (photo-reduction). On the other hand the photo-generated holes react with electron donors such as organic materials (photo-oxidation). Subsequently (e^-/h^+) recombination can occur resulting in the dissipation of heat. These reactions occur synchronously. The recombination reaction step can be considered (Chen, et al., 2000) as one of the main causes for low quantum yield and therefore the drawback of this treatment process.

The energy level at the bottom of the conduction band gives the reduction potential of photo-generated electrons while that at the top of the valence band determines the oxidizing potential of the photo generated holes (Chen and Ray, 1998b; Litter, 1999). When an adsorbed substrate has a redox potential for a thermodynamically feasible reaction to occur, photo-generated hole and electron are involved in these reactions by interfacial electron transfer, so that an adsorbed electron acceptor or donor can either be reduced or oxidized. Semiconductors are utilized in heterogeneous photocatalysis due to their ability to absorb light energy and effectively transport charges (Nguyen, 2006). Degradation of pollutants has been proved to take place on the surface of the photocatalyst instead of the bulk solution (Canterino, et al., 2008).

In recent times, the main goal of photocatalysis has been in its application to the purification of waste water and air. Unlike the conventional process in use currently, which more often than not transfers pollutant from one phase to another (e.g. PAC adsorption), this process transfers pollutants from their harmful states to less harmful substances (Litter, 1999).

Photocatalysis systems have been used in two forms: photocatalyst in suspension in the reactor, or photocatalyst may be immobilized onto inert support. Support materials include glass beads, sand silicate, hollow tubes, vycor glass, woven fabric glass fibre, and quartz optical fibers. Due to mass transfer limitations as a result of the reduction in the number of active sites to target species ratio, immobilized systems are slightly less efficient than slurry or suspension system because there is a higher surface area exposed to illumination. The slurry system is not particularly prone to this challenge, however the disadvantage of using the slurry system, which should be considered, is the separation of

the super fine particles after treatment (Gaya and Abdullah, 2008; Ray, 1998; Ray and Beenackers, 1998). In this work photocatalyst is used in the slurry form.

Reduction by semiconductor photocatalysis technology of dissolved toxic metal ions has been proved to be an advanced and highly feasible process when performed under the right process conditions (Chen and Ray, 2001).

Though currently, photocatalysis has been identified as an effective method for pollutant treatment, photocatalysis is not currently being used on commercial scale in wastewater treatment plants due to low catalyst efficiency and reactor design limitations (Tchobanoglous, et al., 2003). For these reasons further fundamental studies aimed at the improvement of photocatalyst performance to improve photon efficiency, maximize the overall rate of reactions and also extend the ability of the photocatalyst to absorb a wider range of wavelength in the visible region (388-520 nm) of the solar spectrum is required (Nguyen, 2006).

2.2.2 General mechanism of the photocatalytic process

As reported by Chen et al (2000), the general mechanism of photocatalytic reaction can be represented as shown below;

Step1- Catalyst activation

$$TiO_2 \xrightarrow{h_v > E_g} e_{CB}^- + h_{VB}^+ \tag{2-1}$$

Step-2- Oxidation of water and organic compounds present

$$h_{VB}^+ + H_2O_{ads} \rightarrow HO_{ads}^* + H^+ \tag{2-2}$$

(2-3)

(2-4)

Step 3- Reduction of metals present

(2-5)
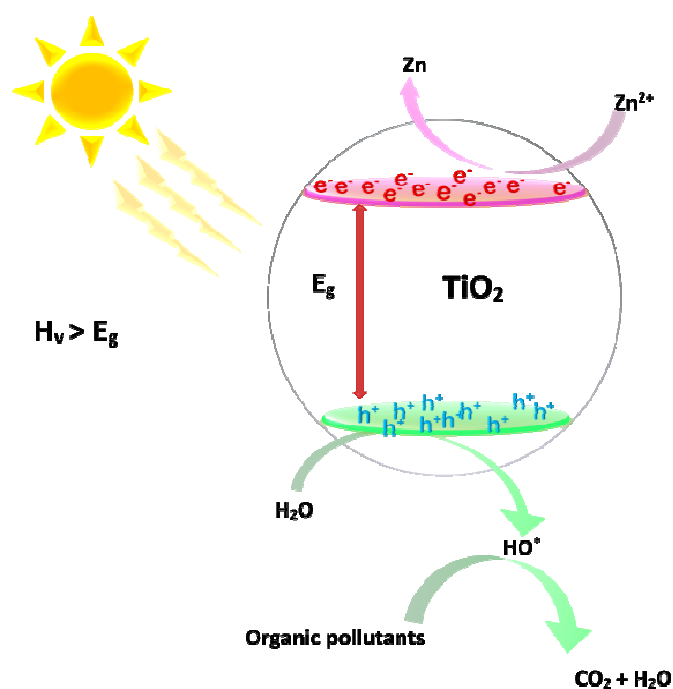
Scheme 2.1 Representation of the photocatalytic process for the metal ion / TiO_2 system

2.2.3 Band theory of semiconductor photocatalyst

Semiconductors are usually crystalline materials characterised by filled valence band and an empty conduction band. There exists a forbidden energy region between the valance band and the conduction band of a semiconductor, where no electrons can be lodged

which is known as the band gap. The energy of different semiconductors range from approximately 1 eV to 4 eV.

The threshold wavelength required in order to activate any semiconductor can be calculated using Plank's equation as shown below;

$$\lambda \, (\mathbf{nm}) = \frac{1240}{E_{bg} \, (eV)} \tag{2-6}$$

Where λ represents the wave length (nanometers), E_{bg} represents the characteristic bandgap of the semiconductor measured in electron Volts (Ming, 2002b).

Nevertheless, the position of valence and conduction bands of the semiconductor can be altered when they come into contact with electrolyte solutions of different ionic strengths and pH (Navío, et al., 1998; Ward, et al., 1983) according to these equations;

$$E_{cb} = -0.3 - 0.59 \, pH \, (At \, 25 \, °C, pH0) \tag{2-7}$$

$$E_{vb} = 2.9 - 0.059 \, pH \, (At \, 25 \, °C, pH0) \tag{2-8}$$

2.3 Adsorption

The first step in photocatalytic reaction process is the adsorption of the pollutant to the surface of the semiconductor photocatalyst. Adsorption is the accumulation of a chemical species (adsorbate) from solution at the solid–liquid interphase of a solid (adsorbent) present (Foo and Hameed, 2010). The adsorption of Zn^{2+} onto several adsorbents have been studied over the years (Malandrino, et al., 2006). The adsorption of molecules or atoms on the surface of the photocatalyst can either be physical, governed by weak van der Waals interaction, or chemical governed by strong ionic bonds or covalent bonds

between the adsorbate and the surface. Chemisorption is the main adsorption mechanism employed in heterogeneous photocatalytic systems (Liu, et al., 2004; Li, et al., 2008).

The fundamental means by which adsorption equilibrium data is described is by using isotherms, which are equilibrium relationships defining how the adsorbates interacts with adsorbent materials. By this, adsorption densities are plotted against the equilibrium concentration of the solute in a dilute solution (Bhattacharya, et al., 2006; Yang, et al., 2007).

For the purposes of design, it is important that isotherm data is described by an equation. In literature, there are three most widely used isotherms applied to solid-liquid systems: the Langmuir, Freundlich and the Redlich-Peterson models. Least-square regression are commonly used in the determination of the parameters for any isotherms. Usually, the most fitted model is determined by comparing the values of 'goodness of fit' (R^2) (Ho, 2004). Recent investigators have expressed concern over the inadequacy of these models to uniquely explain the physical and chemical characteristics of most adsorption studies when linear regression is used. The limitations associated with linear regression and inaccuracy in the determination of parameters is due to alterations in error structures (Veli and Alyüz, 2007a). The best is to use a non-linear regression (such as Marquardt-Levenberg method) together with some error analysis methods.

Bhattacharya, et al (2006) reported the adsorption of zinc onto various adsorbents such as clarified sludge 15.53 mg/g, rice husk ash 14.30 mg/g, activated alumina 13.69 mg/g, neem bark 13.29 mg/g as well a comprehensive review of the capacities of other adsorbents that have been reported. Lee and Yang, (2012) reported the adsorption

capacity of TiO$_2$-GO for Zn^{2+} as 44.8 ± 3.4 mg/g to 88.9 ± 3.3 mg/g depending on the heat treatment time (6 and 12 hours) as compared to 30.1 ± 2.5 mg/g for GO.

The physiochemical parameters determined from the regression analysis gives an understanding into the adsorption mechanism, novel adsorbent surface properties, and the degree of affinity of the adsorbent to the pollutant. The adsorption study aids in the determination of the adsorption mechanism of Zn^{2+} onto the TiO$_2$ and TiO$_2$-G surface. Since adsorption is not being considered as the final treatment method, for the purposes of this study, the Langmuir and Freundlich Isotherms which are the most commonly used, are considered adequate to describe this phase of the study. Both linearized and non-linearized models were used to determine the adsorption parameters in order to ascertain the variation as well as reliability in the values using these two methods.

2.4 Model Compound Selection

In order to evaluate the ability of a treatment method in addressing the challenge of heavy metal removal in CSOs, it is essential to select a model compound not only based on the enormity of its toxicity in relatively low concentrations. It is of great value to select metals that are present as pollutants in surface water run-off after heavy rains as a result of their everyday applications and therefore their abundance in such systems. Zinc and copper are two of such heavy metals. Urban run-off is the most significant contributor of zinc in CSOs while copper can either be attributed to urban run off or municipal waste water (Reemtsma et al., 2000).

Zinc salts are used in inorganic pigments industry (zinc chromate) other sources of zinc contamination come from agricultural applications. Zinc salts are also used for the wide

range of applications such as herbicides to prevent moss on structures and walkways. Zinc oxide is used as an industrial preservative for carpets and fibres to prevent bacterial and fungal growth. It is also used for pressure treatment of lumber. It's therefore no surprise that zinc is the highest in concentration of the metals present in CSOs. It is non-biodegradable and it accumulates in concentration and is transported through food chain and bioaccumulation occurs (Moreno-Barbosa, et al., 2013).

Though zinc was formally considered by the US EPA as generally non-toxic, it became part of the list of priority pollutants in 1992 (EPA, 1992; Turan, et al., 2011). At high levels it can be very toxic to aquatic animals. In small concentrations it is a very essential element for the development of living organisms, and it is useful to the enzymes which are responsible for red blood cell formation in living organisms. It is also used by plants for biosynthesis of nucleus acids and polypeptides (Salim, et al., 2003). A study conducted by (Brix, et al., 2010) concluded that the risk from Zn in storm water runoff to aquatic community is moderate. However, zinc pollution has been of great environmental concern for some time now in the recent decade.

According to the World Health Organization (WHO) and Canadian water quality guidelines, the maximum allowable zinc level in water is 5 mg/L (Wang, et al., 2013). It has also been reported that the threshold limit (TLV) for zinc in drinking water is 3 mg/L; above this limit zinc is toxic to plants animals and humans. More so, studies showing that other severe conditions arise when other heavy metals such as cadmium are also present in significant quantities in water due to synergistic effects (Salim, et al., 2003). Nevertheless, high exposure to zinc in humans can cause stomach cramps, skin and eye irritations, vomiting, nausea, anaemia, lung disorders, metal fume fever, retarded growth,

dehydration, and lack of muscle coordination (Liu, et al., 2011; Turan, et al., 2011; Wang, et al., 2013).

So far, treatment methods have involved the use of soluble calcium compounds such as lime and hydrated lime for zinc hydroxide or calcium zincate formation. In this way the resultant compound is precipitated from solution. Separation is then achieved by coagulation or flocculation with aluminium sulphate (Alum) or Polyaluminium Chloride (PAC) (Liu, et al., 2011).

Copper is another heavy metal of abundance in surface water run-off. It is generally found in the oxidation state of (2+). This form is most abundant in surface waters. Though an essential micronutrient, it may reach toxic limits in much lower concentrations than zinc for aquatic organisms. Cu^{2+} species is the most toxic form. It may contribute to water hardness and the decrease in dissolved oxygen in water. Copper can be toxic when it interferes with oxygen transport and results in hypoxia in vertebrates and invertebrates (Yeber, et al., 2009a).

Natural and industrial activities contribute to copper release into the environment. Activities such as mining, metal production, wood and phosphate fertilizer production are some of the industrial sources of copper (Canterino, et al., 2008). Copper exposure can also be as a result of corrosion of copper plumbing. Like zinc, copper is absorbed in the human body in small proportions. Large quantities of these can cause nose and mouth and eyes irritation, headaches, stomach aches, dizziness, vomiting diarrhea. Chronic copper uptake results in hepatic cirrhosis, brain damage, demyelization, renal disease, and copper deposition on cornea. Copper is non-biodegradable, hence it can accumulate in soils plants and animals. (Lennetech water treatment solutions, Accessed 9/15/2014;

Turan, et al., 2011). The table below summarizes the average concentrations of heavy metals found in urban run-offs.

Table 2.1 Concentration of heavy metals present in urban runoff

Constituent	Concentration in urban run-off µg/L	Typical threshold concentration, µg/L
Arsenic	1.700	20.0
Nickel	16.00	7.10
Lead	90.00	5.60
Selenium	1.600	5.00
Zinc	440.0	58.0
Mercury	0.026	2.10
Copper	19.00	4.90
Chromium	6.400	11.0
Cobalt	2.700	-

Source: (Schroeter, 1997; Tchobanoglous, et al., 2003)

2.5 Photo-reduction of metallic ions

Reduction of metal ions by photocatalysis is a relatively effective method for inorganic waste water treatment. In the absence of oxygen, excited electrons in the conduction band of the semiconductor can react more easily with metallic ions such as Cu(II), (Canterino, et al., 2008; Foster, et al., 1993b; Ollis, 2000), Mn(II), Cr(VI), Au (III), Rh (III) and Pd (II) (Ming, 2002b; Serpone, et al., 1987), Ag(I)(Herrmann, et al., 1988) Hg (II)(Serpone, et al., 1987), Pb(II)(Tanaka, et al., 1986).In addition, Zn (II) and Fe (II) were also photo-reduced in the presence of EDTA and high-pressure mercury lamp. (Litter, 1999c; Ming, 2002).

Since the electron-hole pairs have a very short lifetime before recombination, further steps can be taken to hinder this undesired effect (Canterino, et al., 2008). In order to favour the availability of conduction band electrons, hole scavengers such as organic additives are used to suppress electron/hole recombination (Chen and Ray, 2001).

So far, photo-reduction has also been considered for application in the recovery of noble metals from waste streams, photographic imaging (Pulido Melián, et al., 2012), semiconductor modification for other applications (Chowdhury et al 2013), and light-energy storage systems. This is because after photo-reduction has occurred, metals are deposited onto the surface (Chen, et al., 2000) of the semiconductor and can be extracted by mechanical or chemical means. After the process these deposited metals cannot be easily transferred back into the bulk solution   (Foster, et al., 1993a). Photo-deposition can find immense application in areas such as metal recovery.

The assessment of the theoretical feasibility of this reduction process can be derived from the thermodynamics of the system. Past works by Prairie et al, (1993) established that only metals with half-reaction standard potential greater than or more positive than -0.3 V could be reduced using TiO_2 as a photocatalyst. This can be certainly explained by comparing standard reduction potentials of the metal ion under consideration to that of the semiconductor material. In order for the photo-reduction of a metal ion to be thermodynamically feasible, the standard reduction potential of the semiconductor material should be more negative than that of the metal. On the other hand Cr (III), Ni(II) and Cd(II), Zn(II) with reduction potential more negative than that of TiO_2 semiconductor has not been observed (Kabra, et al., 2007; Kabra, et al., 2008).

However, other investigators reported that Zn^{2+} can be reduced to Zn^0 in the presence of an excess amount of organic additive such as formate under UV irradiation (Chenthamarakshan, et al., 2000). Also, Forouzan et al (1995) established that in the presence of oxalate Ni^{2+} can undergo photo reduction. Cd^{2+} has also been successfully photo reduced under solar light and UV light in the presence of organic species by others (Athapaththu, 2013; Chenthamarakshan, et al., 2000; Nguyen, 2006). It has therefore become of interest to study the reaction conditions and postulate the mechanisms associated with the reduction of such metals in photocatalytic systems. (Litter, 1999).

2.6 Choice of Semiconductor Photocatalyst

In order to develop a sustainable technology in the wastewater treatment of heavy metals, it is imperative to select a durable photocatalyst that is highly photoactive and efficient, photo corrosion resistant, cost effective and readily available. To improve the photocatalytic process, several semiconductors such as ZnO (3.2eV), CdS (2.4eV), ZnS (3.6eV), WO_3 (2.8 eV), and iron oxides (3.1 eV) are used. TiO_2 (3.1 eV) and (ZnO) are the most widely used semiconductor photocatalysts (Chong, et al., 2010b).

2.6.1 Titanium Dioxide

The two main brands of TiO_2 that are commercially available are Degussa P25 and Hombikat UV100. It has been established that Degussa P25 has the highest performance compared to all other TiO_2 catalysts (Martin et al 1994; Chen et al, 2002; Chen and Ray, 2001).

It is naturally occurring in the forms of anatase (most photocatalytically active), rutile (most thermodynamically stable) and brookite. Brookite, unlike anatase and rutile, cannot

be easily synthesized. Titanium dioxide is produced from ilmenite ($FeTiO_3$) ($FeO.TiO_2$) - 36-66% TiO_2 content and is abundant in countries such as Australia, Canada, South Africa Russia, India and the United States of America. Another mineral source of TiO_2 is rutile (90-98%) TiO_2 (Ming, 2002b).

Due to the wide band gap of TiO_2, research attention has been turned toward the structure modification to reduce band gap energy requirements to solar light-compatible levels for boosting the efficiency of electron-hole production and separation. Currently, techniques such as doping with metal ion like rare earth metals, noble metals (Au, Pt Ag and Pd), transition metals (Mn, Fe, Co, Ni, Cu, and Zn) and non-metals have been used (Litter, 1999).

Presently, TiO_2 has been reported to be effective in the removal of Cr(VI), Hg(II), Pb(II), Ni (II) Cu(II) and As(III) (Delgado-Balderas, et al., 2012).

2.6.2 Zinc Oxide

This is another type of semiconductor catalyst which can be used for photocatalytic reduction. Studies have shown that ZnO absorbs a much larger fraction of the visible light spectrum as compared to TiO_2 and so it can be more suitable for use when visible light conditions are being considered. Generally, it has been concluded that ZnO is better photocatalyst under visible light conditions than other semiconductors that have been explored as photocatalysts (Chan, et al., 2011).

However for the purposes of this study, TiO_2 has been selected because it meets majority of the criteria required. It is biologically and chemically stable, nontoxic and insoluble under most conditions and relatively inexpensive. For some of these reasons TiO_2 is used

in a number of domestic products such as sun blocks, vitamin tablets and edible chicken rolls (Ming, 2002b).

2.7 Effect of Processes Parameters on Photocatalytic Reactions

Various factors contribute to the observed reaction rate of photocatalytic systems. These may include but not limited to pH, pollutant concentration, light intensity, catalyst loading, and concentrations of other organic or inorganic species (Bouziane, et al., 2012). In order to evaluate the suitability or otherwise of the photocatalytic process in high rate treatment process such as that required for CSO treatment, it is important to undertake a comprehensive study of the photocatalytic reaction kinetics of the environmentally important but thermodynamically less favoured metal ions such as zinc found in abundance in storm water run–offs.

2.8 Thermodynamics of Zinc Speciation

The conduction band-edge of TiO_2 in neutral pH is -0.4 V vs SHE at pH 7 as compared to -0.3V vs SHE in 0 pH (Chenthamarakshan, et al., 2000). However the standard reduction potentials for zinc and copper, another abundant metal found in CSOs, are;

$$Zn^{2+} + 2e^-, E^0 = -0.76 \text{ V} \tag{2-9}$$

$$Cu^{2+} + 2e^-, \ E^0 = +0.34 \text{ V} \tag{2-10}$$

(Nazeeruddin, et al., 2002). Potentials are quoted in reference to the Standard Hydrogen Electrode (SHE).

From the standard reduction potentials it is thermodynamically more favourable for the photo generated electrons located in the conduction band of the semiconductor photocatalyst to directly reduce Cu^{2+} ions than Zn^{2+} ions. The reduction potential of Zn^{2+} has been shown to be independent of pH (Park, et al., 2009; Singh and Chaudhary, 2013b). So far, conflicting results have been published on the photoreduction of Zn^{2+} to its zero valent form and the reaction pathways present. Chenthamarakshan, et al. (2000), Chenthamarakshan and Rajeshwar (2000b) have established that in the presence of some excess organic additives, the reduction of Zn^{2+} over pure P25 can be achieved under UV irradiation, Singh and Chandan (2013b) established that in the presence of hydrogen peroxide under solar irradiation for 300 min, complete photo reduction of Zn^{2+} is achieved at pH 6 and above. However, (Kabra, et al., 2007; Kabra, et al., 2008) reported that there was no photo reduction of Zn^{2+} to its zero valent form under solar light irradiation in the presence of citric acid as hole scavenger.

Therefore, exploring the possibility of enhancing this reaction using a modified TiO_2 semiconductor catalyst with a reduced band gap aimed at augmenting the absorption of wavelengths in the visible light section of the electromagnetic spectrum, in addition to that in the UV range, is an important research goal. One such modification widely being considered is the use of carbon based materials. Modification of the semiconductor is carried by compositing with Graphene Oxide to produce TiO_2-Graphene (TiO_2-G) composite catalyst for the photoreduction of Zn^{2+} from aqueous solutions.

2.9 Graphene an emerging material in photocatalysis

Interest in the use of carbon-based materials for making composites with TiO_2 is growing. There are currently three different types of carbon-TiO_2 composite materials. TiO_2-mounted activated carbon, carbon - doped TiO_2 and carbon coated TiO_2. (Zhang, et al., 2010a).

Carbon based materials are becoming of great interest because of the promise of chemical inertness, stability in both acidic and basic media as well as the relatively modifiable textural benign nature and abundance. Among these carbon C_{60} structures of interest are carbon nanotubes, fullerenes and graphene nano sheets.

At the center of these carbon-based material is the use of graphene (Gu, et al., 2014; Pastrana-Martínez, et al., 2013; Zhang, et al., 2010;Kumar and Devi, 2011), graphene-based TiO_2 (graphene- TiO_2, graphene- Oxide, TiO_2 and reduced graphene oxide- TiO_2). These composites were considered as the next generation of photocatalyst (Morales-Torres, et al., 2012) Since Novoselov et al (2004) reported its synthesis, there has since been reported several research results of many applications in water and air treatment (Jiang, et al., 2011).

It is considered a promising material because of the excellent mobility of charge carriers, large specific surface area, flexible structure, high transparency and good electrical and thermal conductivity.

Graphene is a material made up of a single layer of graphite. It is an atomic sheet of sp^2-bonded carbon atoms arranged into a honey comb structure. It has a comparatively larger specific surface area and is transparent due to the presence of only 1 layer of atoms for

thickness and composed of hexagonal two-dimensional network of carbon atoms. It is has been labelled the thinnest and hardest material known currently (Brownson and Banks, 2014) So far, it exhibits high adsorptive and conductive abilities for organic pollutants. Currently, similar abilities for dissolved metallic ions has only been sparsely studied (Lee and Yang, 2012; Liu, et al., 2013; Zhang, et al., 2012).

Graphene has the ability of charge carrier's mobility at room temperature (approximately, 100 000 cm^2 V^{-1} s^{-1}), large theoretical surface area (2630 m^2 g^{-1}), mechanical strength of 2.4 +/- 0.4 TPa, and thermal conductivity of 2000- 5000W m K^{-1} (Avouris, 2010).

The use of TiO_2-graphene composite for the photocatalytic removal of organic pollutants is currently receiving enormous attention. It has been demonstrated that TiO_2-graphene composites perform better as adsorbents for organic pollutants than pure TiO_2 for the purposes of photo-oxidation (Zhang, et al., 2010a).

Graphene acts as an inhibiter when combined with metal oxide semiconductors to prevent leaching of metal oxides particles in treated water and it also reduces electron-hole recombination by acting as an electron sink. Recent studies have also indicated that apart from organic materials and heavy metals, graphene and its derived materials exhibit antimicrobial activity which is essential for the disinfection of waste water (Li, et al., 2013; Chowdhury, et al., 2014).

Table 2.2 Zinc photo-reduction as reported by other studies

Title	photocatalyst	Light Source	Organic compound used	Investigators
Visible light induced photocatalytic reduction of metals(Cr, Cu, Ni, Zn) and it's synergism with different pH, TiO_2 and H_2O_2 doses in simulated waste water	0.5-2 g/L TiO_2 suspension	Solar light	Hydrogen Peroxide	(Singh and Chaudhary, 2013b)
Removal of metal ion by means of solar oxidation processes based on pH, TiO_2 and oxidants	1 g/L TiO_2 suspension	Solar light	Hydrogen Peroxide	(Singh and Chaudhary, 2013a)
Photocatalytic reduction of divalent Zinc and Cadmium ion in aqueous TiO_2 suspension: and interfacial induced adsorption – reduction pathway mediated by formate ions	2g/L TiO_2 (Degussa P25) Suspension	UV light	Sodium formate	(Chenthamarakshan, et al., 1999)
Photocatalytic reactivity of Zinc and cadmium ion in UV-irradiated titania suspensions	2g/L TiO_2 (Degussa P25) Suspension	UV light	Isopropanol Methanol Ethanol Isobutanol Sodium formate	(Chenthamarakshan, et al., 2000)
Solar Photocatalytic removal of Cu(II), Ni(II) Zn (II) and Pb(II): Speciation modeling of metal –citric acid complexes	2 g/L TiO_2 suspension	Solar light	Citric Acid	(Kabra, et al., 2008)
Effect of pH of the Solar photocatalytic reduction and deposition of Copper Nickel, Lead and Zinc:	2 g/L TiO_2 suspension	Solar light	Citric acid	(Kabra, et al., 2007)

Speciation modeling and reaction kinetics				
Photocatalytic removal of Zinc(II) in UV –Irradiated Titania suspension	3 g/L TiO_2 (Degussa P25) Suspension	UV	Formic Acid Acetic Acid	(Kajitvichyanukul and Sungkaratana, 2006)

3   EXPERIMENTAL METHODS

3.1 Materials and instruments

This chapter discusses into detail the experimental set up as well as the various chemical

substances and methods of measurements used in the study.

3.1.1 Materials used

Degussa P25 titanium dioxide (Evonic Degussa Corporation), zinc nitrate

[$Zn(NO_3)_2.6H_2O$- 99%)] (Sigma Aldrich), Trizma base (Sigma Aldrich), sodium

hydroxide, hydrochloric acid formic acid (Sigma Aldrich), Milli-Q water Thermo

Scientific. Graphene Oxide (University of Waterloo) were used in the research. All

chemicals were at least reagent grade and were used without further purification.

3.2 Light source for photocatalysis-solar simulator

For the purpose of this work, a 1000 W Xe arc lamp was used as the light source. Solar

light was simulated using a Sciencetech Model SS1 KW solar simulator equipped with

air mass filters which simulate the direct and scattered nature of solar radiations reaching

the surface of the earth. There is a direct radiation filter and a scattered radiation (AM

1.5G) filter fitted in this solar simulator. The maximum light intensity emitted

corresponds to 100 mW/cm^2.

Figure 3.1 Solar simulator used for experiment

3.3 Analytical Instruments for Trace Metal Analysis

Atomic spectrometry is the most commonly used technique for the determination of trace amounts of elements. Atoms absorb energy from an external source and this results in excitation. During excitation, electrons are prompted from the ground state orbital to higher energy levels. Upon losing energy either by photon (s) emission or collision with other particles, electrons return to their original orbitals and the atom is said to be in the ground state. Ionization of the atom is also possible if the absorbed energy by the atom is significant, leaving the atom with a net positive charge. The schematic diagram below depicts the excitation ionization and emission of an atom.
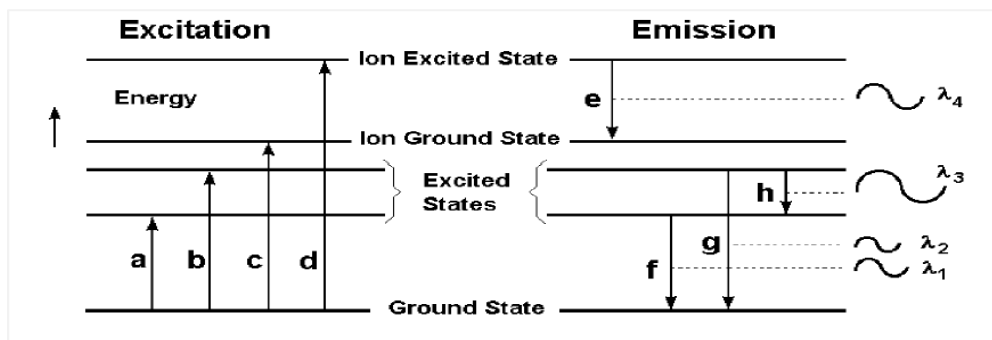
Scheme 3.1 Schematic diagram of energy transitions, a and b excitation c ionization, d ionization/ excitation, e is ion emission and f, g and h are atom emission (Boss and Fredeen, 1997*).*

The techniques most commonly used include atomic absorption spectrometry (AAS), optical emission spectrometry (OES), and atomic fluorescence spectrometry (AFS). In this work, the inductively coupled plasma optical emission spectroscopy (ICP-OES) was used.

3.3.1 Inductively coupled plasma optical emission spectrometer (ICP-OES)

In this study, an axial configuration Vista-Pro CCD simultaneous ICP-OES was used out of three possible configurations which are axial, radial and a combination of axial and radial. This is because the axial configuration gives better sensitivity and therefore provides higher detection at low metal ion concentrations than the radial.

The ICP makes use of plasmas (8000 ˚C); highly energetic ionized gases produced in inert gases, such as argon. Plasmas are orders of magnitude higher in temperature than flames and furnaces and therefore can be applied to detect a wide variety of elements present in different sample types efficiently.

The liquid sample introduced into the ICP is transformed into an aerosol by means of a nebulizer. The aerosol proceeds into the plasma where dissolvation, atomization, and excitation is and or ionization takes place. Characteristic radiations are emitted by the atoms and ions are then sorted by wavelengths and then turned into electronic signals which can then be displayed on a computer as concentration (Boss and Fredeen, 1997).

Measurement was detected using 3 different wavelengths (213.857, 206.200 and 202.548 nm) per sample and the results are reported as average of the 3 measurements. Table 3.1 shows the concentrations as detected by the three different wavelengths.

Table 3.1 ICP-OES Zn^{2+} calibration data

Conc. Prepared, ppm	Analysed Zn^{2+} concentrations, ppm			Average conc., ppm
	202.548 nm	206.200 nm	213.857 nm	
0.10	0 .101	0.108	0.111	0.10±0.01
1.00	1.006	1.025	1.019	1.00±0.01
10.0	9.984	10.003	9.984	10.0±0.01
20.0	20.465	20.623	20.510	20.6±0.08
50.0	50.045	50.180	50.002	50.1±0.09
60.0	59.652	60.009	60.310	60.2±0.33

The axially configured ICP-OES has the ability to detect as low as 0.2 µg/L of Zn^{2+} in aqueous solution. Other sigma detection limits of this instrument can be seen in Table 3.2.

Table 3.2 Three Sigma detection limits of the ICP-OES (Vista-PRO) for some metals

Element	Wavelength	Limits of Detection (3σ) (μg/L)	
	(nm)	Axial	Radial
Zn	213.856	0.20	0.80
Cu	327.396	0.30	1.00
Pb	220.353	0.80	5.00
Cd	214.438	0.05	0.60
As	188.979	1.50	5.00

3.4 Other Instruments and Experimental Conditions Used

The slurry solutions were filtered using a 0.45 micron polypropylene syringe filter. TiO_2 suspension was stirred using a magnetic stirrer while purging continuously with ultrapure nitrogen. pH was monitored using a 780 Metrohm pH meter. The pH was adjusted using 0.1 M NaOH and 0.1M HCl .Unless otherwise stated, the initial metal ion concentration in the simulated wastewater was measured as 20 ± 2 mg/L. Ultra sonication was performed in a Fisher Scientific FS60H bath. A Thermo Scientific furnace and a Rose Scientific OV- 11 Vacuum oven was used for TiO_2-G catalyst preparation. Separation of suspended composite catalyst from solution was achieved using a centrifuge. Dark reaction was performed in a Barnstead Lab line orbital shaker.

3.5 Experimental Procedure

This study focuses on the improvement (solar light activity) of photocatalyst TiO_2 by compositing with graphene and its application to the treatment of Zn^{2+} contaminated water by means of adsorption and photocatalysis. For this reason, an adsorption study was first performed and solar light was used to determine the performance of the photocatalyst under variations in different parameters such as catalyst loading, pH, initial metal ion concentration, light intensity and light source.

3.5.1 Adsorption of metal ions on TiO_2 and surface TiO_2-G (Dark reaction)

It has been established that the first step in the photocatalytic reaction mechanism is the adsorption of species to the surface of the semiconductor catalyst. Prior to light irradiation experiments, metal ion- TiO_2 and TiO_2-G suspensions were equilibrated in the dark.

A detailed adsorption study was performed to determine the equilibrium time and the effects of various process conditions and parameters on the adsorption process. Conditions investigated included the effect of pH, initial catalyst loading and initial metal ion concentration. These investigations were done in the presence of Tris organic buffer to keep the pH reasonably constant and hence provide consistency. Following this, the adsorption of Zn^{2+} on TiO_2-G composite catalyst was also studied under various conditions in the presence of formic acid (FA).

Determination of the adsorption equilibrium time

The initial adsorption studies were performed in the presence of 2-Amino-2-hydroxymethyl-propane-1, 3-diol organic buffer (Tris) to maintain the pH. A Tris buffer solution (0.01 M) was prepared by adding 605.7 mg Trizma base into 500 mL of milli-Q water. Tris has a pKa value of 8.1 and hence its effective pH working range is 6- 9; therefore, adsorption studies were performed within this pH range. With the aid of a magnetic stirrer, the solution was thoroughly stirred for 10 min after which the initial pH was measured to be 10. 2. Next, the pH was adjusted to below 8 with the aid of 0.1 M HCl. To prepare a 20 mg/L Zn^{2+}, 46 mg of zinc salt was dissolved in the buffer solution after which the pH was adjusted to the desired value using 0.1 M NaOH or 0.1 M HCl. The prepared solution was then stirred vigorously for 20 minutes, after which 50 mL of a solution prepared at different initial conditions was transferred into a different conical flask for the dark reaction study. Equilibration time was varied from 5 min to 180 min and samples were taken at the initial time and then onwards at appropriate times, filtered and analysed.

The effect of pH and catalyst loading

For this set of dark reaction experiments, a pH range of 6 – 8 was selected and catalyst loading was varied from 0.5 - 6 g/L. Tris base was used as the buffer and the synthetic wastewater was prepared as described in the section above. For each solution pH, 50 mL of the solution was distributed into seven conical flasks and desired catalyst amounts of 0.025, 0.05, 0.1, 0.15, 0.2, 0.25 and 0.3 g was added, covered with aluminium foil to prevent light penetration and stirred using an orbital shaker at 170 rpm for 1 hour. Initial solution sample was retrieved as well as final sample after 1 hour of equilibration time.

The effect of initial metal ion concentration

For this set of experiments, initial buffer solutions were prepared as described in the section above. Different masses of salt were measured depending on the initial Zn^{2+} desired and dissolved in the buffer solution as shown in Table 3.3 below. The initial metal ion concentration was varied 10 ppm to 50 ppm. The pH of the solution was adjusted to 7.1 ± 0.1 and then the solution was covered and mixed using a magnetic stirrer for 20 minutes before experiments begun. Samples were retrieved at the appropriate times, filtered and then analysed. The molecular mass of $Zn(NO_3)_2.6H_2O$ used was 297.47 g/mol and atomic mass of Zn used was 65.23 g/mol.

Table 3.3 Mass of zinc salt measured

Desired $[Zn^{2+}]$, mg/L	Mass of $Zn(NO_3)_2.6H_2O$ measured, mg
10.00	45.0
20.00	91.9
30.00	136.5
40.00	182.0
50.00	227.5

3.5.2 The hydrothermal method for TiO$_2$-Graphene composite catalyst.

This is a process of loading TiO$_2$ nanoparticles on the platform of the graphene nanosheet. TiO$_2$-Graphene composite was prepared using the hydrothermal process

similar to the method reported by (Malekshoar, et al., 2014) where TiO_2: graphene oxide weight ratio was kept at 1:1. In this method, 2 mg of GO was dissolved in a 20 mL Milli-Q water and 10 mL ethanol mixture followed by ultra-sonication for 1 hour and the addition of 0.2 g P25 TiO_2. This was followed by 2 hours of stirring with a magnetic stirrer and then transfer to a 50 mL Teflon-sealed autoclave and placed in a furnace at a temperature of 120 ˚C for 3 hours. The cooled suspension was then centrifuged and washed three times with distilled water then dried at 60 ˚C in a vacuum oven for 7 hours.

Graphite Oxide GO was obtained from graphite powder using the modified Hummers method (Hummers and Offeman, 1958).

```
┌─────────────────────┐        ┌─────────────────────┐
│     2 mg GO         │        │  Sonicate mixture   │
│        +            │   →    │      2 hours        │
│ 10 mL Milli-Q water │        │                     │
│        +            │        │                     │
│   10 ml Ethanol     │        └─────────────────────┘
└─────────────────────┘
           │
           ↓
┌─────────────────────┐        ┌─────────────────────┐
│        +            │        │       Stir          │
│     200 mg          │   →    │     2 hours         │
│        +            │        │                     │
│ 10 ml Milli-Q water │        └─────────────────────┘
└─────────────────────┘
           │
           ↓
┌─────────────────────┐        ┌─────────────────────┐
│ Pour into Teflon –  │        │  Cool overnight     │
│  lined autoclave    │   →    │                     │
│  Heat at 120 °C     │        └─────────────────────┘
│     3 hours         │
└─────────────────────┘
           │
           ↓
┌─────────────────────┐        ┌─────────────────────┐
│ Centrifuge and wash │        │   Vacuum dry        │
│     with DI         │   →    │    (60 °C)          │
│     3 times         │        │    7 hours          │
└─────────────────────┘        └─────────────────────┘
           │
           ↓
┌─────────────────────┐
│     Pulverise       │
└─────────────────────┘
```
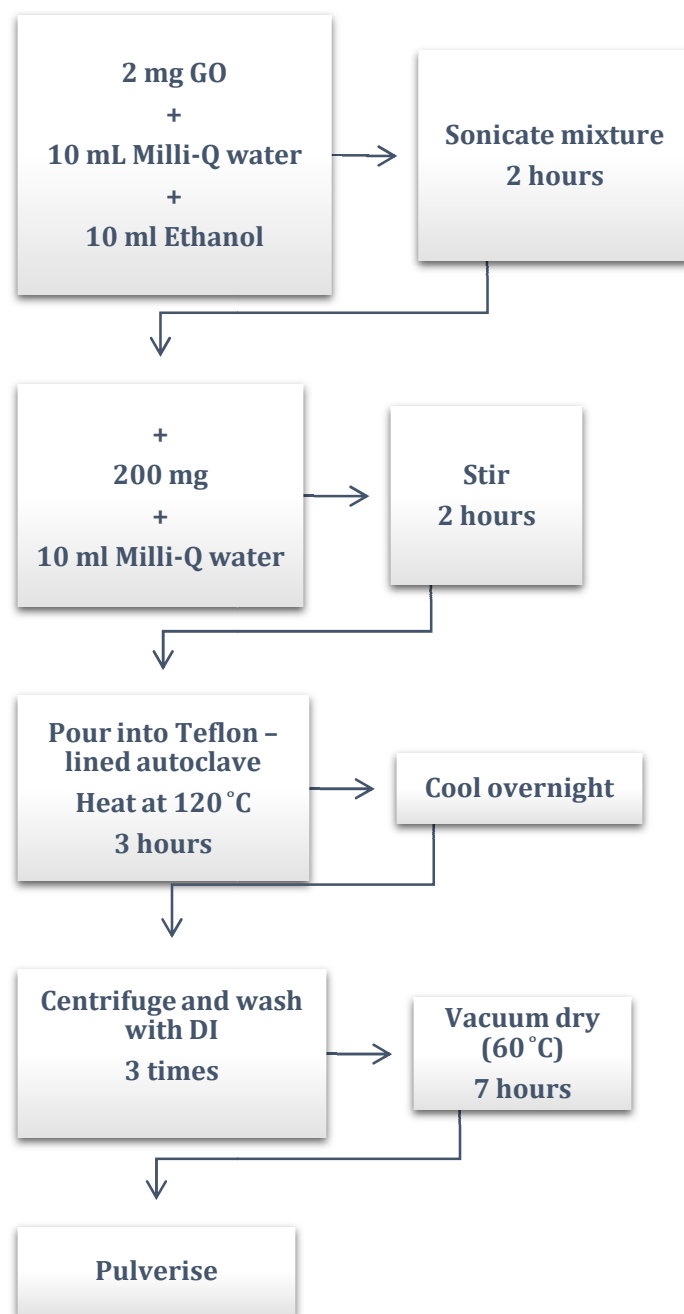
Scheme 3.2 Flow diagram for TiO$_2$-G synthesis from GO and TiO$_2$

3.5.3 Determination of the isoelectric point for TiO$_2$-Graphene composite catalyst

The isoelectric point of the prepared composite catalyst was determined using a Brookhaven ZetaPlus zeta potential analyzer. Surface properties of semiconductors in aqueous media play an important role in photocatalysis. By this experiment the pH range at which the surface charge of TiO$_2$-G will enhance the photocatalytic reduction of Zn^{2+} is determined.

Theory

The zeta potential (ζ) is defined as the electrostatic potential at the interfacial boundary layer on the surface of a particle (Brookhaven Instruments Corporation, 2002). This measurement is based on the ability of charged particles in a solution to move either to positive or to negative poles of an electrode when an electrical field is applied. Also, the charged particles are translated to these poles at a velocity proportional to the magnitude of the charge on them. This phenomenon is known as electrophoresis. During the measurement, a laser beam is passed through the solution in the cuvette with the inserted electrodes. The doppler shifted scattered light particles are proportional to the velocity of the particles in the electrical field which are then detected.

From these two sets of information under a known electrical field the mobility is determined from which zeta potential can be calculated. The mobility is determined from the equation below.

$$\mathbf{V_s = \mu_e E} \tag{3-1}$$

Where E (Volts/cm) is the electric field, V_s (microns/second) average velocity of moving particles and μ_e ($\mu s^{-1}V^{-1}$ cm) is the electrophoretic mobility.

In general the relationship between zeta potential and mobility for colloidal particles dispersed in aqueous solutions is determined as follows

$$\mu_e = \frac{2\varepsilon\zeta}{(3\eta)f\,(\kappa a,\zeta)} \hspace{3cm} (3\text{-}2)$$

Where, $\square$ is the dielectric constant, η is the viscosity ,ζ is the zeta potential, κ^{-1} is the thickness of the electrical double layer, **a** is the radius of the particles, **κa** is the ratio of particle radius to electrical double layer and   f(ka, ζ) is Henry's function which is model-dependent (Brookhaven Instruments Corporation, 2002),

Experimental method

In this experiment, 1 mg of the catalyst was dissolved in 100 mL solution of 250 mg/L formic acid in 8 different glass beakers. The solution pH was adjusted to a pH range of 1 to 12, one pH per glass beaker. The resulting mixture was then sonicated for 10 minutes to keep the particles evenly dispersed in the solution. Exactly 1.5 mL of solution was pipetted into a zeta analyzer cuvette or sample cell and then the electrode was fully inserted into the solution, while thoroughly cleaning any spills on the outer part. The sample cell was then inserted into the sample holder and covered for zeta potential measurement. A graph of pH verses zeta potential was then plotted from the data to give the isoelectric point of the new composite TiO_2-G catalyst which is the point on the graph where zeta potential is zero.

3.5.4 Photo-reduction of Zn^{2+}

TiO_2 or TiO_2-G was added in appropriate quantity to a volume of 150 mL of the prepared simulated wastewater comprising 20.0 ± 1 mg/L Zn^{2+} and formic acid unless otherwise stated. After the pH was adjusted to the required value using a 780 Metrohm Ltd. pH meter, 5 minutes of ultrasonic bath dispersion then followed. After this, the resulting suspension was carefully transferred to a pyrex glass photocatalytic reactor of 600 mL maximum capacity (6.3 cm height and 11 cm diameter) as described in previous work (Chowdhury, 2012).

Adsorption or dark reaction stage (30 min) followed while stirring continuously with a magnetic stirrer. After this a sample was taken, filtered and then stored for further analysis. Ultra-pure nitrogen gas was bubbled through the reaction mixture continuously throughout the entire reaction time. Liquid samples were collected regularly and filtered through a polypropylene 0.45 µm, 25 mm diameter filter before analysis.

3.6 Experimental set up
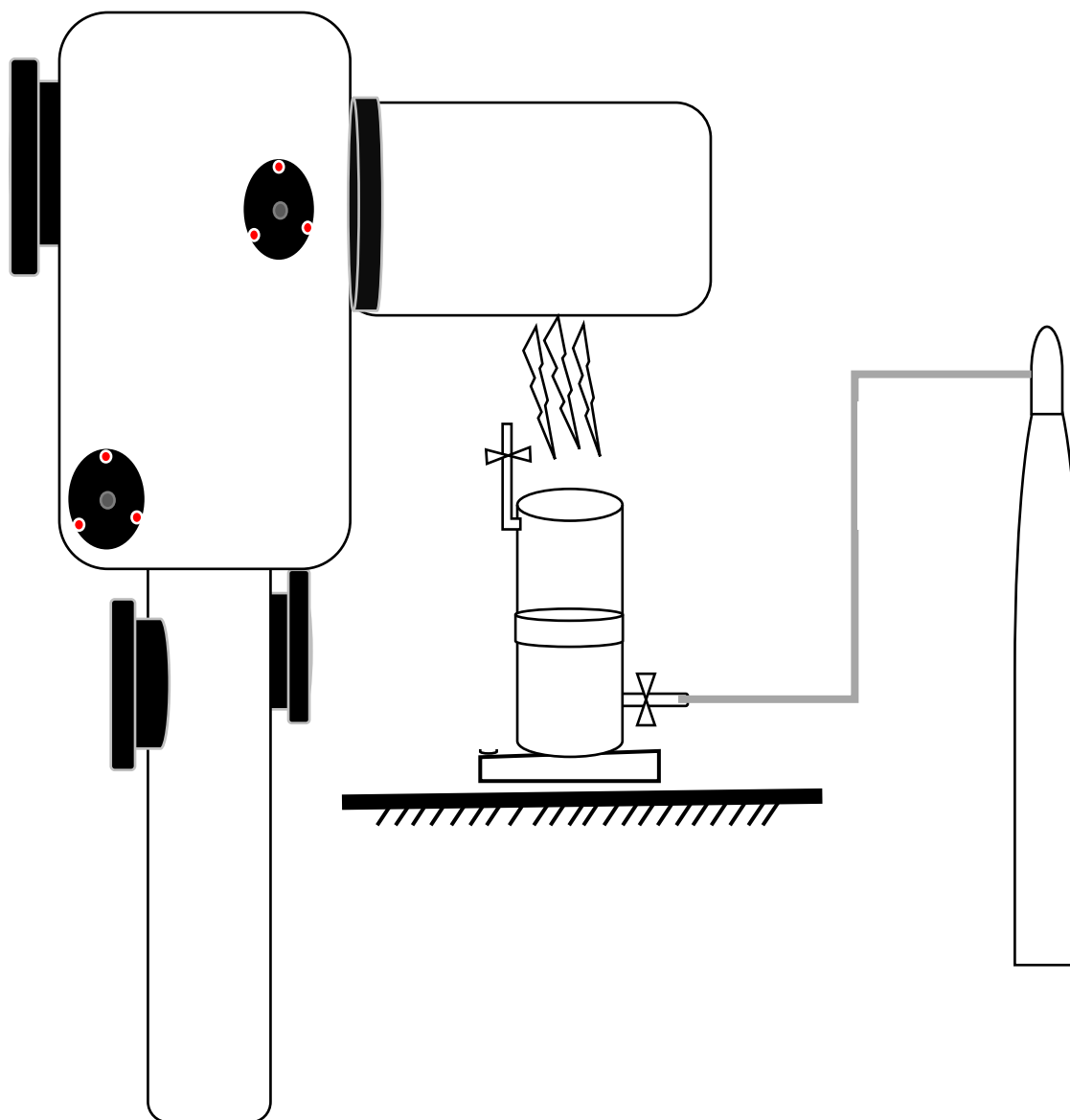
Scheme 3.3 Experimental set up for photo-reduction

4 RESULTS AND DISCUSSION

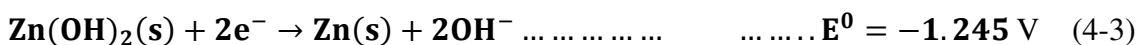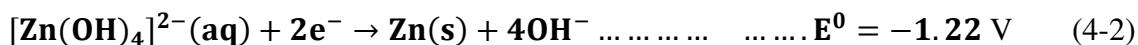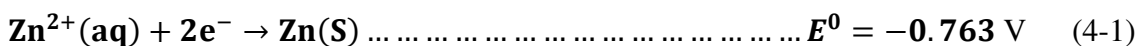This chapter presents experimental results and discussion of solar photocatalytic reduction of Zn^{2+} using graphene-based TiO_2 composite catalyst.

4.1 pH and its Effect on Metal Speciation

Any aqueous system comprising various metal ions will have a wide variety of complex metal ion species depending on the pH of the wastewater under consideration (Kabra, et al., 2008). It has also been established that the rate and feasibility of any photo-reduction process greatly depends on the disposition of the standard reduction potential as compared to that of the conduction band edge of the semiconductor under consideration (Chen and Ray, 2001). Again, various metal ion and ion complexes have different standard reduction potentials as shown below:

$$Zn^{2+}(aq) + 2e^- \rightarrow Zn(S) \ldots \ldots \ldots \ldots \ldots \ldots \ldots \ldots \ldots E^0 = -0.763 \text{ V} \quad (4\text{-}1)$$

$$[Zn(OH)_4]^{2-}(aq) + 2e^- \rightarrow Zn(s) + 4OH^- \ldots \ldots \ldots \quad \ldots \ldots E^0 = -1.22 \text{ V} \quad (4\text{-}2)$$

$$Zn(OH)_2(s) + 2e^- \rightarrow Zn(s) + 2OH^- \ldots \ldots \ldots \ldots \ldots \quad \ldots \ldots . E^0 = -1.245 \text{ V} \quad (4\text{-}3)$$

As mentioned in earlier chapters, the pH of the wastewater also affects the semiconductor surface charge as well as the position of the conduction and valence band edges of the photocatalyst. While increasing the pH of the solution will theoretically favour the photoreduction of Zn^{2+}, the investigation of the most effective pH range for which a

comprehensive assessment of the effectiveness of the photocatalytic treatment process would be possible is of great concern. It was therefore of interest to investigate the effect of pH on the ion species distribution of zinc in the simulated wastewater. With the aid of Visual MINTEQ 3.1 chemical equilibrium software, zinc metal speciation over pH range 0-14 was modeled for the synthetic wastewater composition. The species represented in figure 4.1 are those that showed relatively significant percentages in abundance.
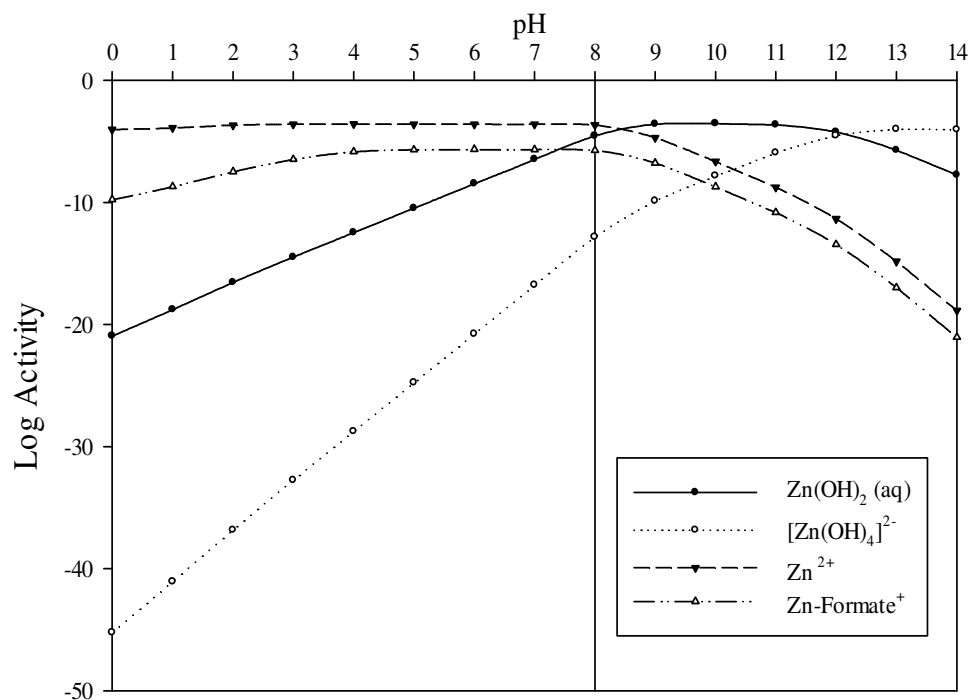
Figure 4.1 Zinc species distribution profile as a function of pH.

Zinc is present in aqueous solution as various species with different standard reduction potentials. From the speciation profile in Figure. 4.1, it is observed that the major species in solution are Zn^{2+}, $Zn(OH)_2$, $Zn(OH)_3^-$ and $Zn(OH)_4^{2-}$. As the pH increases from 0 to 8 there is a steady increase in the activity of $Zn(OH)_2$ which reaches a plateau between pH

8 and 12. Within the same range pH (8 – 12), Zn^{2+} activity begins to decline. This gives an indication that as the Zn^{2+} activity decreases, there is simultaneous precipitation of zinc as $Zn(OH)_2$ from solution. This was physically observed as a white gelatinous precipitate, that settles at the bottom of the reactor prior to addition of TiO_2 as shown in figure 4.2. This precipitate may be retained on a filter paper as residue.

.
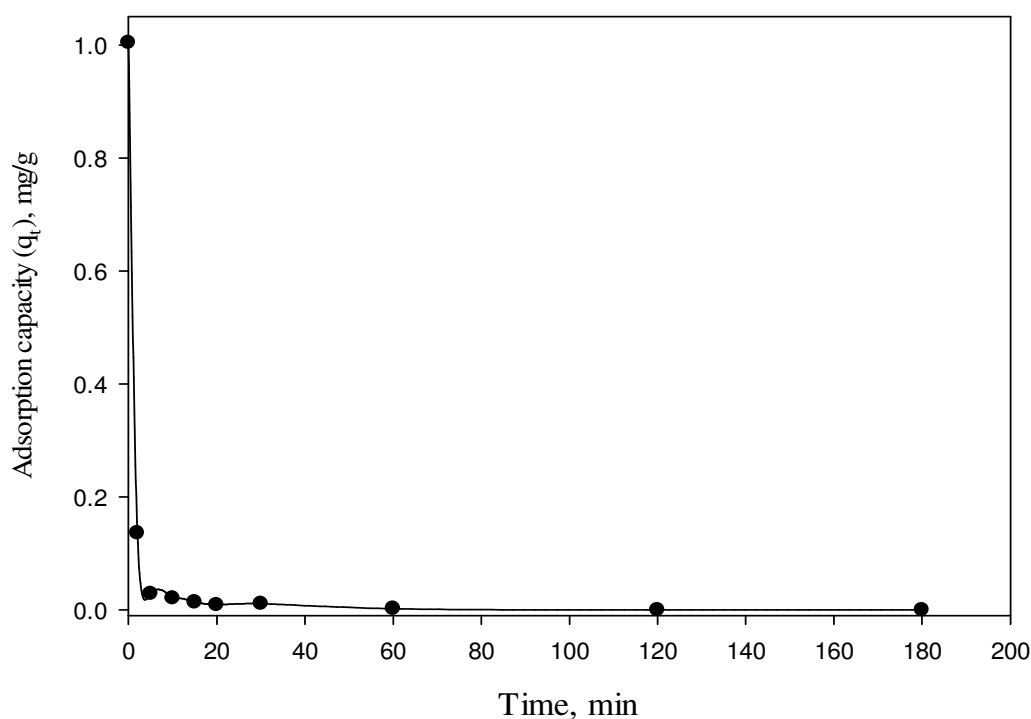
Figure 4.2 Adsorption of Zn^{2+} at pH 8.

[Experimental conditions: $C_0 = 20$ ppm, $C_{cat} = 2$ g/L, 0.01 M Tris buffer]

As seen from Figure 4.2, 86 % of Zn^{2+} was quickly removed from solution after TiO_2 addition. At 20 minutes, there is nearly 100% removal of Zn^{2+} from solution. This high percentage removal of Zn^{2+} could partly be as a result of the precipitation of Zn^{2+} and retention on filter as residue of $Zn(OH)_2$. In addition to this, the neutral $Zn(OH)_2$ does not

have an affinity for the charged catalyst surface, and therefore, cannot be removed by adsorption (Kabra, et al., 2008). This is because according to figure 4.1, at pH ~ 7.5, $Zn(OH)_2$ formation begins and its formation is independent of the initial zinc concentration present (Albrecht, et al., 2011). This experimental results clearly support the theoretical speciation model shown in figure 4.1. Therefore, at this stage it can be proposed that in accounting for the mass balance of Zn^{2+}, adsorption onto TiO_2 or any other adsorbent material cannot account to a significant extent for the high removal efficiency. For consistency and certainty in the data obtained, it has been established that the most effective pH working range for the removal of Zn^{2+} from solution by adsorption is between 6 and 8 (Bhattacharya, et al., 2006; Lu and Chiu, 2006; Wang, et al., 2013).

4.2 Adsorption study

In photocatalytic systems adsorption of pollutants to the semiconductor catalyst is the first step in the reaction process since the reaction occurs between the adsorbed species on the surface of catalyst and the radicals via photo-generated charges that have migrated to the surface. For this reason, the study of conditions under which there will be efficient adsorption of the pollutant species onto the surface of the semiconductor catalyst as well as the subsequent reaction process associated with this adsorption step is very important.

In industry, the limitations of wastewater discharge regulations imposes the safe disposal limits between 6-9 pH units. The pH range of this study, however, was limited to 6 - 8. This is because, study at pH values above 8 will provide an inconclusive and skewed result due to excessive precipitation of the model compound as discussed earlier.

Therefore, in order to clearly distinguish between the adsorption phase and the photodegradation, hereafter the highest pH was capped at 8. The adsorption equilibrium time was determined, followed by the effect of various parameters, such as the initial metal ion concentration, catalyst loading and catalyst type.

4.2.1 Adsorption equilibrium time for Zn^{2+}

The kinetics of Zn^{2+} adsorption at different pH are shown in Figure 4.3. This experiment was performed to determine the dark reaction time, (adsorption in absence of light) in the presence of tris organic buffer. This graph shows that irrespective of the chosen pH, in the absence of light after about 30 min of continuous stirring there is no significant removal of Zn^{2+}. Hence, this time was chosen as the adsorption equilibration time required in subsequent experiments prior to photodegradation experiments.

Chenthamarakshan et al (2000), also observed that approximately 30 min was the time required for zinc reach an adsorption/desorption equilibrium. Depending on the pH, the adsorbent photocatalyst has a high affinity for target pollutant materials, which implies that photocatalytic degradation can be considered in this step as a possible treatment candidate for dissolved metal ions. However, for the purposes of the adsorption study, the equilibration time was extended to 1 hour to ensure complete adsorption/desorption equilibrium was attained. After this step, further studies were performed to explain the type of adsorption mechanism that effectively describes this system.
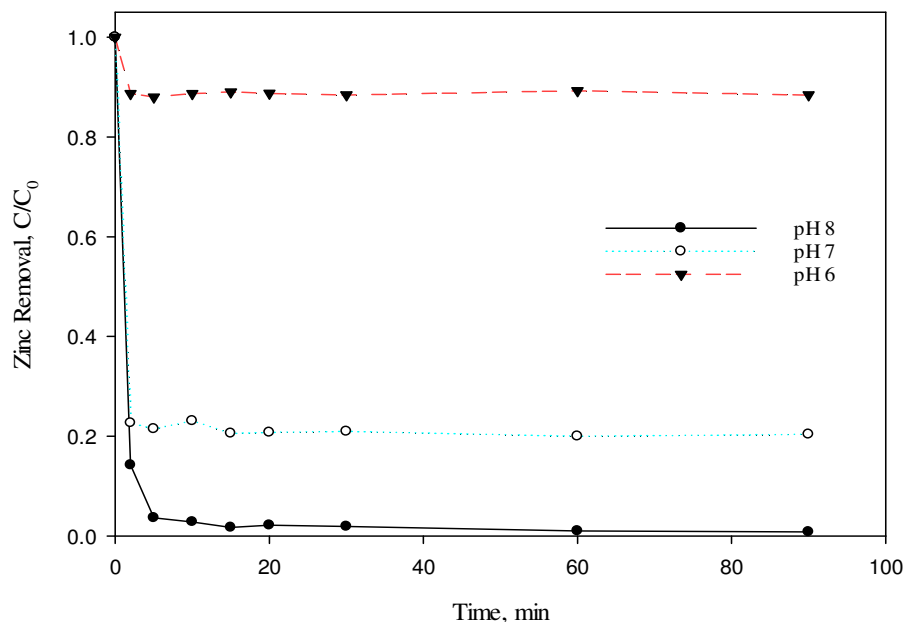
Figure 4.3 Adsorption of Zn^{2+} on TiO_2 at different pH.

[Experimental conditions: $C_0 = 21 \pm 1$ mg/L, pH = 6, 7, 8, $V_r = 200$ ml, $C_m = 2$ g/L,

0.01M Tris Buffer.]

4.2.2 Effect of catalyst loading on adsorption

The concentration of adsorbent has been proved to be directly related to the amount of metal ion removed and therefore, the determination of exact relationship of the catalyst loading to adsorption of target pollutant is of great importance. Experiments were performed over three different pH values (pH 6-8).

The percentage removal of Zn^{2+} was calculated as follows,

$$\% \text{ Zinc(II) Removal} = \left(\frac{C_0 - C_e}{C_0}\right) \times 100 \tag{4-4}$$

Where C_0 is the initial Zn^{2+} concentration, C_e is the equilibrium concentration measured.
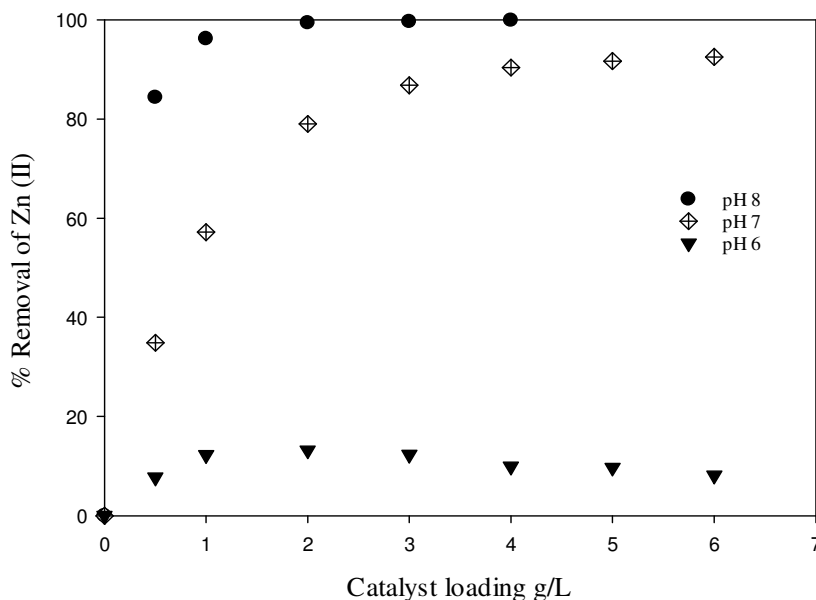
Figure 4.4 Effect of catalyst loading on the adsorption of Zn^{2+} onto TiO_2 at different

pH values.

[Experimental conditions: C_0 = 20± 0.2 mg/L, V_r = 50 ml each, 0.01M Tris buffer]

This experiment evaluates the effect of varying catalyst loading on the removal of Zn^{2+} as well as the impact the initial pH of the solution has on the removal. From Figure 4.4, the trends show that increasing the initial catalyst loading for a constant initial metal ion concentration gives a positive response for Zn^{2+} removal at pH 7 and 8, while the effect is insignificant at pH 6. As the TiO_2 concentration for pH 6, 7 and 8 is increased, there is also an initial increase in the % removal of Zn^{2+} until a catalyst concentration of about 2 g/L. This shows that the dependence of the removal via adsorption of Zn^{2+} on the catalyst loading is not a linear relationship. After the threshold point, any further increase of TiO_2 concentration for pH 7 and 8 causes the % removal to approach a limiting value of

approximately 90% and 100% respectively. However at pH 6, there was only a maximum of 12% removal recorded at 2 g/L TiO_2 concentration after which the % Zn^{2+} removed with increase in catalyst concentration starts to decline.

The initial increase in the amount of Zn^{2+} removed is a result of the availability of a larger specific surface area with respect to the initial concentration, which in turn translates to availability of more adsorption cites for the metal ion. Conversely, higher initial concentration to catalyst loading results in the saturation of all the active adsorption sites on the TiO_2 surface. Optimum catalyst loading for this system was found at 2 g/L for pH 8 and 6 and 4 g/L at pH 7 in terms of percentage Zn^{2+} adsorbed. However, the adsorption capacity mg/g of the TiO_2 does not increase with increasing TiO_2 loading but decreases due to shielding of reactive sites caused by overcrowding (agglomeration) of the TiO_2 particles. This saturation behavior may also be due to flocculation of the TiO_2 particles (Athapaththu, 2013). Particle concentration effect resulting in the decrease of adsorption efficiency was also observed by Chen et al. (2007). While greater amount of TiO_2 catalyst will result in higher percentage removal by adsorption it should be noted that an overly turbid solution may not be favorable for the next stage of the experiment, which is the introduction of a light source for the photocatalysis.

The adsorption of Zn^{2+} in relation to the pH of the aqueous solution can also be explained with respect to the effect of pH on the surface charge on the TiO_2. At pH values less than 7 there is a resultant net positive charge on the TiO_2 surfaces as a result of the accumulation of protons on the surface sites. This in turn leads to relatively strong

electrostatic repulsion of cationic metal species from the surface of the TiO_2. As pH becomes more alkaline, there is a reduction in the electrostatic repulsion on the TiO_2 sorption sites thereby enhancing the adsorption of Zn^{2+} onto the TiO_2 surface. This trend greatly conforms to that of many other others (Bhattacharya, et al., 2006; Lu and Chiu, 2006).

This elucidates the adsorption behavior at pH 6 where there is considerable competition of H^+ ions with the cationic species for the sites available on the adsorbent surface. Coupled with the saturation behavior noticed at catalyst loadings above the optimum values it can be observed that, the percentage of Zn^{2+} removed begins to decline. Again, other investigations have shown that the isoelectric point of P25 TiO_2 is in the range of pH 6.0-6.9 (Yang, et al., 2007). For this reason, the surface of the catalyst is highly negatively charged above this pH, hence attracting the positively charged cations to the surface while the converse occurs at pH values below this 6.2 accounting for the low adsorption of Zn^{2+} at pH 6. This could also be the reason for the lack of decline in the percentage removal of Zn^{2+} at pH 8 after the threshold value (Farghali, et al., 2013; Low, et al., 1995).

The solution pH is one of the most significant process parameters in adsorption of Zn^{2+} on TiO_2. It is therefore vital to maintain a near neutral pH during the treatment process. (Xiaofu, Wu et al 2010). Unless stated otherwise initial pH was kept at a constant value of 7.1 ± 0.1.

4.2.3 Determination of adsorption isotherm parameters

The most important parameter that is useful for the description of every adsorption relationship is the equilibrium adsorbed Zn^{2+} per unit adsorbent mass, q_e (mg/g). This was determined as shown in equation 4-5;

$$q_e = \frac{(C_0 - C_e)\,V}{m} \qquad\qquad (4\text{-}5)$$

Where, C_o (mg/L) is the initial metal ion concentration, C_e (mg/L) is the equilibrium concentration of Zn^{2+} remaining in solution as measured using the ICP-OES while m (g) is the mass of catalyst and V is the initial volume of the solution (L)(Lu and Chiu, 2006).

4.2.4 Freundlich isotherm for adsorption of Zn^{2+} on TiO_2

The Freundlich isotherm is an empirical model applied to describe adsorption on an adsorbent (Veli and Alyüz, 2007b). This isotherm is expressed using equation 4-6.

$$q_e = K_f C_e^{1/n} \qquad\qquad (4\text{-}6)$$

Where K_f, represents the Freundlich constant (mg/g) and 1/n is the adsorption intensity. Using the first method (linear regression), the approximations of Freundlich adsorption parameters are determined from equation 4-6 by fitting the experimental data to the linearized form of the model as follows;

$$\text{Log } q_e = \log K_f + \frac{1}{n}\log C_e \qquad\qquad (4\text{-}7)$$

Plotting the results of Log C_e vs Log q_e yields a straight line whose Y-intercept and slope corresponds to log K_f and the 1/n parameters as shown in Figure 4.5. The slope (1/n), known as the intensity of adsorption usually is a value within the range of 0 to 1. This

gives an indication of the extent of the heterogeneity of the system. The closer this value is to 0 the more heterogeneous the system is. This provides a parameter for the comparison of different adsorbent materials (Foo and Hameed, 2010).
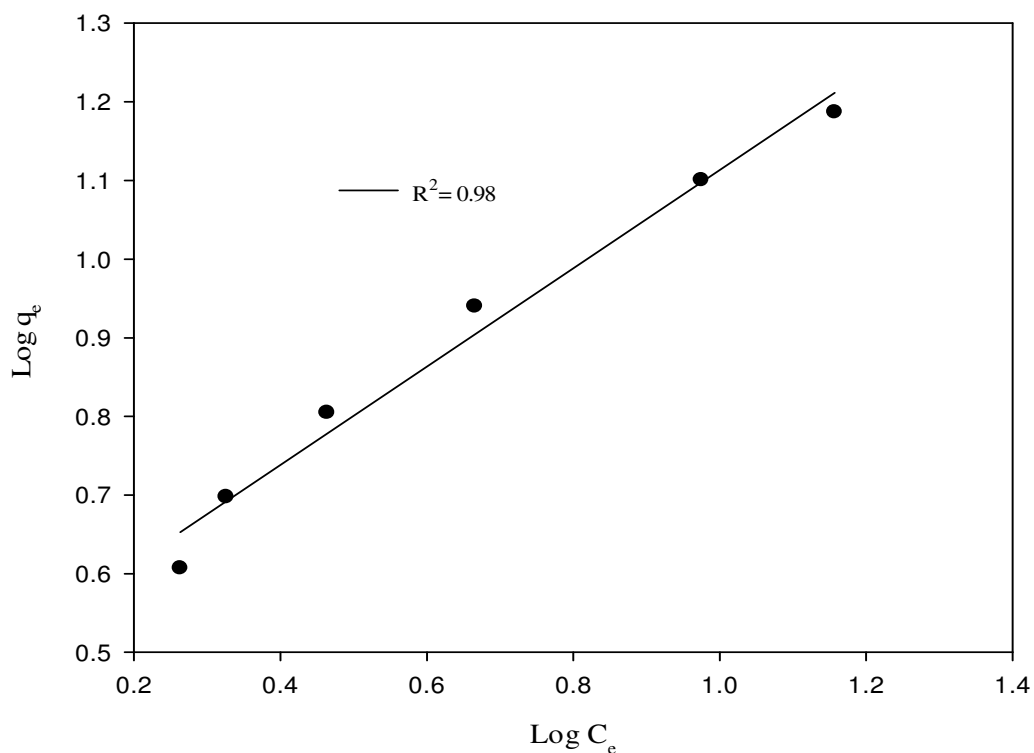
Figure 4.5 Linearized Freundlich Isotherm for adsorption of Zn^{2+} on TiO_2

[Experimental conditions: C_0 = 22.0 mg/L, pH = 7, V_r = 50 ml each, 0.01M Tris buffer]

From the Figure 4.5 above it can be observed that the fitted line yields an R^2 value of 0.98, the resulting in equation 4-8a as seen bellow for the Freundlich type adsorption of Zn^{2+} onto TiO_2.
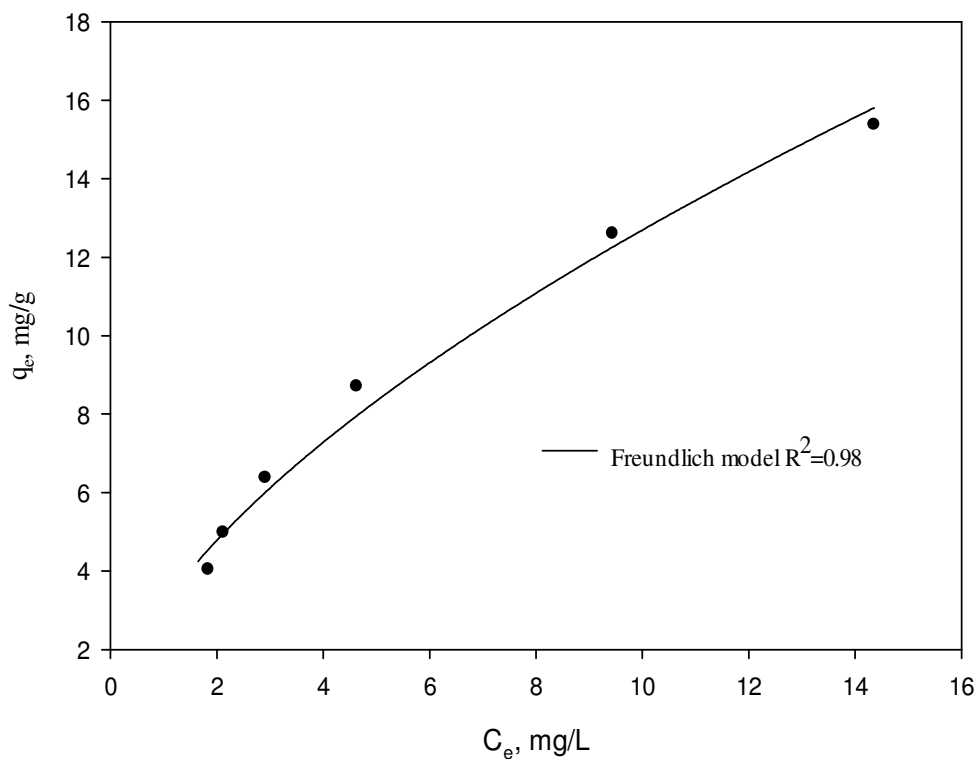
$$\mathbf{q_e = 3.07C_e^{0.63}}$$ (4-8 a)

Figure 4.6 Freundlich Isotherm for adsorption of Zn^{2+} on TiO$_2$

[Experimental conditions: $C_0 = 22.0$ mg/L, pH = 7, $V_r = 50$ ml each, 0.01M Tris buffer]

Secondly, fitting the isotherm model to the obtained data by means of a non-linear regression yielded the results for the Freundlich parameters as seen in equation 4-8b.

$$\mathbf{q_e = 3.33C_e^{0.58}}$$
(4-8 b)

K_f and 1/n was determined as 3.07 and 0.63 respectively for method A (linear regression) and 3.33 mg/g and 0.67 respectively for method B (non-linear regression). Since round-

off errors are introduced while linearizing, it is best to use the value obtained from non-linear regression analysis.

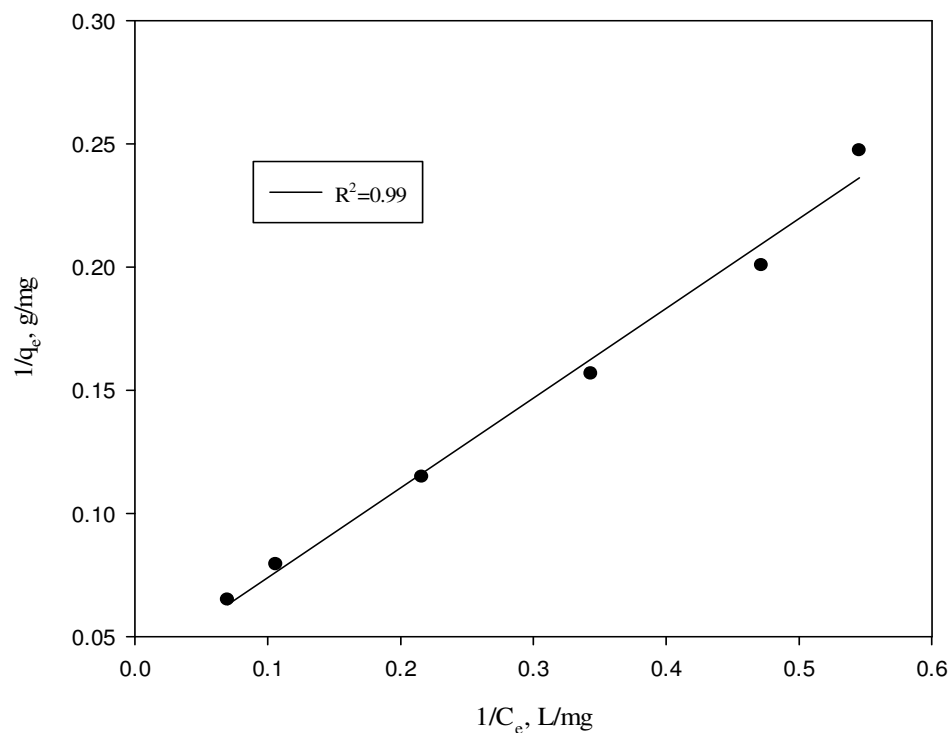## 4.2.5 Langmuir isotherm for adsorption of Zn^{2+} on TiO_2

The Langmuir Isotherm describes a type of adsorption where only a single layer of adsorbate coats the surface of the adsorbent (Veli and Alyüz, 2007b). This model is represented as follows;

$$q_e = \frac{Q_o K_{ad} C_e}{1 + K_{ads} C_e} \tag{4-9}$$

Where q_e is the equilibrium amount of Zn^{2+} adsorbed per unit mass of catalyst (mg/g), Q_o (mg/g) is the maximum (saturation) capacity of adsorbent which corresponds to the amount of Zn^{2+} that is adsorbed per unit mass of catalyst that forms a complete monolayer coverage, K_{ads} is the equilibrium constant of adsorption, also known as the Langmuir constant (L/mg), and C_e is the equilibrium concentration of ions in solution (mg/L) (Bhattacharya, et al., 2006).

Again, to determine the model parameters, the data obtained is fitted to the linear form of equation 4-10 that is derived by rearranging equation 4.9 as follows:

$$\frac{1}{q_e} = \frac{1}{Q_0} + \frac{1}{K_{ads} Q_0} \left(\frac{1}{C_e}\right) \tag{4-10}$$

Figure 4.7 Linearized Langmuir Isotherm for adsorption of Zn^{2+} onto TiO_2

[Experimental conditions: C_0 = 22.0 mg/L, pH = 7, V_r = 50 ml each, 0.01M Tris buffer]

As shown in Figure 4.5, a graph of $1/C_e$ vs $1/q_e$ resulting in the linear equation of the Langmuir type adsorption for Zn^{2+} onto TiO_2 is given as follows in equation 4-11a ;

$$\frac{1}{q_e} = 0.037 + 0.364\frac{1}{C_e}$$ (4-11 a)

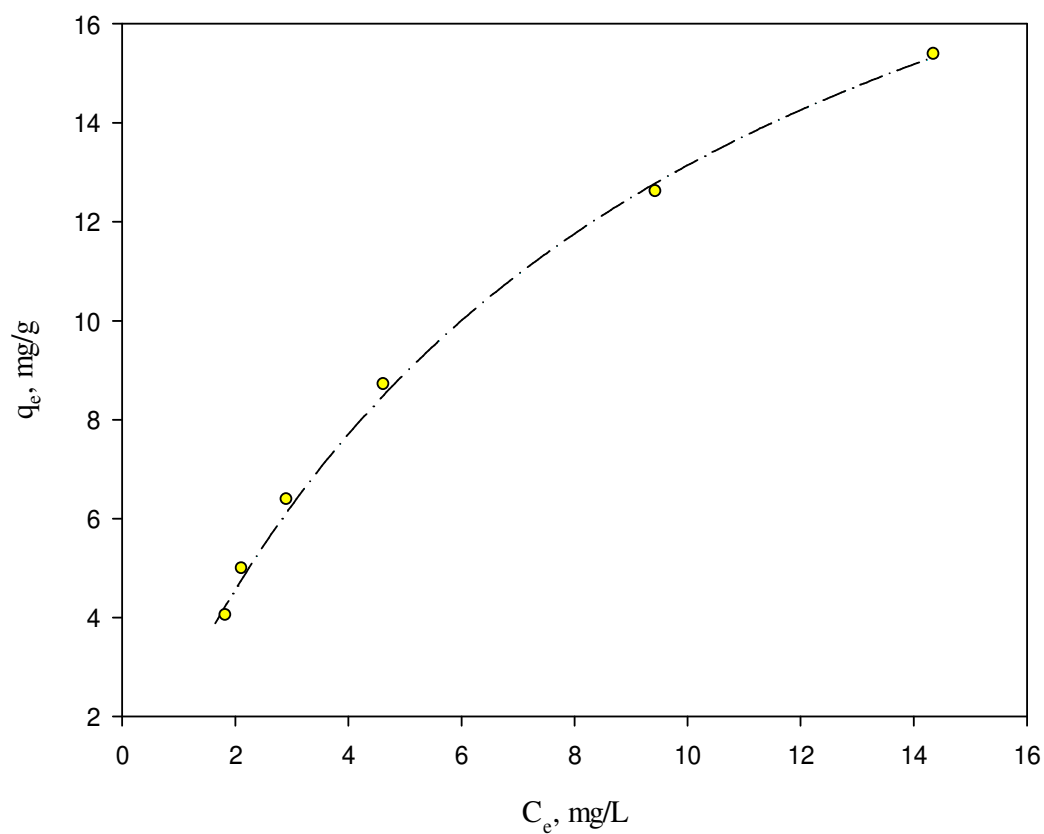Therefore, Q_o is calculated as 26.58 mg/g and K_{ads} as 0.10 L/mg for the adsorption of Zn^{2+} onto TiO_2.

Figure 4.8 Langmuir Isotherm for adsorption of Zn^{2+} on TiO$_2$

[Experimental conditions: $C_0 = 22.0$ mg/L, pH = 7, V_r =50 ml each, 0.01M Tris buffer]

Secondly, fitting the non-linear Langmuir isotherm model to the data gives a Q_o of 24.25 mg/g and K_{ads} as 0.12 L/mg for the adsorption of Zn^{2+} onto TiO$_2$. The resulting equation is shown in equation 4-11b.

$$\mathbf{q_e} = \frac{\mathbf{2.91}C_e}{\mathbf{1+0.12}C_e} \tag{4-11b}$$

4.2.6 The adsorption of Zn^{2+} on Graphene-Based TiO_2 photocatalyst

The performance of coupling graphene, a relatively new carbon material with TiO_2 is investigated in this section. Similar experiments were performed under various conditions to determine the adsorption parameters. Equilibrium data were obtained for the TiO_2-G (1 wt. % GO) composite catalyst and fitted to both the Freundlich and Langmuir type adsorption isotherms. These parameters are compared to that of adsorption on TiO_2 only as adsorbent. Currently, Lee and Yang (2012) have reported the effect of the TiO_2-G composite catalyst hydrothermal treatment time on the adsorption capacities of zinc, lead and cadmium ions. Other metal oxide-graphene or reduced graphene oxide prepared under various conditions has been investigated for the removal of heavy metal ions by others adsorbents. Meanwhile, the mechanisms involved in the adsorption of metal ions on various graphene-based composite materials is not fully understood and is currently also under investigation (Upadhyay, et al., 2013)

In this study, parameters such as the initial TiO_2-G catalyst amount and the effect of pH on adsorption was compared to that of TiO_2. It been established from the results in section 4.1 above that the pH of the aqueous solution is one of the most important parameters that affects the adsorption of metal ions to the surface of any adsorbent. The point of zero charge (PZC) is significant in explaining and understanding this behaviour. Therefore, the PZC for the synthesized composite catalyst material was measured. In addition a complete characterization of the prepared catalyst as described by (Malekshoar, et al., 2014) is summarized.

4.2.7 Characterization of TiO$_2$-Graphene catalyst

X-ray powder diffraction (XRD), X-ray photoelectron spectroscopy (XPS), UV spectra analysis transmission electron microscope (TEM) and the scanning electron microscope (SEM) for structural and morphological analysis of the composite TiO$_2$-G (1 wt.% GO) was carried out and discussed in an earlier work (Malekshoar, et al., 2014). The Band gap of TiO$_2$ was measured to have reduced from 3.1 to 2.2 eV when composited with graphene.

4.2.8 The isoelectric point for TiO$_2$-Graphene composite

Figure 4.9 below shows the surface charge of the synthesized TiO$_2$-Graphene composite as a function of pH. The point of zero charge (pH$_{zpc}$) is defined as the pH at which the concentration of the protonated and deprotonated surface groups are equal. The measured pH$_{pzc}$ for this new catalyst material (1 wt.% GO) was found to be at 4.9 pH as compared to that of the pH$_{ZPc}$ of 1 wt.% TiO$_2$-G photocatalyst to be 4.1 (Morales-Torres, et al., 2013). They also showed that increasing the Graphite Oxide (GO) to 6 wt. % decreased the pH$_{ZPc}$ to pH 3.0.
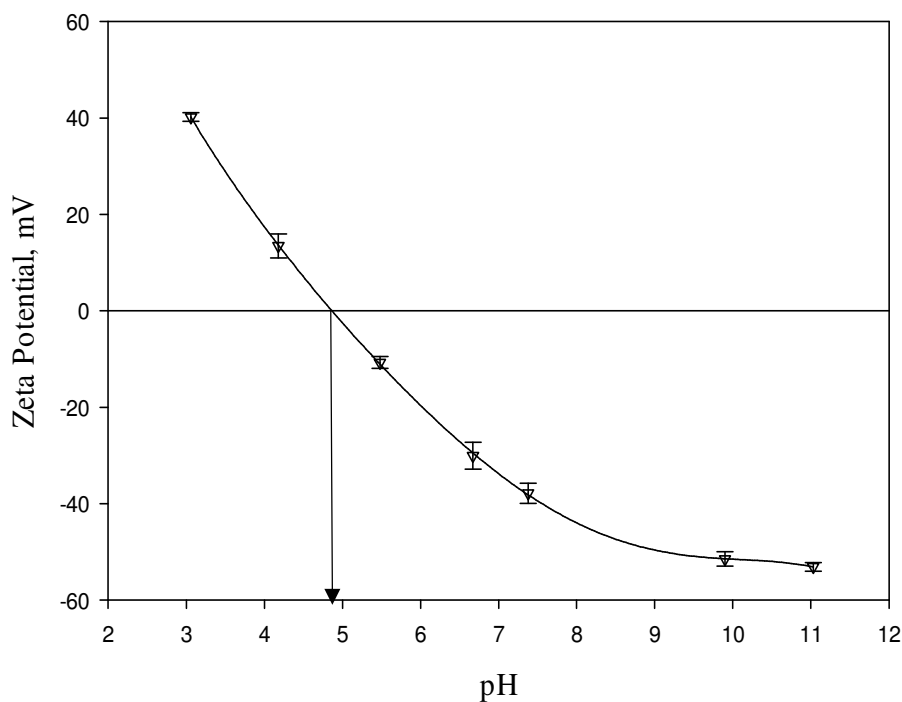
Figure 4.9 The Isoelectric point of TiO$_2$-G composite

[Experimental conditions: 1 mg TiO$_2$-G, 100 mL Milli-Q water each, 250 ppm FA]

The higher pH$_{pzc}$ of TiO$_2$ (6.2-6.9) as compared to TiO$_2$-G (4.9) indicates that the net surface charge of these two materials might be significantly different in aqueous solution between pH 4.9 and 6.0 such that at a pH greater than 5 the net positive charge on the surface of TiO$_2$-G is negative attracting the cations while a net positive charge on the surface of TiO$_2$ will be positive repelling the cations until pH increases above 6.2. Therefore, the adsorption capacity of TiO$_2$-G is expected to be higher than that of TiO$_2$ between pH 5 to 6. Figure 4.10 shows the adsorption capacities of the two catalyst materials at different pH at a constant catalyst loading of 2 g/L.
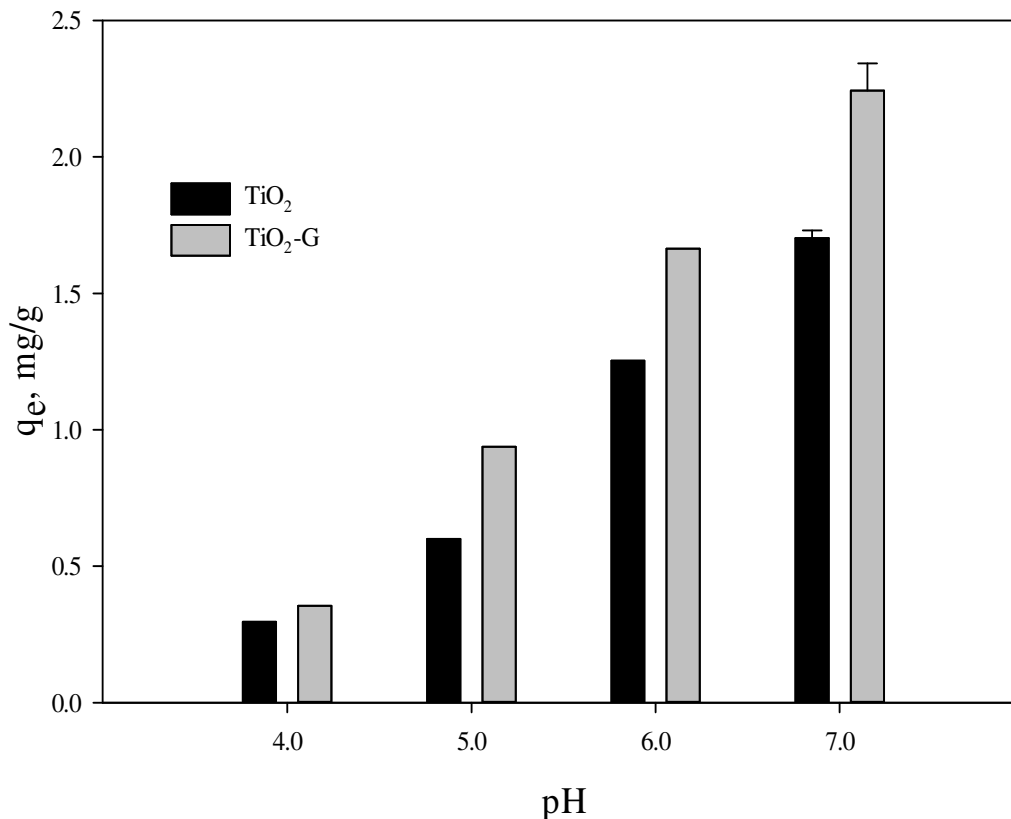
Figure 4.10 Equilibrium Zn^{2+} adsorbed (mg/g) at different pH

[Experimental conditions: C_0 = 21.2 mg/L; pH = 4, 5, 6, 7; V_r = 50 ml each, C_m = 2 g/L]

Figure 4.10 indicates that below the pH$_{pzc}$ of both TiO$_2$ and TiO$_2$-G at pH 4, the maximum amount of Zn^{2+} adsorbed is less than 0.5 mg/g. TiO$_2$-G at this pH adsorbed 16.5% more Zn^{2+} than TiO$_2$ only. Increasing the pH resulted in an increase in Zn^{2+} adsorption on TiO$_2$ and TiO$_2$-G. The observed adsorption capacity values of TiO$_2$-G are 36.1%, 24.6% and 24.06 % more than TiO$_2$ only at pH 5, 6 and 7 respectively.

This can be explained by the change in surface properties of the composite catalyst material as compared to pure TiO$_2$. The presence of graphene in the composite contributes to the formation of various complexes with the metal ions thereby increasing

the overall sorption capacity of the material. This result therefore shows that the adsorption of metal ions onto TiO_2-G is favoured over a wider pH range than that of TiO_2 only.
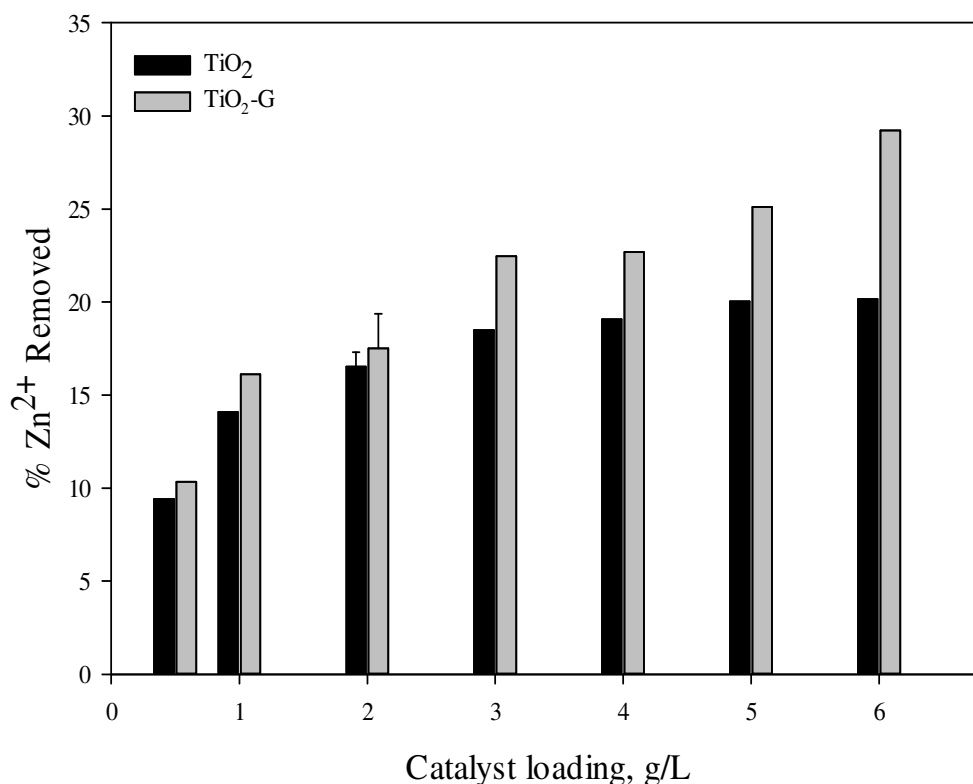
Figure 4.11 Effect of catalyst loading on the adsorption of Zn^{2+} in presence of FA.

[Experimental conditions: C_0 = 22.0 mg/L, pH = 7, V_r = 50 ml each, 250 ppm FA]

Figure 4.11 shows that varying the photocatalyst loading from 0.5 to 6 g/L, the percentage of Zn^{2+} removed by TiO_2 is less than that of TiO_2-G for all photocatalyst loadings. However, after the 2 g/L dose of TiO_2 there is no significant increase (2.0 %) in the adsorption of Zn^{2+} with increasing catalyst loading to 6 g/L. Increasing the catalyst dosage for TiO_2-G from 2 g/L to 6 g/L however shows a relatively significant increase (12.9 %) in the amount of Zn^{2+} removed. The trend for TiO_2-G does not follow a

saturation behaviour as seen for TiO_2 within the same catalyst concentration range considered. This could be as a result of an increase in binding sites due to the higher specific surface area of TiO_2-G the TiO_2-G loading increases as compared to bare TiO_2.

4.2.9 Isotherms for Graphene based TiO_2 Catalyst

The equilibrium data obtained for the adsorption of Zn^{2+} onto TiO_2-G semiconductor was also fitted to linearized and non-linearized adsorption isotherms and the isotherm parameters were determined and compared to that of TiO_2 only.

4.2.10 Freundlich isotherm for the adsorption of Zn^{2+} on TiO_2-G

As seen from figure 4.12, the results from the fitted data yields equation 4-12a with an R^2 value of 0.98.

$$q_e = 2.22C_e^{0.689} \qquad \text{(4-12 a)}$$

From this result, K_f and 1/n was calculated as 2.22 mg/g and 0.69 respectively.
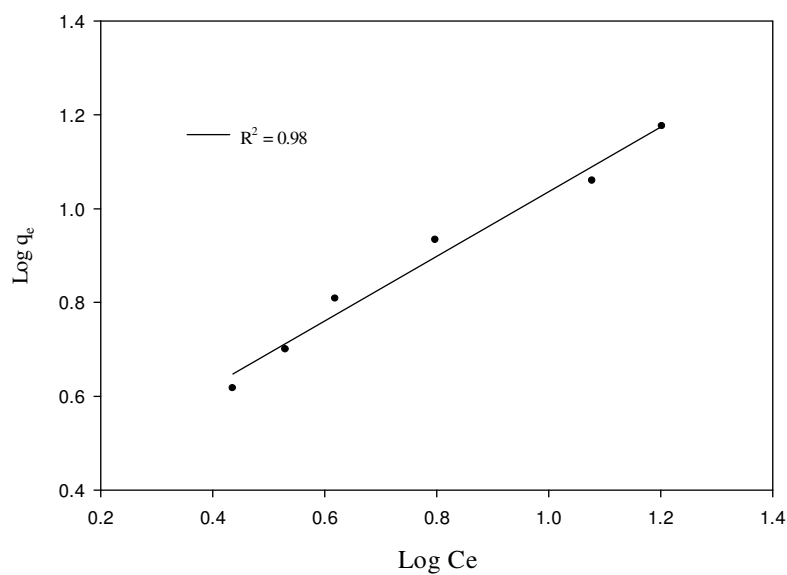
Figure 4.12 Freundlich Isotherm for adsorption of Zn^{2+} on TiO_2-G

[Experimental conditions: C_0 = 22.0 mg/L, pH = 7 V_r = 50 ml each, 0.01 M Tris buffer]
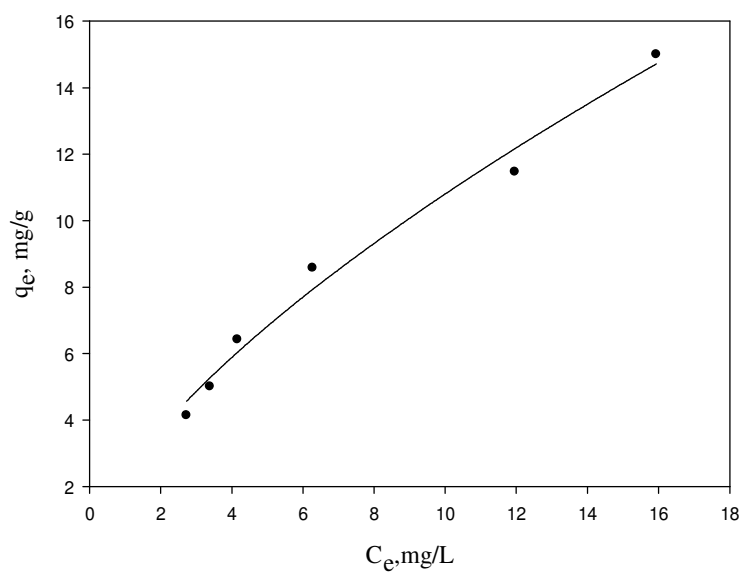
Figure 4.13 Freundlich Isotherm for adsorption of Zn^{2+} on TiO_2-G

[Experimental conditions: C_0 = 22.0 mg/L, pH = 7, V_r = 50 ml each, 0.01M Tris buffer]

From figure 4.13, the fitted data to the Freundlich equation gives rise to the equation 4-12b. K_f and $1/n$ was determined as 2.35 and 0.66 respectively.

$$q_e = 2.35C_e^{0.66} \hspace{4cm} \text{(4-12 b)}$$

4.2.11 Langmuir isotherm for adsorption of Zn^{2+} on TiO_2-G

As seen from figure 4.14, the results from fitting the data to the linearized Langmuir equation produces equation 4-13a as seen below.

$$\frac{1}{q_e} = 0.032 + 0.556\frac{1}{C_e} \hspace{3cm} \text{(4-13a)}$$

Therefore, Q_o is calculated as 30.81 mg/g and K_{ads} as 0.06 L/mg for the adsorption of Zn^{2+} onto TiO_2-G.
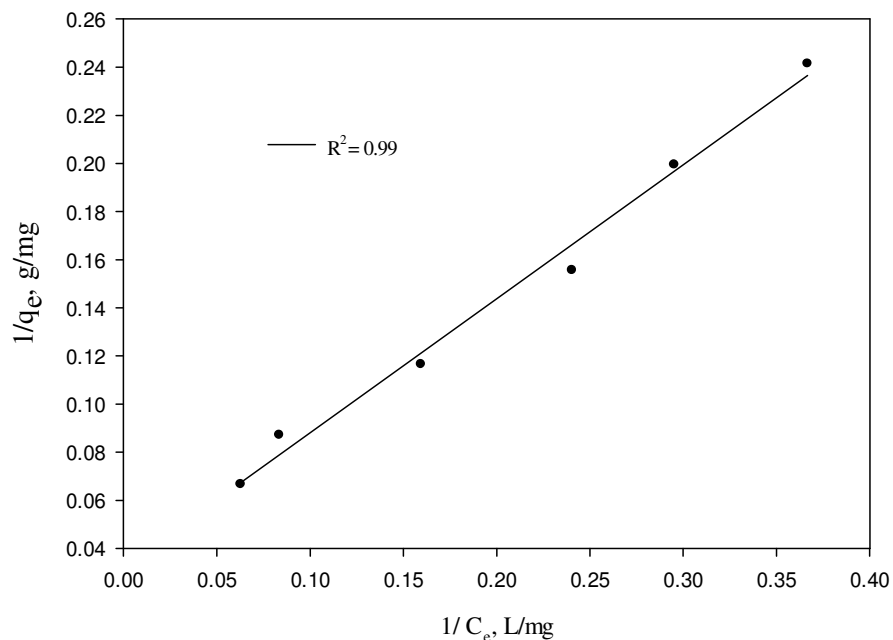
Figure 4.14 Langmuir Isotherm for adsorption of Zn^{2+} on TiO_2-G

[Experimental conditions: C_0 = 22.0 mg/L, pH = 7, V_r = 50 ml each, 0.01M Tris buffer]
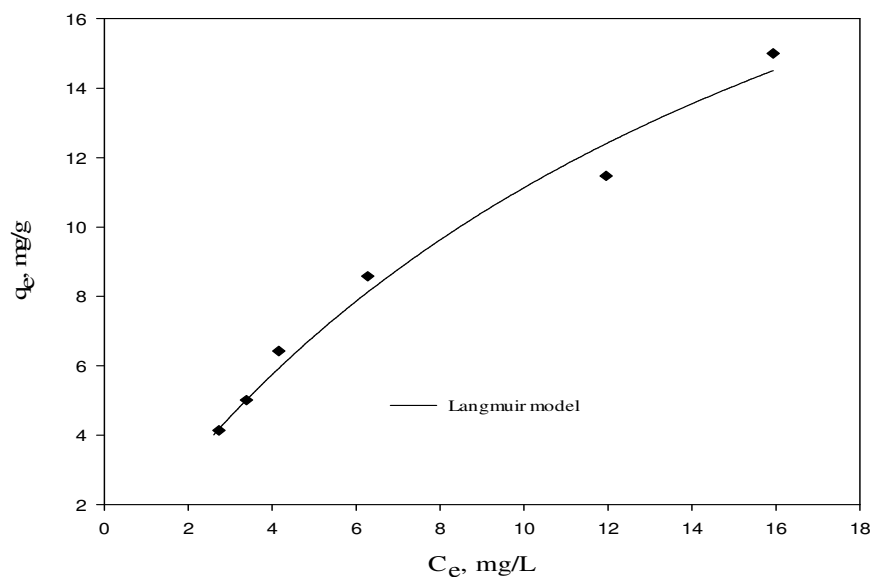
Figure 4.15 Langmuir Isotherm for adsorption of Zn^{2+} on TiO_2-G

[Experimental conditions: C_0 = 22.0 mg/L, pH = 7, V_r = 50 ml each, 0.01M Tris buffer]

Here also, fitting the non-linear model to the data gives a Q_o of 28.28 mg/g and K_{ads} as 0.07 L/mg for the adsorption of Zn^{2+} onto TiO_2. The resulting equation is shown in equation 4-13b.

$$q_e = \frac{1.87C_e}{1+0.07C_e} \tag{4-13b}$$

4.2.12 Separation constant for Langmuir isotherms

Determination of the separation constant (R_L) values for the Langmuir isotherms which is a dimensionless constant is shown in equation 4.14.

$$R_L = \frac{1}{1+K_L C_0} \tag{4-14}$$

The lower the R_L value the more favourable the adsorption when the comparison of adsorbents is being considered. When the R_L is > 1 then adsorption is unfavourable. When 0 <R_L<1 adsorption is considered favourable (Foo and Hameed, 2010).

Table 4.1 summarises the results of the isotherm parameters determined using the two methods.

Table 4.1 Summary of adsorption isotherm parameters

	Langmuir Isotherm Constants			Freundlich Isotherm Constants	
Catalyst type	Q_o, mg/g	K_{ads}, L/mg	R_L	K_f	1/n
TiO$_2$ Non-linear	24.25±0.78	0.12±0.01	0.28	3.33±0.25	0.58±0.03
TiO$_2$-G Non-linear	28.28±3.89	0.07±0.02	0.39	2.35±0.26	0.66±0.05

From the summary of parameters in Table 4.1, it can be observed that all the 1/n values for the Freundlich isotherms are less than unity. This is indicative that adsorption of Zn^{2+} on TiO$_2$ and TiO$_2$-G is a chemisorption process characterized by strong bonds which are not easily reversible. (Yang, et al., 2007) showed from adsorption/desorption experiments that the adsorption of Zn^{2+} on TiO$_2$ was an irreversible process. Comparing the R_L values of TiO$_2$ and TiO$_2$-G shows that adsorption onto both catalyst materials is favourable. Due to round-off errors the linear method overestimated the isotherm parameters as compared to the non-linear method.

4.3 The Effect of Initial Metal Ion Concentration

Effect of initial metal ion concentration (10-60 ppm) was investigated keeping pH constant at 7.1±0.1 and catalyst loading of TiO_2 as 2 g/L. From Figure 4.16, it can be observed that the percentage Zn^{2+} removed decreased with increasing initial metal ion concentration. This is due to the decrease in specific surface area available for adsorption as the Zn^{2+} concentration increases.

More ions are available for the same surface area and hence there may be a saturation on the surface of the TiO_2, hence the decrease in the amount that can be removed from solution. Similar trends were observed by other authors (Chandan, 2013).The maximum adsorption capacity on TiO_2 from the experiments done with varying initial Zn^{2+} concentration was found out to be 10.62 ± 0.37 mg/g as seen in Figure 4.17.
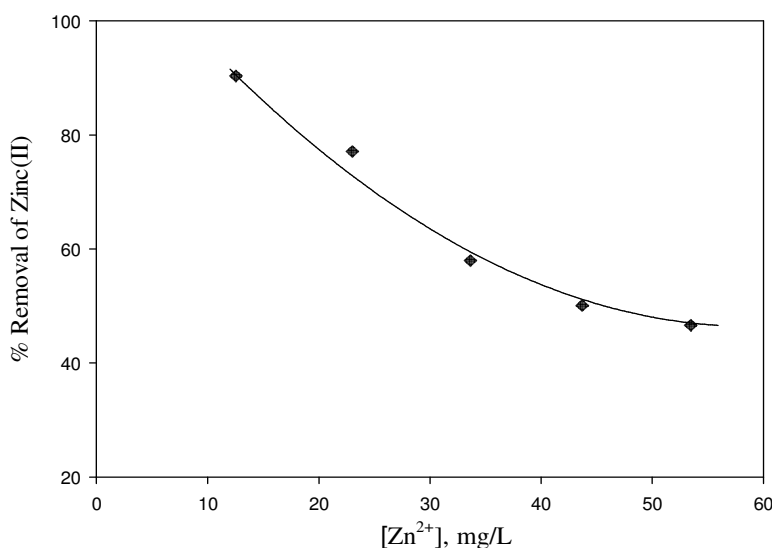
Figure 4.16 Effect of Initial Zn^{2+} concentration on Zn $^{2+}$ removal on TiO_2.

[Experimental conditions: pH = 7, V_r = 50 ml each C_{cat} = 2g/L, 0.01M Tris buffer]
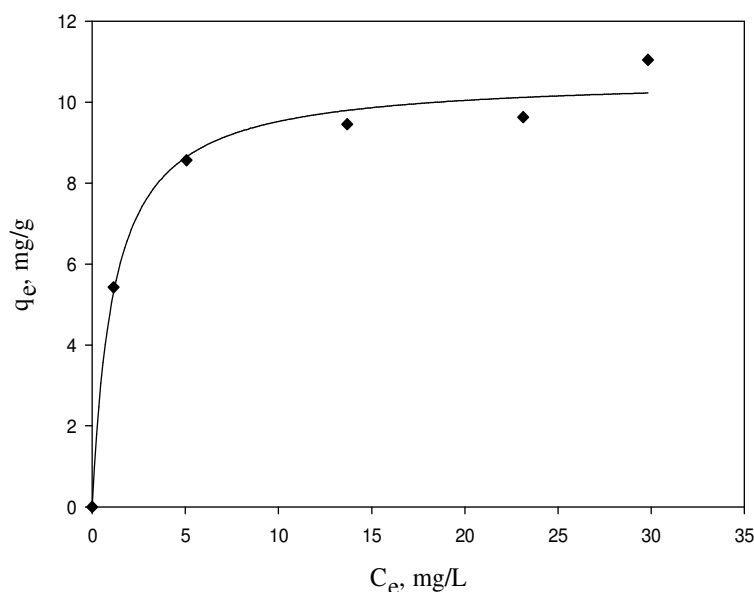
Figure 4.17 Effect of initial Zn^{2+} concentration on adsorption capacity of TiO$_2$

[Experimental conditions: pH = 7, V$_r$ = 50 ml each C$_m$ = 2g/L, 0.01M Tris buffer]

4.4 Adsorption kinetics Zn^{2+}on TiO$_2$ and TiO$_2$-G

As part of assessing the adsorption efficiency of an adsorbent, the need to evaluate the kinetic performance, which provides information on the adsorption residence time and solute uptake rate is imperative. Adsorption kinetics also offers insight into the adsorption mechanism of the system. Over the years, a number of kinetic-based models have been reported and employed to describe adsorption of various pollutants. These models are either based on solution concentration or the adsorption capacity of the adsorbent (Ho and Mackay, 1998b).

Generally, two types of adsorption capacity based kinetic models have been used to describe adsorption data. These are adsorption diffusion models and adsorption reaction models. However, the reaction models have been more widely used to describe

adsorption kinetic process. These include the Lagergren (1898) pseudo first-order rate equation, the pseudo second-order rate equation (Ho, 1995; Sheela, et al., 2012), Elovich's equation (adsorption of gases onto solid) and the second-order rate equation (Ho, 2006).

Figure 4.18 shows that the adsorption of Zn^{2+} onto TiO_2 and TiO_2-G is a very rapid process, occurring within a few minutes of the addition of the catalysts. The adsorption equilibrium time is relatively short. After 25 min of dark (in absence of light) reaction time, there is no significant change in the concentration of Zn^{2+} removed. Other studies involving other carbon and non-carbon based adsorbents recorded adsorption/desorption equilibrium times between 3 to 4 hours at 25 mg/L Zn^{2+} initial concentration and 10 g/L adsorbent dose (Bhattacharya, et al., 2006). Also, increasing the catalyst loading for TiO_2 from 1.6 to 2 g/L increased the adsorption capacity. Previous experiments showed that the optimum catalyst loading is 2 g/L for TiO_2. Therefore comparing the kinetics for TiO_2 and TiO_2-G shows that at 30 min equilibration time, the maximum adsorption capacity was 7.55 ± 0.16 mg/g for TiO_2 and 8.17 ± 0.025 mg/g for TiO_2-G.
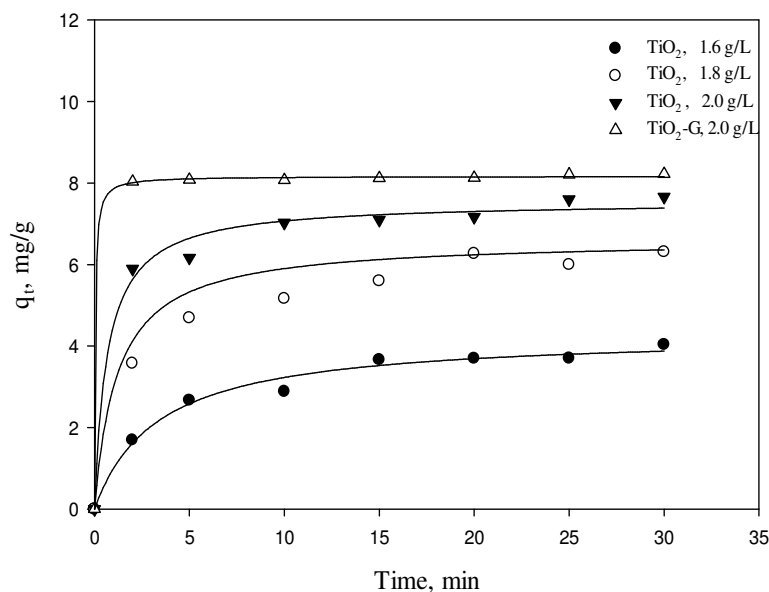
Figure 4.18 Equilibrium adsorption of Zn^{2+} in the absence of organic buffer

[Experimental conditions: $C_0 = 22.7$ mg/L, pH = 7, $V_r = 50$ ml each, 250 ppm FA]

4.4.1 The Lagergren Pseudo-first-order rate

This is a kinetic model that describes liquid-solid phase adsorption rate based on the adsorption capacity of the adsorbent. The equation is as follows:

$$\frac{dq_t}{dt} = k_1(q_e - q_t) \tag{4-15}$$

Where k_1 (min^{-1}) is the pseudo first-order rate constant for adsorption. Applying the boundary conditions of $q_t = 0$ at $t = 0$ and $q_t = q_t$ at $t = t$, and integrating and then rearranging,

$$\ln(q_e - q_t) = \ln q_e - k_1 t \tag{4-16}$$
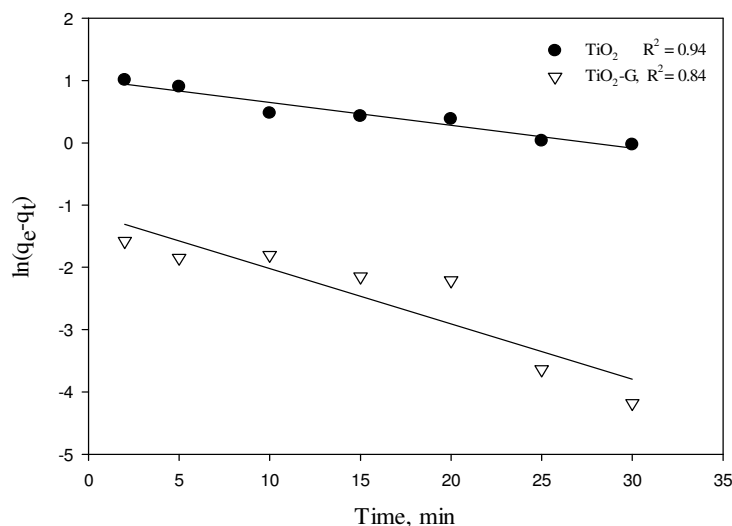
Figure 4.19 Largergren's pseudo first-order model

[Experimental conditions: $C_0 = 20 \pm 0.2$ mg/L, pH = 7, $V_r = 200$ ml, 0.01M Tris buffer]

k_1 is then determined from the slope of the plot of t vs ln (q_e-q_t) as shown in Figure 4.19. From this graph k_1 was calculated as 0.04 min^{-1} for TiO_2 as adsorbent with an R^2 of 0.94 and 0.09 min^{-1} with R^2 of 0.84 for TiO_2-G as adsorbent.

4.4.2 Ho's Pseudo- second-order rate

The Pseudo second-order rate, which has been applied to describe the adsorption of other divalent metal ions onto several adsorbents (Ho, 2006) is derived from integrating equation 14-17 with applicable boundary conditions as shown before. Rearranging the resulting equation gives equation 14-18.

$$\frac{dq_t}{dt} = k_2(q_e - q_t)^2 \tag{4-17}$$

$$\frac{t}{q_t} = \frac{1}{k_2 q_e^2} + \frac{t}{q_e} \tag{4-18}$$

Where k_2 (g/ mg.min) is the pseudo second- order rate constant of adsorption.

The value of k_2 is determined from Figure 4.20 as 0.16 g/mg. min for the adsorption of Zn^{2+} on TiO_2 and 1.33 g/ mg. min for TiO_2-G. From the trends it can be observed that the adsorption of Zn^{2+} onto TiO_2 fits to the pseudo-second order model quite well because the R^2 value is 0.99 as compared to the pseudo-first-order where the R^2 is 0.94 for TiO_2 and 1.00 as compared to 0.84 for TiO_2-G. This is because the pseudo-second order model assumes that chemisorption which involves electron exchange between Zn^{2+} and catalysts and may involve more than one reaction step. Zinc as a divalent metal ion requires two sites on the surface of the adsorbent. Therefore, since q_t represents the active sites already occupied, then the rate at which the active sites is being occupied by Zn^{2+}, $\left(\frac{dq_t}{dt}\right)$ will follow the pseudo-second-order reaction model (Ho and Mackay, 1998b). This trend conforms clearly with adsorption of Zn^{2+} as well as other divalent metal ions onto other materials (Wang, et al., 2013).
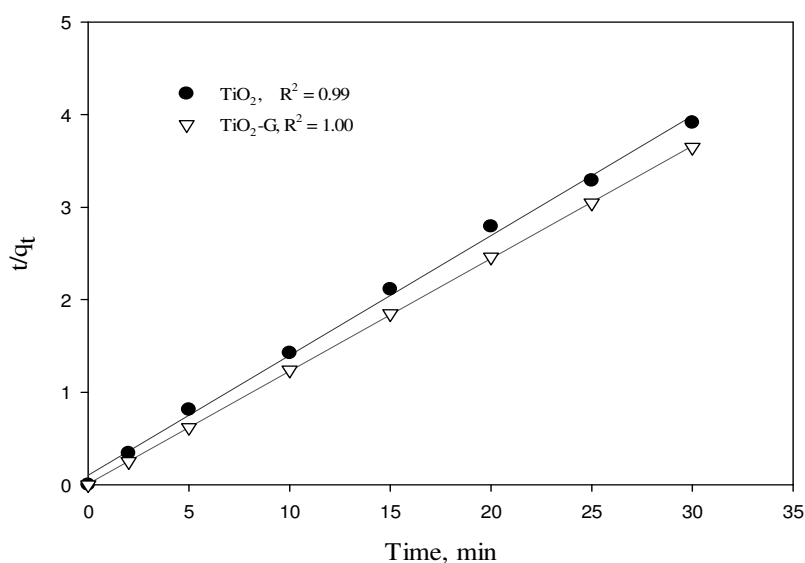
Figure 4.20 Pseudo second-order rate model

[Experimental conditions: $C_0 = 20\pm 0.2$ mg/L, pH = 7, $V_r = 200$ ml, 0.01M Tris buffer]

4.5 Solar Photocatalytic Reduction of Zn^{2+} using TiO_2 and TiO_2-G

4.5.1 Introduction

In the previous section, the adsorption of Zn^{2+} and the effect of various parameters (catalyst amount, pH, initial metal ion concentration and catalyst type) on the adsorption of Zn^{2+} were reported. This section looks into the kinetics and mechanism of the reduction of the adsorbed Zn^{2+} by photocatalysis in the presence of formic acid as the hole scavenger, as well as assessing the efficiency of TiO_2-G composite catalyst compared to TiO_2 only. Optimum reaction conditions and kinetic parameters are determined for TiO_2 and TiO_2-G catalyst under similar conditions in order to enable effective comparison.

In the presence of pure TiO_2, Kabra (2007) established the fact that Zn^{2+} photo-reduction was not significant under solar light primarily because of the wide band-gap and the absence of anoxic conditions. In addition to this, the photo-reduction by TiO_2 is generally considered thermodynamically not favourable due to the position of the standard reduction potential. That is, Zn^{2+} is more positive than TiO_2, hence thermodynamically there exists low driving force for the reaction to occur unaided. However, the introduction of a suitable hole scavenger (such as formic acid) decreases the electron-hole recombination. This has been observed to increase the photo-reduction rate of such metal ions (Chenthamarakshan, et al., 2000; Ming, 2002a; Nguyen, 2006; Tan, et al., 2003).

In addition, modification of the catalyst is considered vital to reducing the band-gap of pure TiO_2 as well as the improvement in catalyst activity under solar visible light conditions. This catalyst enhancement falls in two categories: augmenting the band-gap by modifying the electronic properties (band-gap engineering). Band-gap reduction is achieved by techniques such as the introduction of transition metal, noble metal and non-metal dopants. However, due to the cost involved when considering large scale applications, these methods tend to become inefficient (Chong, et al., 2010a; Fujishima, et al., 2008) Secondly, Photo-sensitisation by the introduction of dyes is another useful technique (Chowdhury, et al., 2013). Because of the time sensitive nature of combined sewer overflows the need for fast reactions rates for high rate treatment of target species is more preferable.

The main focus of this work is to explore the effectiveness of the modified catalyst in terms of activity under solar and visible light regions of the electromagnetic spectrum for the photo-reduction of a thermodynamically less favored reaction as well as high rate treatment for a CSO abundant metal ion, Zn^{2+} and the associated reaction mechanisms involved.

So far, the use of graphene modified TiO_2 has not been explored for the photo reduction of Zn^{2+} from aqueous solution to the best of our knowledge, and hence the focus of this current research.

4.5.2   Effect of initial catalyst loading on photo-reduction of Zn^{2+}

As the catalyst used in this batch reaction system is in suspension, the catalyst amount should be chosen such that it does not contribute to the turbidity of the system. Though it has been shown that efficiency of photo-reduction process is linearly proportional to the quantity of catalyst present particularly at low catalyst loading, a turbid system may lead to particle agglomeration and light screening effect which in turn reduces the active surface area of TiO_2 that is exposed to the light being irradiated (Bamba, et al., 2008; Chen, et al., 2007).   This can then negatively affect the apparent reaction rate even though the presence of more catalyst particles will translate into the availability of more active sites.   Increasing the catalyst dosage above the threshold value is therefore detrimental to the overall reaction rate due to particle agglomeration (which leads to internal mass transfer resistance) and light shielding effect (Chen and Ray, 1998a). For this reason, it is important to determine the optimum catalyst dosage which is able to absorb the photons available to give the most effective and efficient pollutant removal in terms of catalyst material required. The optimum catalyst dosage is a function of the concentration of metal ion present, the reactor geometry, light intensity as well as the properties of the semiconductor particles in use. In literature, optimum catalyst dosage ranged from 0.5-2 g/L for TiO_2 (Athapaththu, 2013b; Kabra, et al., 2008).

In this study, the catalyst concentration was varied from 0.5 g/L to 6 g/L and the equilibrium concentration of Zn^{2+} was measured in the presence of formic acid. The hole scavenger is useful to prevent electron hole recombination during the photo-reduction

process. The optimum catalyst loading for adsorption was determined as shown in figure 4.21 after 30 minutes of equilibration time.
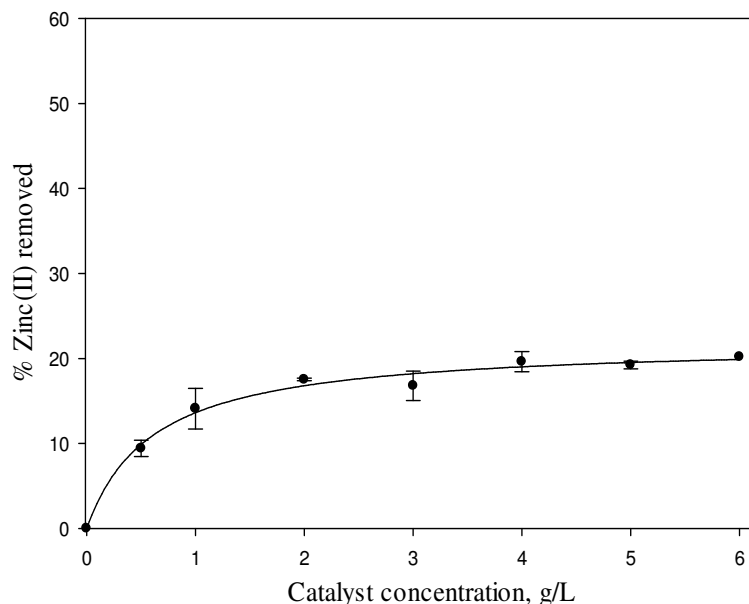
Figure 4.21 Effect of Catalyst loading in the presence of Formic acid

[Experimental conditions: C_0 = 22 mg/L, pH = 7, V_r = 50 ml each, 250 ppm FA]

It was observed from the above experiment that a catalyst loading in excess of 2 g/L yielded no significant increase in the percentage Zn^{2+} removed. For instance increasing the catalyst loading, three times showed only a 12% increase in the removal of Zn^{2+} by adsorption. After ensuring that the adsorption equilibrium had been reached, the light was turned on to measure photocatalytic reduction of Zn^{2+} for each catalyst concentration and samples collected at regular intervals.
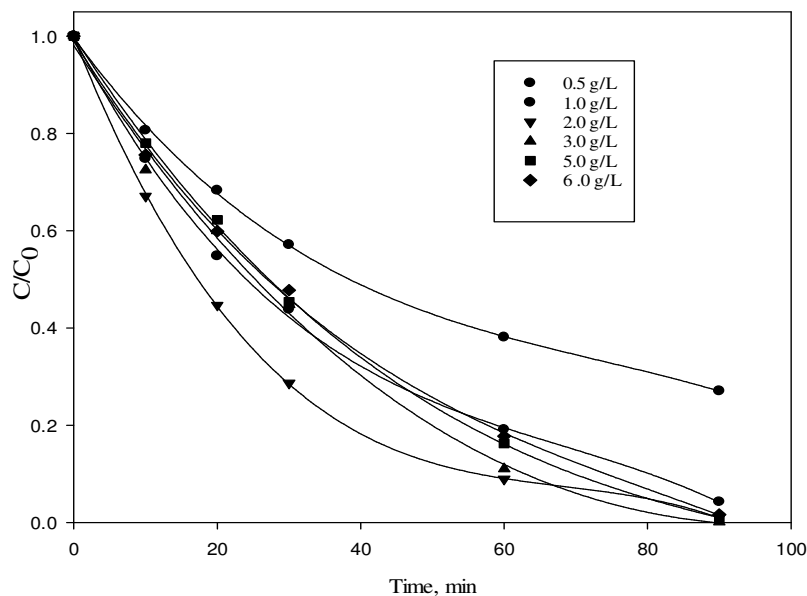
Figure 4.22 Effect of TiO$_2$ concentration on the photoreduction of Zn^{2+}

[Experimental conditions: C$_0$ = 21± 1 mg/L, pH = 7.1±0.1, V$_r$ = 150 ml each, 250 ppm

FA, I = 100 mW/cm^2 N$_2$ saturated].

This experiment reports the effect of catalyst loading on Zn^{2+} photo-reduction. Figure 4.22 shows the kinetics of various catalyst loadings. There is an increase in the removal of Zn^{2+} with time up to 2 g/L of catalyst loading. Beyond this point any additional increase in TiO$_2$ concentration does not improve the rate of Zn^{2+} removal. Table 4.2 clearly shows that the photo-reduction reaction follows a pseudo first-order kinetic pattern with respect to initial catalyst loading when reaction rate constants are compared. The reaction rate constant increases until a threshold value of 2 g/L after which reaction rate constant does not change significantly as shown in Table 4.2 .

Table 4.2 Pseudo first-order rate constants for different catalyst concentrations

[TiO$_2$] (g/L)	k$_{app}$ min^{-1}	(R^2)
0.5	0.016	0.99
1.0	0.027	1.00
2.0	0.038	0.99
3.0	0.037	0.97
4.0	0.031	0.97
5.0	0.031	0.99

[Experimental conditions: C$_0$ = 21± 1 mg/L, pH = 7.1±0.1, V$_r$ = 150 ml each, 250 ppm

FA, I = 100 mW/cm^2 N$_2$ saturated]

Furthermore, when the effect of the variation of the initial catalyst concentration was determined for the initial reaction rate, it was observed from Figure 4.23 that the rate increases with increasing concentration until 2 g/L. Above this concentration, the initial rate of the reaction is observed to be independent of the TiO$_2$ concentration. This Photocatalytic reaction is observed to follow a Langmuir-Hinshelwood type reaction mechanism with respect of catalyst loading. This has been observed by other researchers (Athapaththu, 2013; Chowdhury, 2012).

As TiO$_2$ concentration is increased, the solution becomes turbid. Turbidity which is referred to as the insoluble particulates that are present in water is very unfavorable for the photocatalysis process. The particles obstruct and impede the penetration of light by

scattering and absorbing some of the rays. They also shield some of the target pollutants limiting the amount of light that is able to penetrate. This phenomenon is known as the shielding effect (Zhou, 2001). Also, some researchers have reported that high TiO_2 concentration leads to agglomeration which in turn reduces the total number active sites on the surface available for adsorption   and   there after photo-reduction of pollutant.(Chen and Ray, 1998a). This is the reason for the lack of increase in initial reaction rate with the increase in catalyst loading as observed in this study. Therefore, the rate of degradation per unit mass r_1 is seen to decline steadily with the increase in the initial TiO_2 concentration as seen if figure 4.23.
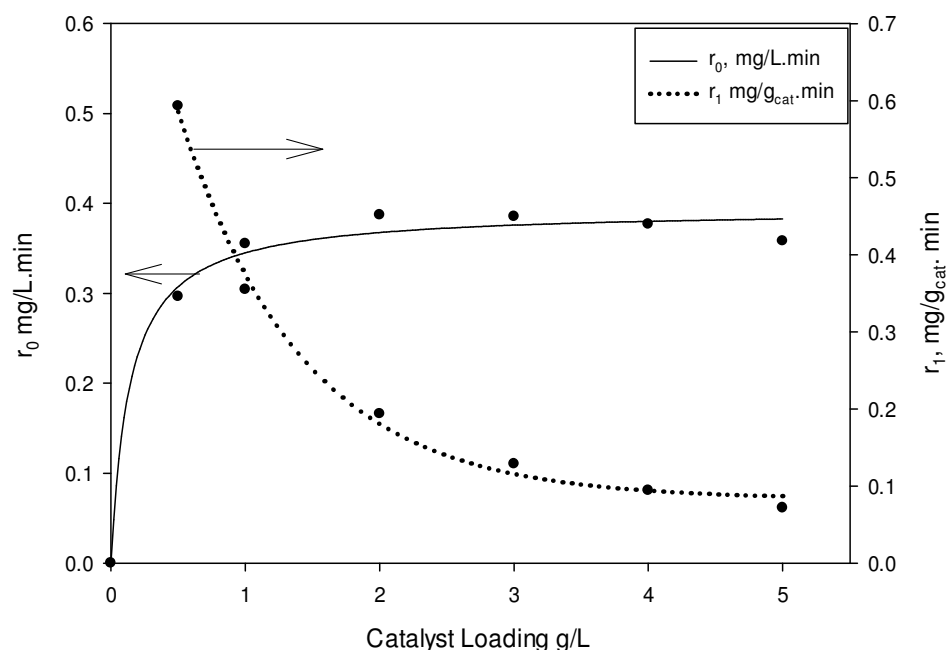
Figure 4.23 Effect of catalyst dosage on the photo-degradation rate

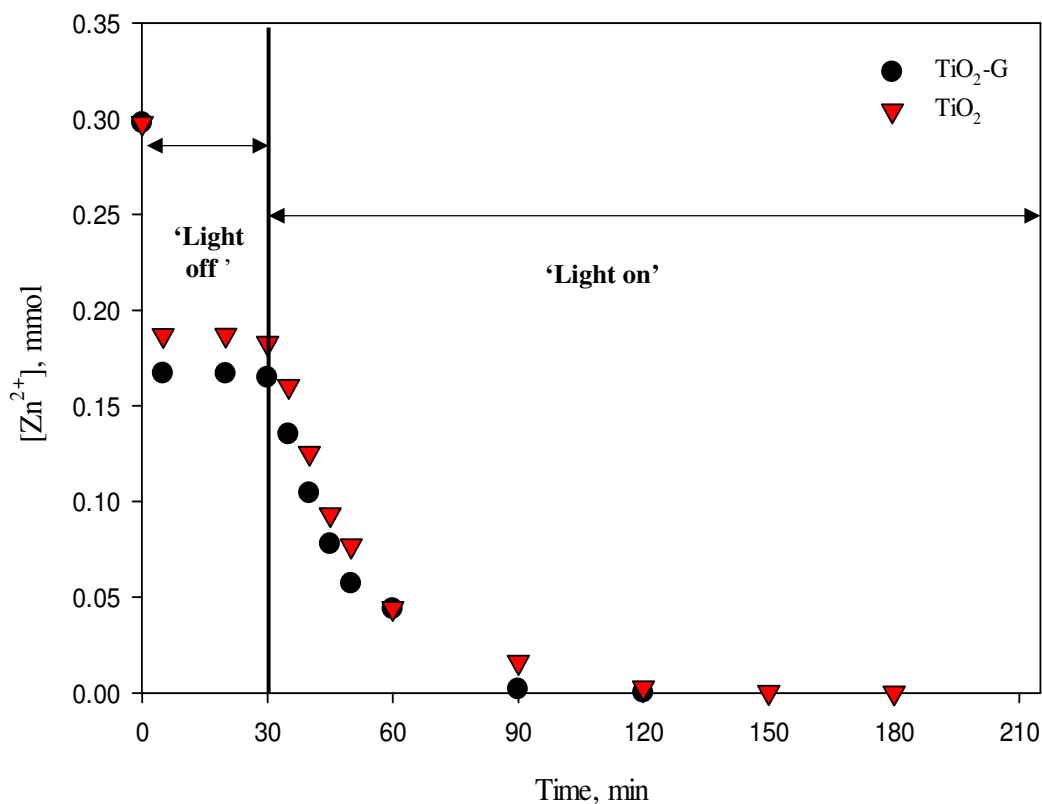[$C_0 = 21\pm 1$ mg/L, pH = 7.1$\pm$0.1, V_r = 150 ml each, 250 ppm FA, I = 100 mW/cm^2

N_2 saturated].

Generally in waste water, suspended solids contribute to the turbidity of the system and this may eventually decrease the efficiency of the photocatalytic process. Therefore, to ensure good efficiency it has been reported that turbidity should be below 5 nephalometric turbidity units (NTU) (Chong, et al., 2010a). Hence, catalyst concentration should be chosen such that it does not impede the reaction. For this reason, 2 g/L TiO_2 was chosen as the optimum catalyst loading for this study. All other experiments were conducted using this concentration unless otherwise stated. In this study, it was also observed that after the photo-reduction a color change from white to gray occurred as reported by others (Chenthamarakshan, et al., 2000).

Photo-reduction profile for TiO_2 and TiO_2-G

The photo-reduction profiles for each catalyst type are shown in Figure 4.24 for catalyst loading of 2 g/L. The first 30 minutes represents the dark reaction time (adsorption only). After this when adsorption equilibrium has reached the light was turned on to measure photo-reduction rate only. A steady reduction in the Zn^{2+} concentration was observed. At this catalyst concentration, the reaction time for complete reduction was determined as 90 min and 60 min using TiO_2 and TiO_2-G respectively.

Figure 4.24 Photo-reduction reaction time for the reduction of Zn^{2+} using TiO_2 and

TiO_2-G.

[Experimental conditions: C_0 = 20 mg/L, pH = 7.1±0.1, V_r = 200 ml each, 250 ppm FA

C_{cat} = 2 g/L, I = 100 mW/cm^2, N_2 saturated].

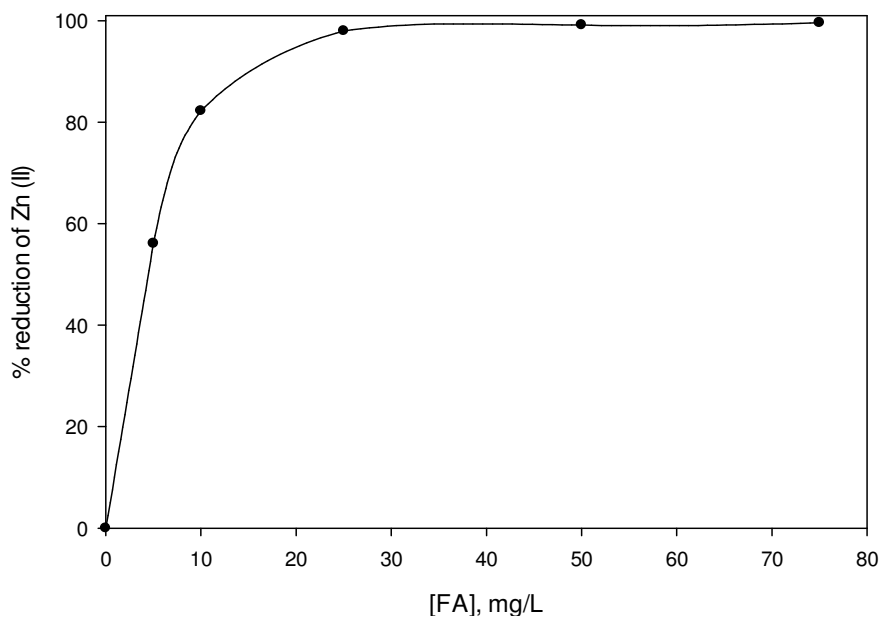### 4.5.3 Effect of formic acid concentration

For photo-reduction of metal ions, it is important that some organic compound is added

to remove the hydroxyl radicals, otherwise oxidation-reduction slows down or stops. In

addition to this, the reaction should be studied in absence of oxygen otherwise oxygen

competes with metal ions for the electrons. Of all the organics, it is best to add formic

acid as after reaction, it is easy to remove formic acid as it breaks down to CO_2 and H_2O only with no other intermediate formation. It is also reported in literature that during the photocatalytic reduction of Zn^{2+} using UV illumination with TiO_2 the addition of formate ions brings about a large enhancement in the rate of reduction of Zn^{2+} in a pH medium of 7 (Chenthamarakshan and Rajeshwar, 2000a). Also, Ming (2002) determined that sodium formate out performed some other organic compounds such as isopronanol, ethanol, methanol t-butanol and sodium oxalate in the photoreduction of other metals such as Mn^{2+} (- 1.18 V) and Cd^{2+} (- 0.40 V). This was because formic acid is more easily oxidized by photo generated holes. For these reasons formic acid was chosen as the hole scavenger for this study.

This particular study was important because it offered a unique advantage in assessing the performance of the system in the presence of excess amount of organic compounds in our system. This is because wastewater is filled with an innumerable number of dissolved organic compounds in various proportions and concentrations. In this study, formic acid concentration was varied from 50-750 ppm to obtain the optimum concentration required at which the overall reaction is not limited to the presence of organic for the photo reduction of the pollutant species and the results are shown in the Figure 4.25 below.

Increasing the FA concentration increases the initial amount of Zn^{2+} that is adsorbed during the dark reaction. During the photo-reduction reaction, increasing the initial FA concentration results in an increase in the % Zn^{2+} removed within 60 minutes. At 250 ppm of FA, 98% of initial Zn^{2+} concentration was photo-reduced. At this point,

increasing the FA concentration further does not increase the removal since the reaction was almost complete.

Figure 4.25 Effect of formic Acid concentration on the removal of Zn^{2+}

[Experimental conditions: C_0 = 19.8 ± 1 mg/L, pH = 7.1±0.1, V_r = 150 ml each, C_{cat} = 2 g/L, I = 100 mW/cm^2 N$_2$ saturated]

Figure 4.26 shows the effect of initial concentration of FA on the initial reaction rate. It was observed that the trend follows a Langmuir-Hinshelwood type kinetics, where a saturation trend is seen beyond that obtained at 250 ppm. Therefore, 250 ppm was chosen as the optimum organic content. This corresponds to approximately 65 ppm Carbon.
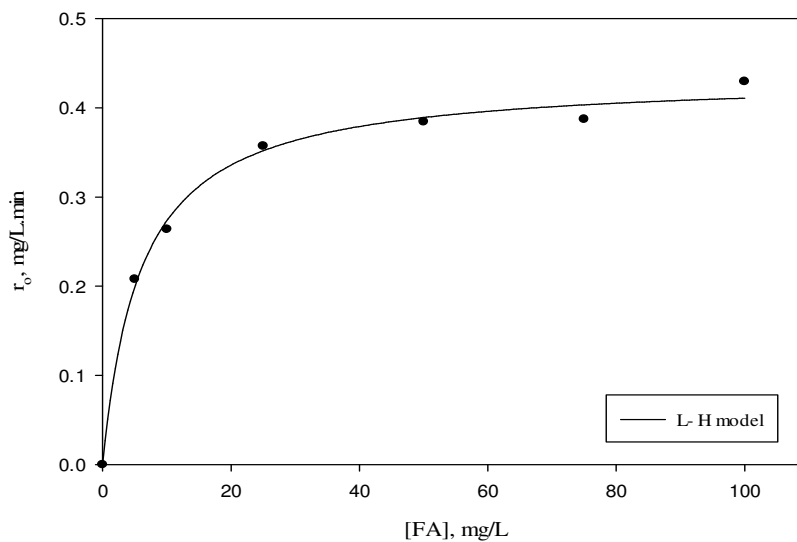
Figure 4.26 Effect of Formic acid concentration on the initial rate of Zn^{2+} photo-

reduction

[Experimental conditions: $C_0 = 19.8 \pm 1$ mg/L, pH = 7.1±0.1, $V_r = 150$ ml each, $C_m = 2g/L$, I = 100 mW/cm^2]

4.5.4 Effect of initial pH on photo-reduction of Zn^{2+}

As photo-degradation takes place on the surface of the semiconductor catalyst, pH is shown to contribute significantly to the performance of heterogeneous photocatalysis in aqueous systems. In that, it affects the charge on the surface of the catalyst particles, and the positions of the valence and conduction bands of the catalyst as mentioned in previous sections (Moreno-Barbosa, et al., 2013; Chen and Ray, 1998a).

The surface charge density is affected by pH according to the equations;

$$pH < PZC : \textbf{TiOH} + \textbf{H}^+ \leftrightarrow \textbf{TiOH}_2^+$$

$$pH > PZC: \textbf{TiOH} + \textbf{OH}^- \leftrightarrow \textbf{TiO}^- + \textbf{H}_2\textbf{O} \text{ (Rincón and Pulgarin, 2004)}$$
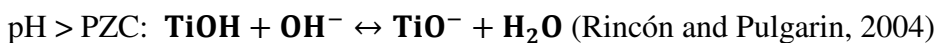
For catalyst particles, which exist in a system below this pH the net charge on the surface becomes positive, and hence attracts anionic organic compounds onto the surface for adsorption. On the other hand, when the pH is above this value, the net charge on the surface becomes negative, and hence the adsorption of cations is favored. It has also been observed that during photocatalytic reaction operating pH change occurs (Chong et al., 2010). In addition to this, it has been reported that the pH of CSOs from light rain is lower than that from storm events, and this is lower than that from dry weather flow, and hence, the need to look into the extent at which this parameter affects the system.

In this study, the pH was adjusted to the desired initial pH before the addition of the catalyst. All other experimental conditions were kept constant. The pH was varied from 4 to 7. The results are shown in Figure 4.27. As the pH changes from acidic to neutral, the % Zn^{2+} removal is also increased due to the favourable adsorption of the cation. It can be observed that as the pH value changed from 4 to 7, a remarkable increase in the apparent initial reaction rate occurs, as shown in Table 4.3.

Also, because the position of the valence and conduction band edges are influenced by the solution pH, neutral to slightly alkaline pH also increases the conduction band edge of TiO_2, which provides more thermodynamic driving force for the reaction to occur. It can

also be explained that, acidic pH decreases the ionization of the hole scavenger (formic acid) and hence reduced the amount of formic acid adsorbed onto the surface of the TiO_2 and this lowers the efficiency of the system. In addition, the availability of more hydroxyl ions (OH^-) leads to the effective scavenging of photo generated holes by forming hydroxyl free radicals (HO^*) which is beneficial to the reaction (Athapaththu, 2013b).

Table 4.3 Effect of pH on the reaction rate constant.

Initial pH	Final pH	k_{app}, min^{-1}
4.10	5.90	0.001
5.10	6.70	0.012
6.30	7.50	0.031
7.20	7.90	0.065

[Experimental conditions: C_0 = 21.0 mg/L, V_r = 150 ml each, C_{cat} = 2 g/L, 250 ppm FA, I = 100 mW/cm^2, N_2 saturated]

It is, therefore, concluded from the experimental results that acidic pH values retard photocatalytic reduction of Zn^{2+}. For this reason, pH values close to neutral is the optimum for photo-degradation of Zn^{2+}. Table 4.3 shows the experimental values for the initial and final pH recorded and the observed rate constants of reduction of Zn^{2+}.
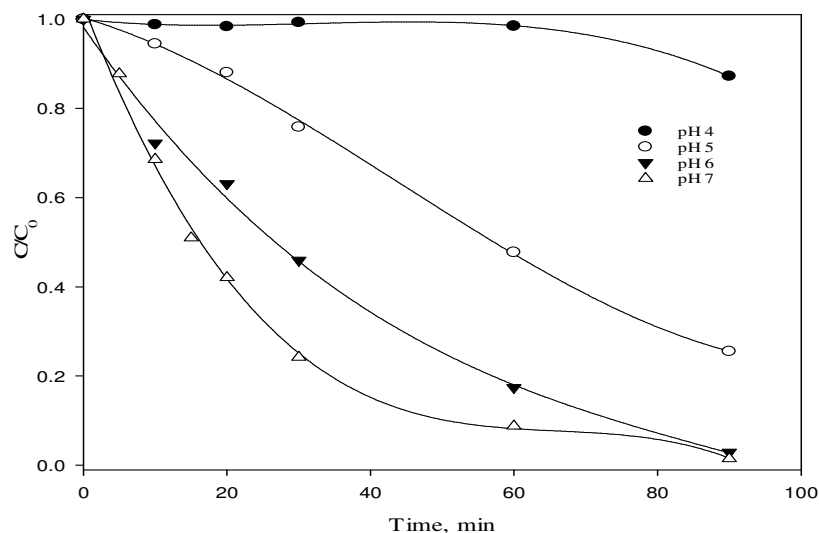
Figure 4.27 Effect of pH on the removal of Zn^{2+}

[Experimental conditions: C_0 = 21.0 mg/L, V_r = 150 ml each, C_{cat}= 2g/L, 250 ppm FA,

I = 100 mW/cm^2, N_2 saturated]

4.5.5 Effect of initial metal ion concentration

In this study, the rate of photo-reduction of Zn^{2+} was studied at various initial metal ion concentration. This is because wastewater at every instantaneous point contains varying amount of pollutant in concentration. It is, therefore, necessary to assess the effect of the concentration available for treatment.

This study was done by varying the initial Zn^{2+} concentration between 10 and 50 ppm as shown in Figure 4.28. After 90 minutes of reaction time, 98.7%, 94.1%, 70.8%, 56.6% of the initial concentration of 10, 20, 28, 38, 50 ppm was removed respectively. Therefore, at higher initial concentration the time required for complete degradation also increases.
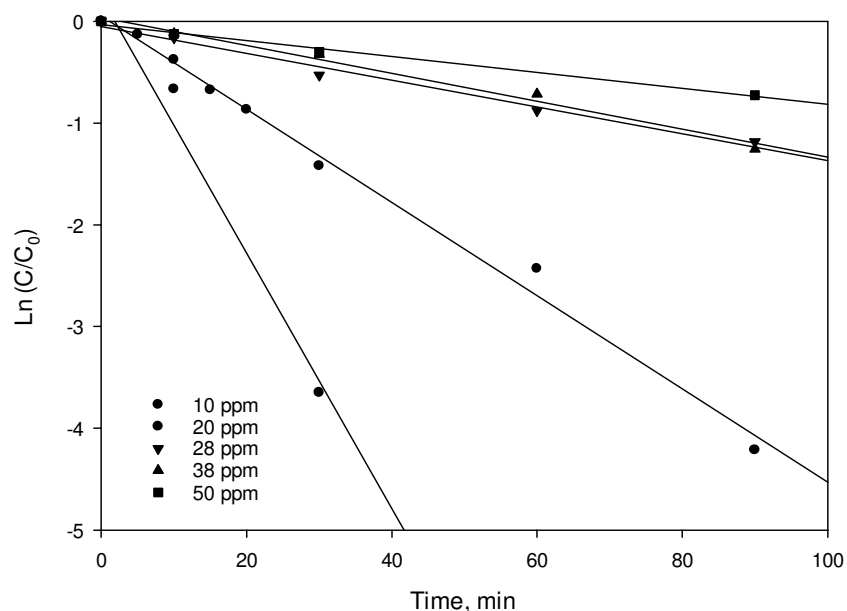
Figure 4.28 Effect of initial metal ion concentration on the reaction rate constant

[Experimental conditions: V_r = 150 ml each, pH = 7.1 ± 0.1 C_m = 2g/L, 250 ppm FA,

$I = 100$ mW/cm^2]

This result could be explained by the fact that as initial Zn^{2+} concentration increases, the active sites on the surface of the catalyst become saturated. However, since the catalyst concentration remains the same, the instantaneous availability of conduction band electrons remain the same. Therefore, more ions would remain in solution at the specified time as compared to a system with fewer Zn^{2+} ions.

According to the results of this experiment, it is evident in Figure 4.28 that within the chosen range, the reaction follows a pseudo-first-order reaction model with respect to each initial metal ion studied. By this, the experimental data can be correlated with great precision using equation 4-19 which has a linearized version as 4-20 (Zhou, 2001).

$$C = C_0 \exp(-k_{app}t) \tag{4-19}$$

$$\ln\left(\frac{C}{C_0}\right) = k_{app}t \tag{4-20}$$

Where k_{app} (min^{-1}) is the apparent rate constant of the reaction and t is the reaction time.

Increasing the initial metal ion concentration significantly affects the photo-reduction reaction rate in that, as the concentration of ions increase, reaction rate constants decreases when other parameters were kept constant.

The initial reaction rate of heterogeneous photocatalytic reduction of heavy metals was shown to follow a Langmuir-Hinshelwood mechanism with respect to the initial metal ion concentration in Figure 4.29 as observed by others (Chowdhury, et al., 2014). This model takes into account the contribution of the initial concentration of pollutant while incorporating the role of adsorption of pollutant onto the catalyst surface as the reaction progresses. This is because the adsorption, which is an important step in the photo-reduction does contribute significantly to the rate of degradation of the pollutant. The Langmuir-Hinshelwood model is represented below;

$$\frac{dC_{Zn}}{dt} = r_0 = \frac{k_{red}K_{ads}C_0}{1+K_{ads}C_0} \tag{4- 20}$$

Where r_0 is the initial reaction rate, K_{ads} (ppm^{-1}) is the adsorption constant and k_{red} is the reaction rate constant, C_0 is the initial concentration of Zn^{2+}.

Therefore, the apparent reaction rate constant is given as;

$$k_{app} = k_{red}\ K_{ads} \tag{4-21}$$

Therefore at high Zn^{2+} concentration, $\mathbf{K_{ads}C_0 \gg 1}$. Meaning that the reaction rate is independent of the initial concentration present. The rate is maximum and can be equated to k_{red}. This describes a zero-order rate. However at low concentrations of Zn^{2+} $\mathbf{K_{ads}C_0 \ll 1}$ therefore, reaction rate is first order (Chowdhury, et al., 2014).

For the photo-reduction of Zn^{2+} the initial reaction rate is observed to increase with increase in the initial metal ion concentration while the apparent rate constant reduced with increase in initial concentration. Fitting the experimental data to the model as showed in Figure 4.29, k_{red} and K_{ads} was determined as 0.530 ± 0.012 ppm/min and 0.107 ± 0.008 ppm^{-1}. Therefore, the apparent reaction rate constant is calculated as 0.057 ± 0.008 min^{-1}.
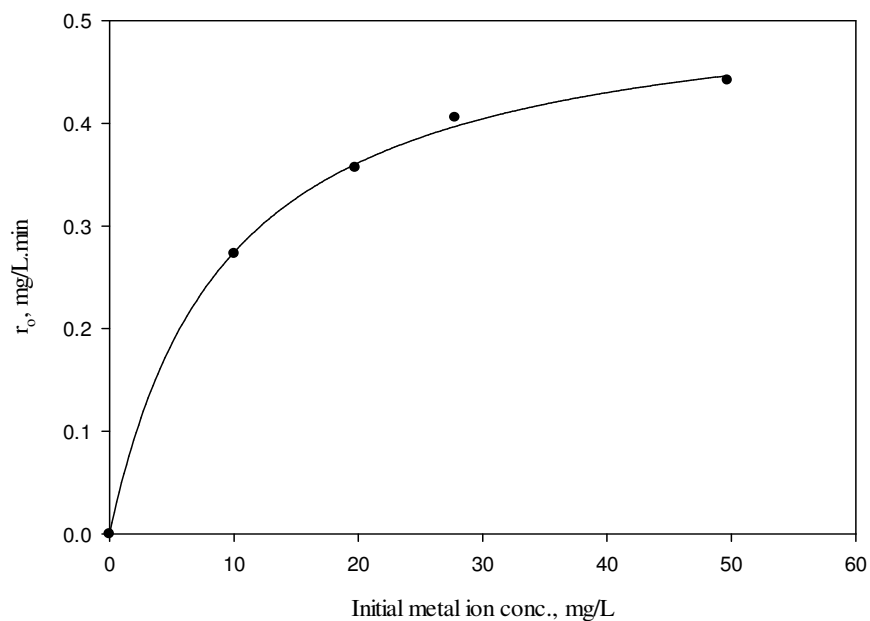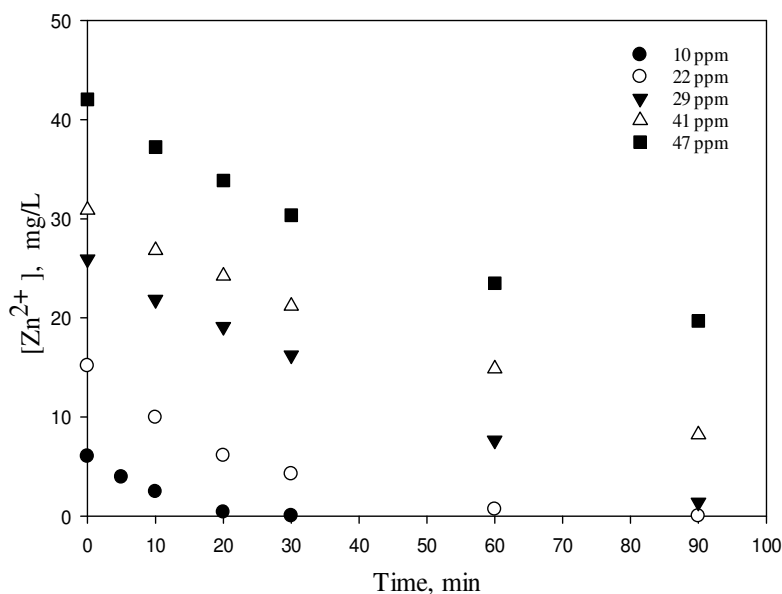

Figure 4.29 Effect of initial metal ion concentration on the initial photodegradation rate

[Experimental conditions: V_r = 150 ml each, pH = 7.1±0.1 $C_{cat\ =}$ 2 g/L, 250 ppm FA, N_2

saturated, I = 100 mW/cm^2]

4.5.6 Effect of initial metal ion concentration using TiO$_2$-G

Using similar experimental conditions as those of TiO$_2$, the influence of the initial metal

ion concentration on the removal of Zn^{2+} was investigated for TiO$_2$-G. Figure 4.30 shows

the kinetics of Zn^{2+} using TiO$_2$-G. After 60 min of reaction time, 100%, 95 %, 71 %, 52

% and 44 % was removed for the initial Zn^{2+} concentration of 10, 20, 29, 41, 47 ppm

respectively. This indicates that higher concentration would require longer time interval

for complete removal.

Figure 4.30 Effect of initial concentration metal ion concentration on the removal of

Zn^{2+} using TiO$_2$-G

[Experimental conditions: V_r = 150 ml each, pH = 7.1±0.1 C_{cat} = 2g/L, 250 ppm FA,

N_2 saturated, I= 100 mW/cm^2]

The data obtained fitted well to equation 4-19 and the slopes of the plot of time vs ln(C/C$_o$) (Figure 4.31) yields the apparent rate constants k$_{app}$ for each initial concentration. As shown in Table 4.4, the apparent rate constants decreased with increasing initial concentration of Zn^{2+}. Therefore, the photo-reduction rate of Zn^{2+} on TiO$_2$-G was found to be pseudo first-order with respect of the initial concentration.
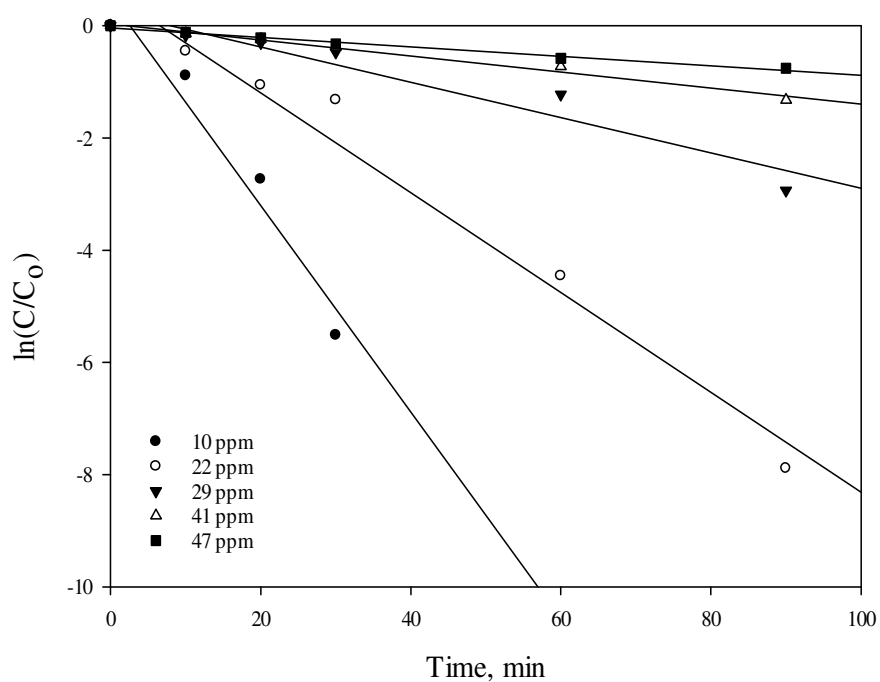
Figure 4.31 Effect of initial metal ion concentration on the rate of reduction

[Experimental conditions: V$_r$ = 150 ml each, pH = 7.1±0.1 C$_{cat}$ = 2g/L, 250 ppm FA,

N$_2$ saturated, I = 100 mW/cm^2]

Table 4.4 Effect of initial concentration on the reaction rate constant on TiO_2-G

$[Zn^{2+}]$, ppm	Reduction rate (k, min^{-1})	R^2
10.0	0.184	0.95
22.0	0.084	0.97
29.0	0.032	0.93
41.0	0.014	0.97
47.0	0.008	1.00

[Experimental conditions: V_r = 150 ml each, pH = 7.1±0.1 $C_{cat} = $ 2 g/L, 250 ppm FA, N_2
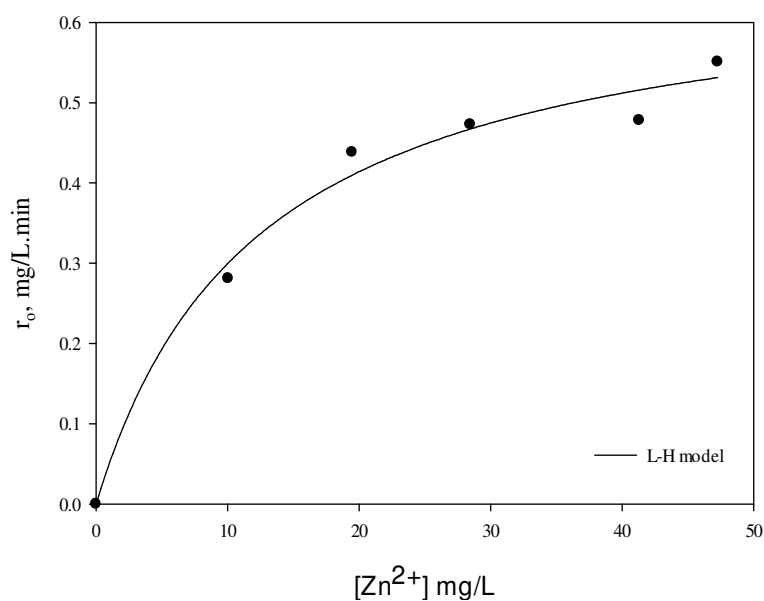
saturated, I = 100 mW/cm^2]

Figure 4.32 Effect of initial metal ion concentration on the initial photodegradation rate

[Experimental conditions: V_r = 150 ml each, pH = 7.1±0.1 $C_{cat} = $ 2 g/L, 250 ppm FA, N_2

saturated, I = 100 mW/cm^2]

Fitting the experimental data to the model as showed in Figure 4.32, k_{red} and K_{ads} was determined as 0.671 ± 0.055 ppm/min and 0.081 ± 0.021 ppm^{-1}. Therefore, the apparent reaction rate constant is calculated as 0.543 ± 0.002 min^{-1}.
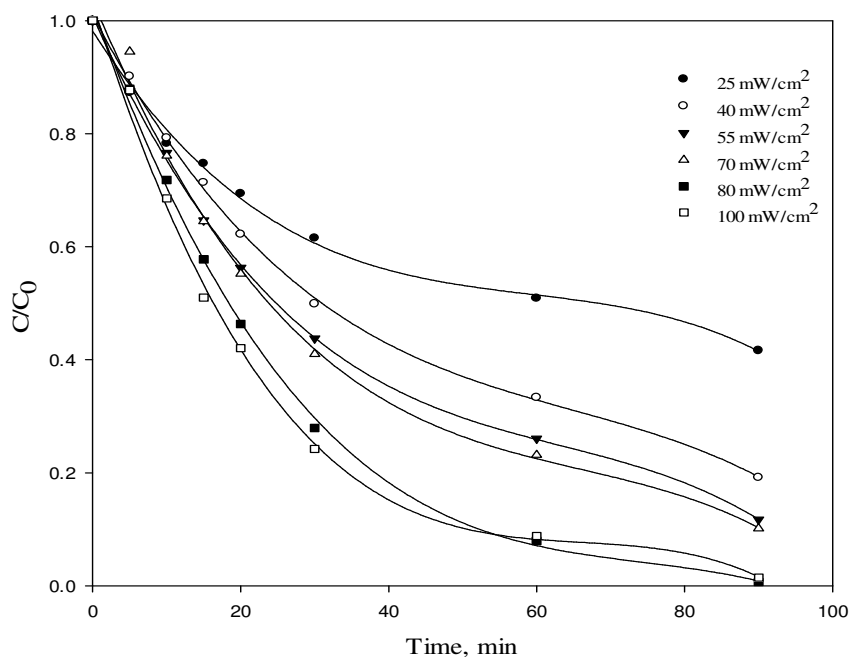
4.5.7 Effect of light intensity

Light which is the source of the photons required to activate the semiconductor by the production of electron-hole pairs, is one of the most important rate controlling parameters in the study of photocatalytic systems that needs to be evaluated (Malekshoar, et al., 2014; Zhou, 2001). In view of the fact that solar light has varying intensities with altitude and geographical location, it's worthwhile to perform a comprehensive analysis of how the light intensity influences the efficiency of the system (Chowdhury, 2012). Light intensity, however, does not exceed 1,300 W/m^2 on any part of the earth surface because according to NASA this is the average intensity that is recorded at the top part of the atmosphere in areas around the equator.

As part of the main objectives of this work, the study of the improvement of the pure TiO$_2$ to respond to longer wavelengths in the solar spectrum by compositing with graphene. A comparative study is then performed on the solar light response of TiO$_2$ to that of TiO$_2$-G composite catalyst. In this study, the solar light intensity was varied from 25-100 mW/cm^2 to determine the relationship between the light intensity, the reaction rate constant and the initial reaction rate.

The kinetics for the photo-degradation of Zn^{2+} are shown in Figure 4.33. It is evident that the increase in the intensity of light increases the removal of Zn^{2+} and the reaction rate.

This is because as the intensity of light increases the density of photons available to initiate the electron-hole pair generation also increases.

Figure 4.33 Effect of light Intensity on the photo-reduction of Zn^{2+} at pH 7

[Experimental conditions: Co = 20 ±1 mg/L V_r = 150 ml each, pH = 7.1±0.1 C_m = 2 g/L,

250 ppm FA, N_2 saturated]

As shown in Figure 4.34 and 4.35, the apparent reaction rate constant and the initial rate of reaction increases with increasing light intensity. The k_{app} was found to be related to the light intensity by a power law as follows.

$$\mathbf{k_{app} \propto I_s^{\beta}} \tag{4-21}$$

Where β is the kinetic order and I_s represents the solar light intensity (mW/cm^2). Fitting the data shown in the graph 4.34, the values of the constant obtained are $\beta = 1.4 \pm 0.1$ and α (the proportionality constant) $= 1.3 \times 10^{-4} \pm 7.2 \times 10^{-5}$.

Figure 4.35 represents the relationship between the initial reaction rate and the light intensity. As the light intensity increases there is a corresponding increase in the initial reaction rate when all other parameters remains constant. This relationship follows a Langmuir-Hinshelwood type reaction. As the light intensity increases, there is a corresponding increase in the photons available to initial electron/hole separation. Therefore, the initial light intensity and the initial metal ion concentration are characteristic parameters that determine the reaction rate. It is, therefore, evident that lower light intensities can be the limiting factor on the reaction rate. Using the optimum light intensity ensures that there is no waste of energy as excess photons are wasted as it heats in the system. 100 mW/cm^2 is obtained as the optimum light intensity and was therefore used in the entire study unless otherwise stated.
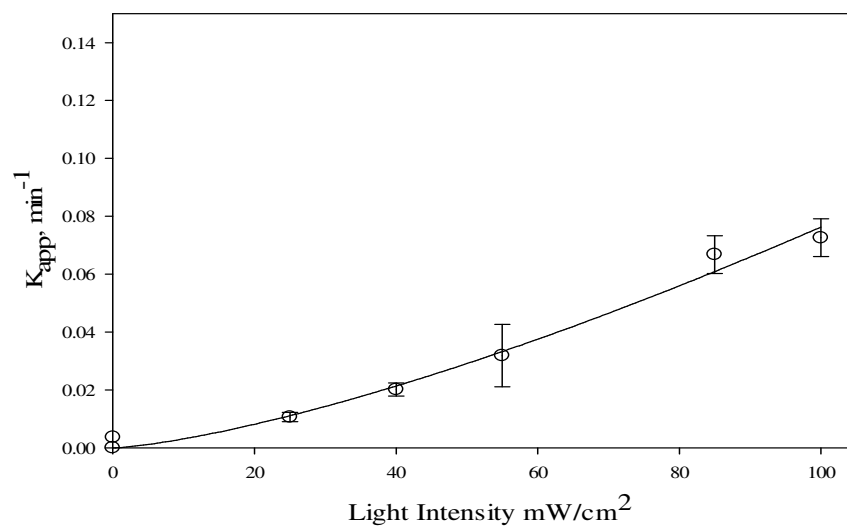
Figure 4.34 Effect of light intensity on reduction rate constant

[Experimental condition: $C_0 = 20 \pm 0.2$ mg/L, pH = 7.1±0.1, $V_r = 150$ ml each, $C_{cat} =$

2g/L, N_2 = saturated, I = 100 mW/cm^2]
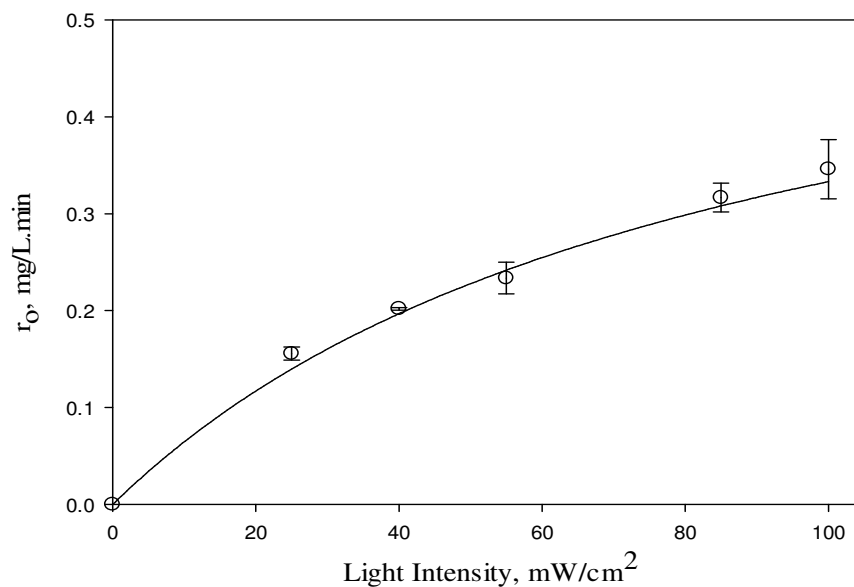
Figure 4.35 Effect of light intensity on the initial reaction rate

[Experimental condition: $C_0 = 20.0 \pm 1$ mg/L, pH = 7.1±0.1, $V_r = 150$ ml each,

$C_{cat} = 2$ g/L, N_2 = saturated, I = 100 mW/cm^2]

4.5.8 Effect of light intensity on TiO$_2$-G

Similarly, the effect of light intensity on TiO$_2$-G was studied. In this section, the light intensity was varied from 25 to100 mW/cm^2. The kinetics of Zn^{2+} photo-reduction with variation in light intensity are shown in Figure 4.36. Increasing the light intensity resulted in the increase in the removal of Zn^{2+}. After 90 min of irradiation, 55%, 70%, 84%, 100% and 100% was removed with 25, 40, 55, 70, 85 and 100 mW/cm^2 respectively. The reaction rate constants obtained from the plot of t vs ln(C/C$_o$) was obtained. The plot of the light intensity vs reaction rate constants also fitted well to the power law model. Therefore, α and β values obtained from Figure 4.37 as 1.1 x 10^{-6} ± 9.1 x 10^{-7}and 2.4 ± 0.2 respectively.
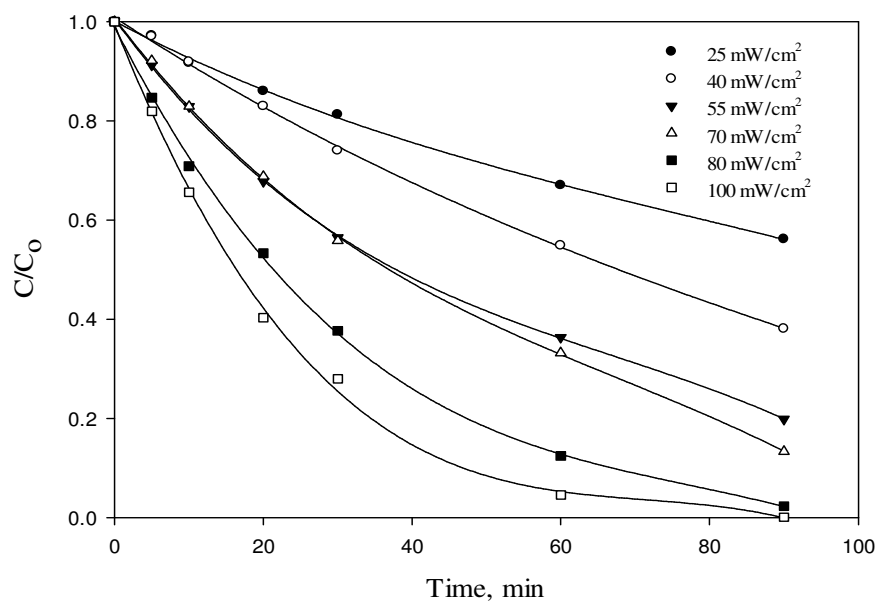
Figure 4.36 Effect light intensity on the removal of Zn (II) using TiO$_2$-G

[Experimental condition: C$_0$ = 21± 1 mg/L, pH = 7.1±0.1, V$_r$ = 150 ml each, C$_m$= 2 g/L, N$_2$ saturated, I = 100 mW/cm^2]
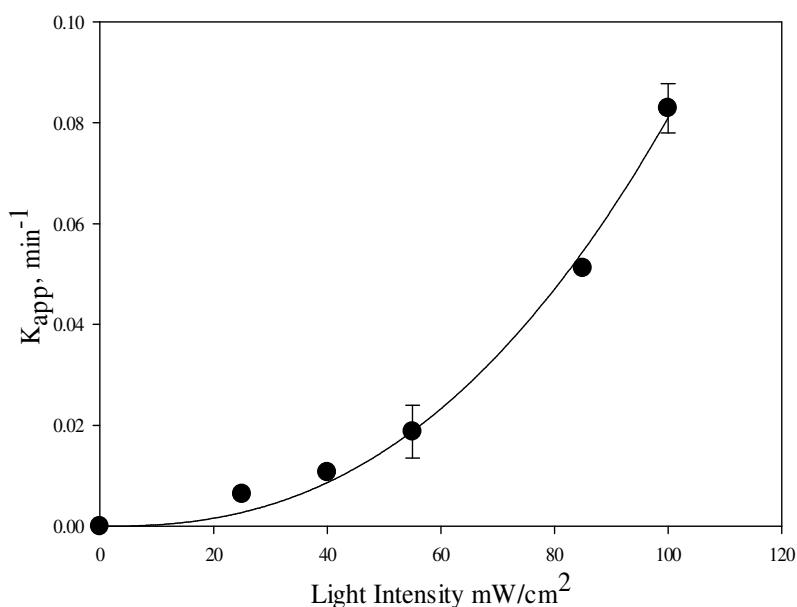
Figure 4.37 Effect of light Intensity on reaction rate on TiO$_2$-G

[Experimental condition: $C_0 = 21 \pm 1$ mg/L, pH = 7.1±0.1, $V_r = 150$ ml each, $C_m = 2$ g/L,

$I = 100$ mW/cm^2]

4.5.9   Effect of light source on reduction of Zn^{2+}

In order to evaluate the contribution of the improvement in activity of the composite

catalyst, this experiment was performed under three different light conditions using the

same light intensity of 100 mW/cm^2. The full solar spectrum (wavelength 300-650 nm),

Ultraviolet light only (wavelength 300-388 nm) and Visible light only (wavelength 420-

650 nm). The ultraviolet conditions were set in the solar simulator by placing a long pass

or visible light cut-off filter by the help of an external attachment. This removed all

wavelengths above 388 nm from the incident radiation. The visible light conditions were

obtained by placing a UV cut-off filter inside the simulator which removed wavelengths

lower than 338 nm from the incident radiation. As per the band-gap measured 3.1 eV

(Malekshoar, et al., 2014) of the TiO_2 catalyst, it can be derived from equation 2-6 that the wavelengths of 400 nm and below are sufficient to produce electron-hole pairs required for the reaction to occur.

The first set of experiments conducted using only TiO_2 as shown in Figure 4.38. It was observed that the rate of photo-reduction was 62 % higher for full solar spectrum (k_{app} = 0.067 ± 0.006 min^{-1}) than that of only UV light (k_{app} = 0.025 ± 0.007 min^{-1}) when the apparent reaction rate constants are compared. Though it was expected that the rate of degradation under both conditions will not be insignificantly different, this experiment proved otherwise. This could be as a result of the cut-off wavelength of the filter which does not permit light above 388 nm from passing through. Since this catalyst will theoretically be activated by wavelengths of up to 400 nm there is therefore a decrease in the rate of photo-reduction. When only visible light conditions were considered, the trend showed a rather slow reaction rate. This is as a result of the inability of the TiO_2 to be activated by the longer wavelengths which are above 400 nm in the visible region. The apparent reaction rate constants were determined from the slope of the graph of time vs $ln(C/C_0)$ as represented in Figure 4.39.
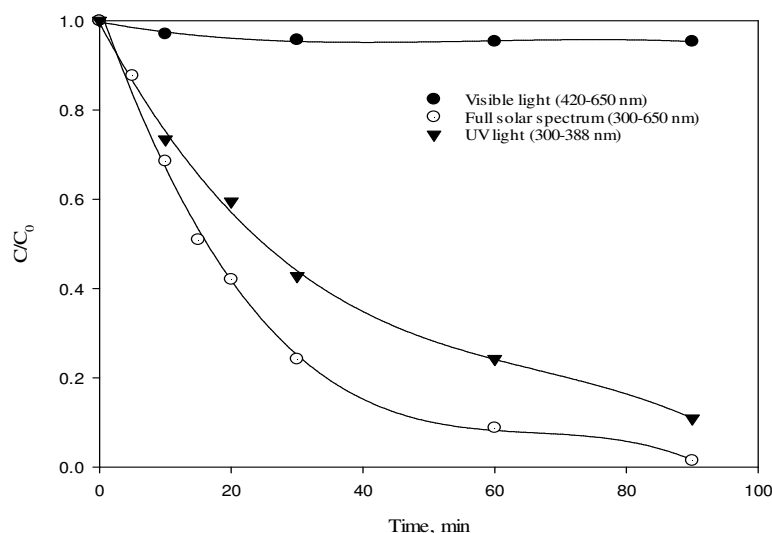
Figure 4.38 Effect of light source on the removal of Zn^{2+} using TiO$_2$

[Experimental conditions: C$_0$ = 21± 1 mg/L, pH = 7.1±0.1, V$_r$ = 150 ml each, C$_{cat}$ = 2 g/L,

N$_2$-saturated, I = 100 mW/cm^2].
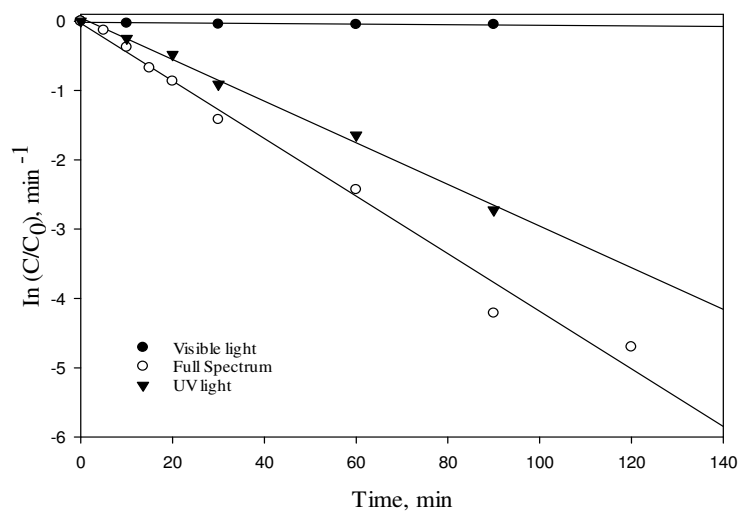
Figure 4.39 Effect of light source on the apparent reaction rate constant using TiO$_2$.

[C$_0$ = 21± 1 mg/L, pH = 7.1±0.1, V$_r$ = 150 ml each, C$_{cat}$ = 2 g/L, N$_2$-saturated,

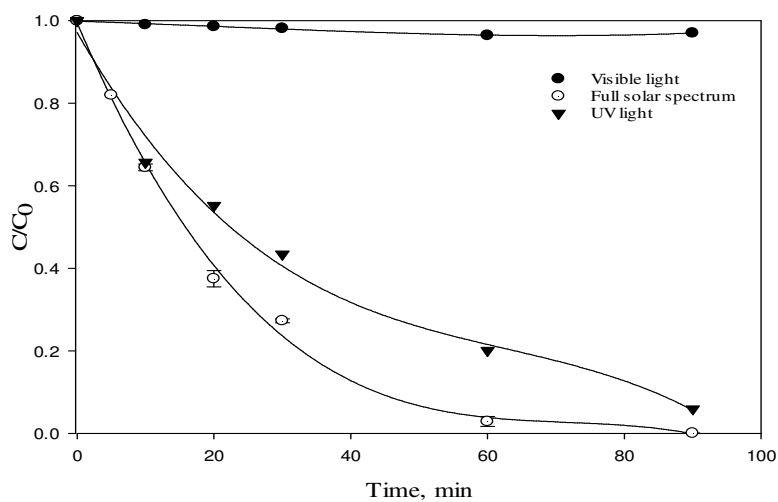I = 100 mW/cm^2]

Following this, a second set of experiments were performed under similar conditions as above using the composite TiO_2-G catalyst. It was observed that the photo-reduction rate under solar light (k_{app} = 0.083± 0.005 min^{-1}) out-performed that of only UV light (k_{app} = 0.030 min^{-1}) by 63.3% when the apparent rate constants were compared. Here again, it can be seen from Figure 4.40 that when only visible light conditions were applied by cutting off UV light, it was evident that reaction rate was still very slow. As per the band-gap measurement of the synthesised TiO_2-G, it was observed that the bandgap reduced from 3.1 to 2.2 eV. At 2.2 eV, it is expected according to equation 2-6 that wavelength of up to 563 nm should theoretically be able to activate and sustain the reaction.

Figure 4.41 showed that photo-reduction reaction of Zn^{2+} continued 20 minutes after the UV-cut-off filter was placed. After this, there was a noticeable slowing down of the reaction, implying that the photons produced were not capable of sustaining the e^-/h^+ separation. However, though the new catalyst did not show significant activity under visible light conditions for the reduction of Zn^{2+}, it showed significant improvement in performance in the full solar spectrum as shown in Figures 4.38 - 4.40. This observation is possible because combining graphene with TiO_2, produces two advantages to the catalyst. First of all compositing with graphene, reduces the band-gap of TiO_2 through energy favoured hybridization of O2p and C2p atomic orbital enabling the formation of a new valence band (Li, et al., 2013). Secondly, Graphene when combined with TiO_2 also reduces charge recombination (Upadhyay et al., 2013).

Figure 4.40 Removal of Zn^{2+} under different light sources using TiO$_2$-G

[Experimental condition: C$_0$ = 21± 1 mg/L, pH = 7.1±0.1, V$_r$ = 150 ml each, C$_{cat}$ = 2 g/L,

N$_2$-saturated I = 100 mW/cm^2].
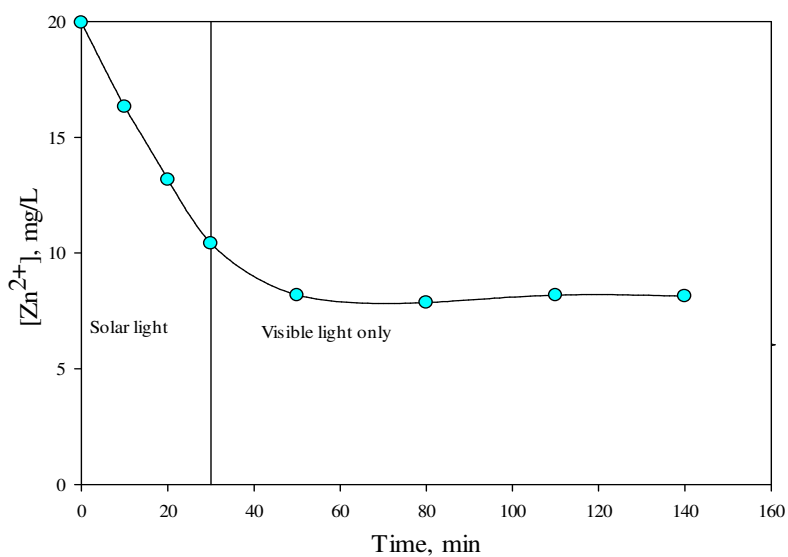
Figure 4.41 Effect of full solar and visible light conditions on the photo-reduction of

Zn^{2+} using TiO$_2$-G

[Experimental condition: C$_0$ = 22.7 mg/L, pH = 7.1±0.1, V$_r$ = 150 ml each, C$_{cat}$ = 2 g/L,

N$_2$-saturated, I= 100 mW/cm^2]

When the TiO_2-G composite is irradiated with photons, electrons excited into the conduction band of the TiO_2 from the valence band are transferred to the adjacent carbon films which then act as electron sinks and aid charge carrier separation in TiO_2. This charge is therefore available for the reaction to occur thereby increasing the reaction rate. As a result of these experiments, the increased reaction rate associated with the use of the composite TiO_2-G can be attributed to increased charged separation efficiency of the composite.

4.6 Effect of catalyst type together with other parameters on photoreduction of Zn^{2+}

This section seeks to provide a clear comparison between the performance of TiO_2-G and TiO_2 under the various conditions to give clarity to the overall study.

4.6.1 Effect of catalyst type and light intensity

Figure 4.42 shows the kinetics of the two catalysts at optimum conditions. The reaction conditions used are 250 ppm FA, 2 g/L catalyst loading, 21 ppm initial Zn^{2+} concentration, 100 mW/cm^2 light intensity and neutral pH. TiO_2-G ($k_{app} = 0.083\pm 0.005$ min^{-1}) showed a 19.2 ± 0.04 % higher photo activity than bare TiO_2 ($k_{app} = 0.067 \pm 0.006$ min^{-1}) under solar light conditions when the apparent reaction rate constants are compared. TiO_2-G also performed 21% higher than TiO_2 when initial reaction rates are compared under solar light.
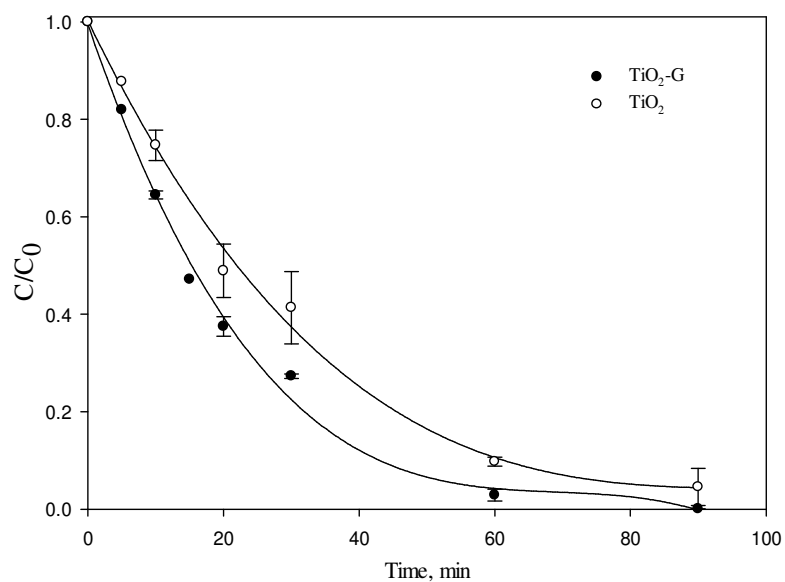
Figure 4.42 Effect of catalyst type and light intensity on the reduction of Zn^{2+}

[Experimental condition: $C_0 = 21\pm 1$ mg/L, pH = 7.1±0.1, $V_r = 150$ ml each, $C_{cat} = 2$g/L,

N_2-saturated, I = 100 mW/cm^2].

4.6.2 Effect of catalyst type and light sources

When the effect of the catalyst type and light source (solar and UV) were compared for the two different catalyst, that the initial rate of reaction in the TiO_2-G ($r_0 = 0.45 \pm 0.06$ mg/L. min) suspended system was significantly higher (20.0 %) than that of TiO_2 ($r_0 = 0.36 \pm 0.05$ mg/L. min)   under solar light conditions. Under UV conditions there is 16 % higher photo-activity for TiO_2-G catalyst than TiO_2, when the apparent reaction rate constants are compared.
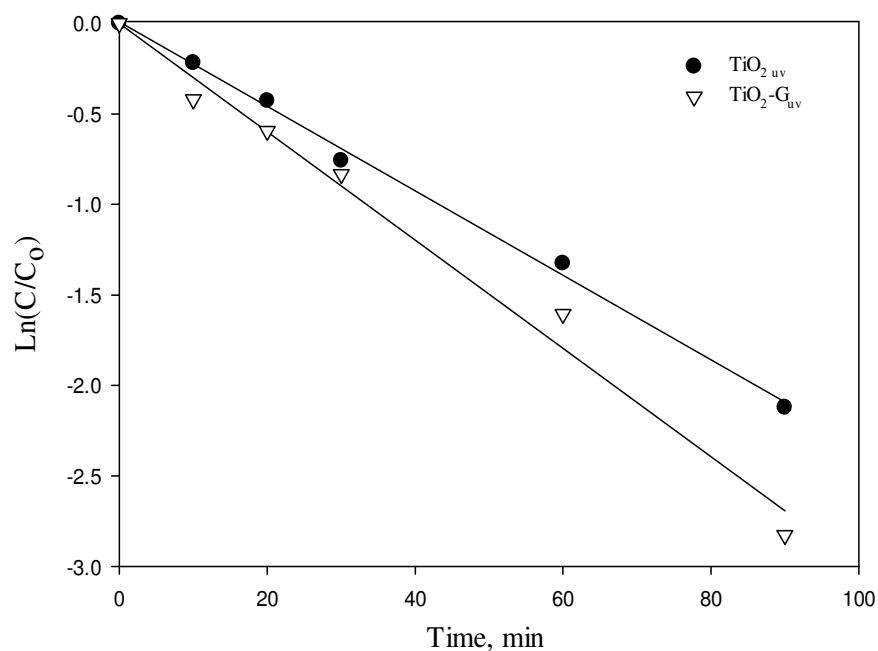
Figure 4.43 Effect of catalyst type and UV light source on the reduction rate

constant of Zn^{2+}

[Experimental condition: $C_0 = 21 \pm 1$ mg/L, pH $= 7.1 \pm 0.1$, $V_r = 150$ ml each, $C_{cat} = 2$ g/L, N_2-saturated, I $= 100$ mW/cm^2].

4.6.3 Effect of catalyst type and pH

After the initial experiments using the TiO_2 only, the performance of the composite catalyst TiO_2-G was also determined in the presences of varying pH conditions. It can be seen that at every pH value the apparent reaction rate for the modified catalyst outperforms that of TiO_2. The result from Figure 4.44 shows that TiO_2-G performs by 51.4%, 58.6% 56.1% and 25.5% over TiO_2 only at pH 4, 5, 6 and 7 respectively. Table 4.5 below shows the percentage removal of Zn^{2+} after 60 minutes of irradiation time in TiO_2 and TiO_2-G suspensions.

Table 4.5 Percentage removal of Zn^{2+} with pH variation

pH	% Zn^{2+} Removed	
	TiO_2	TiO_2-G
4.1	4.3	6.7
5.1	55.0	74.2
6.3	74.2	99.0
7.2	94.6	99.4

[Experimental condition: C_0 = 21 mg/L, V_r = 150 ml each, C_{cat} = 2 g/L, N_2-saturated,

I= 100 mW/cm^2].

Figure 4.45 illustrates the removal of Zn^{2+} with varying pH and time. TiO_2-G at pH value of approximately 6, results in a higher removal and reaction rate constant than TiO_2 at a pH value of 7.

The high performance of TiO_2-G at low pH values can be attributed to the PZC being much lower (4.9) than that of TiO_2 only (6.2-6.9). This changes the dynamics of the surface interaction with the Zn^{2+}. The lower PZC as seen in previous section increases adsorption capacity and therefore enhances the photo-reduction rate. Furthermore, the presence of the graphene also enhances electron-hole separation life-time and in the presence of excess amount of hole scavenges the density of electrons available for the photo-reduction increases. Due to the variable nature of CSO pH, it is important to note that this improvement is of major importance to the improvement of photocatalytic reaction systems as a whole.
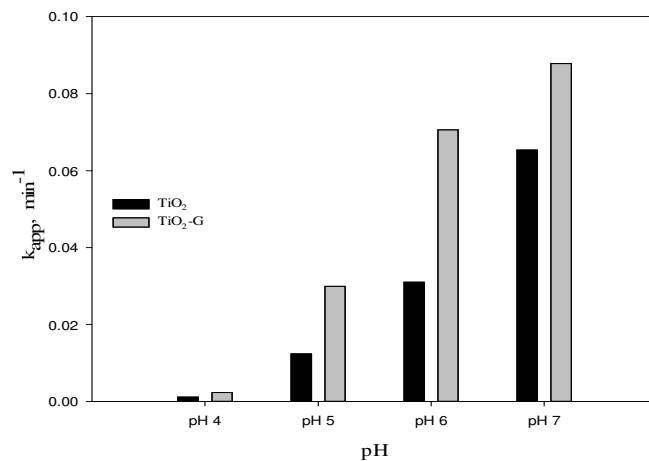
Figure 4.44 Effect of pH and catalyst type on the apparent reaction rate constant

[Experimental condition: C_0 = 21 mg/L, V_r = 150 ml each, C_{cat} = 2 g/L, N_2 saturated,
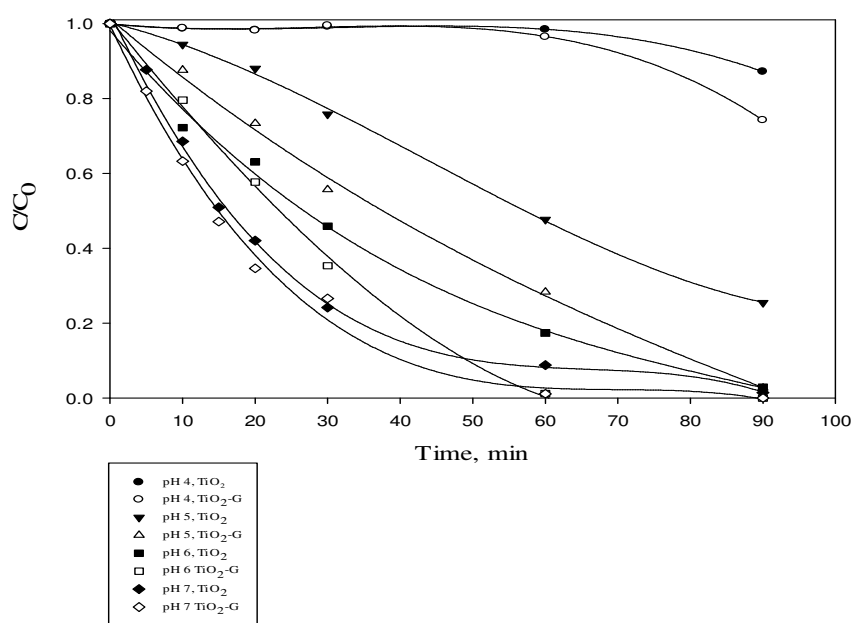
I = 100 mW/cm^2]

Figure 4.45 Effect of pH and catalyst type on the removal of Zn^{2+}

[Experimental condition: C_0 = 21 mg/L, V_r = 150 ml each, C_{cat} = 2 g/L, N_2-saturated,

I = 100 mW/cm^2]

4.6.4 Effect of catalyst type and initial metal ion concentration

Figure 4.46 compared the reaction rate constant for the reduction of Zn^{2+} at different initial concentration of the metal ion. The apparent reaction rate constant for TiO_2-G for every initial concentration is higher than that of TiO_2 only. Lower values of initial Zn^{2+} led to a much higher difference in the reaction rate.
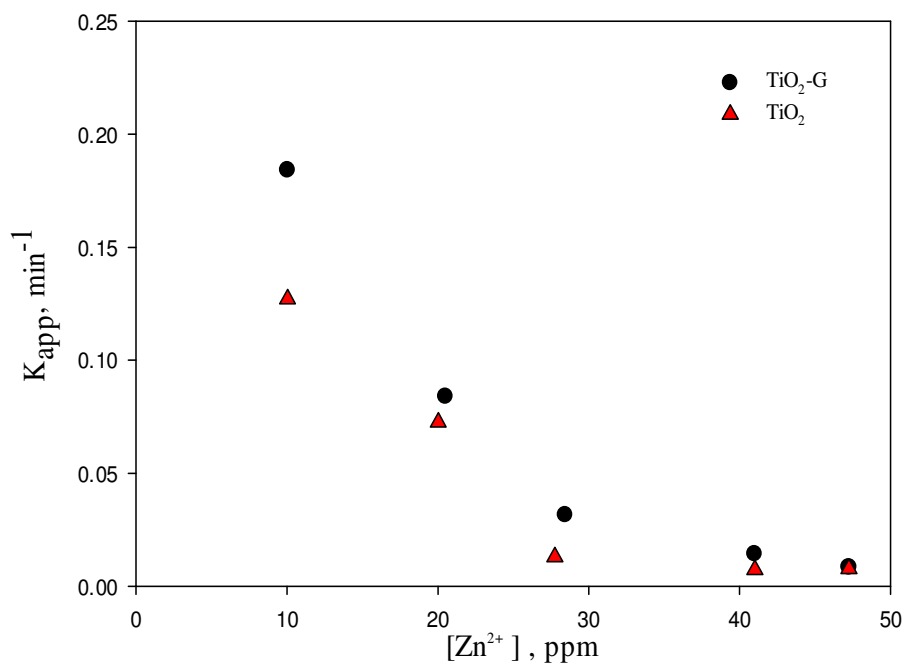
Figure 4.46 Effect of catalyst type on the reaction rate constant at different initial

Zn^{2+} concentration

[Experimental condition: pH = 7.1±0.1, V_r = 150 ml each, C_{cat} = 2 g/L, N_2-saturated I = 100 mW/cm^2].

5 CONCLUSIONS AND RECOMMENDATIONS

5.1 Conclusions

The aim of this research work was to evaluate the use of photocatalytic treatment method for removal dissolved metal ions found in CSOs. Zn^{2+} was identified as one of the most abundant heavy metals found in CSOs, and therefore, used as a model compound for this work. The main aim of the photocatalytic process was to utilize solar energy, which is an abundant resource of energy on earth today, for the activation of the semiconductor catalyst. However, TiO_2, the most widely used semiconductor photocatalyst, due to its unique physical and chemical characteristics has a major disadvantage of only being able to utilize less 4 % of the wavelengths in the entire solar spectrum, which are in the UV region. For commercialization of this technology it is important to modify the semiconductor catalyst in order to provide a higher efficiency under solar spectrum. In order to achieve this, graphene oxide was composited with TiO_2 to improve its performance in the solar spectrum. As a result of the detailed experiments discussed in chapter 4 the following conclusions can be arrived at:

- Adsorption of Zn^{2+} on TiO_2 and TiO_2-G is a very rapid process occurring within 30 minutes of contact time.
- The pH, initial catalyst loading, initial metal ion concentrations were found to have various effects on the removal of Zn^{2+} by adsorption. Of these, pH contributed the most profound effect. In slightly acidic solution, there is less adsorption than in alkaline solution. TiO_2-G recorded a higher adsorption capacity for Zn^{2+} than pure TiO_2 for every pH value.

- The TiO$_2$-G$_{pzc}$ was determined as pH 4.9 compared to TiO$_2$ at 6.2-6.9, hence, the higher adsorption of Zn^{2+} was observed for TiO$_2$-G at pH 6 over TiO$_2$.

- In the presence of a hole scavenger such as formic acid, 100% removal of 20 ppm initial concentration of Zn^{2+} was achieved.

- At an initial metal ion concentration of 20 ppm, the optimum conditions for TiO$_2$ were 2 g/L catalyst loading, 250 ppm FA concentration and pH 7 resulting in a complete reaction time of 90 min.

- There was no significant improvement in the reaction rate under visible light conditions only when TiO$_2$-G was compared to TiO$_2$ under similar experimental conditions.

- Under solar irradiation, TiO$_2$-G, however, recorded a higher reaction rate than that of TiO$_2$ even though reaction under UV light was not significantly different.

- 100 mW/cm^2 resulted in the highest reaction rate even though this is the ideal situation under natural sunlight.

- The enhancement in reaction rate of TiO$_2$-G system can be explained as a result of the effective electron-hole separation.

Compositing Graphene with TiO$_2$ provides an improvement in the adsorption as well as photo-reduction process within the solar spectrum.

5.2 Recommendation for future work

- To design an improved large-scale photocatalytic reactor for the photo-reduction experiments.

- To perform a properly designed multivariate experimental process to determine the optimum conditions more accurately.

- Investigate further into the reason for the inability of the TiO_2-G catalyst to be active under visible light conditions only.

- Investigate the effect of other competing metal ions on the photo-reduction process.

- Investigate separation methods of catalyst from treatment process.

- Investigate the effect of the deposited metals on the rate of the reaction.

REFERENCES

Albrecht, T.W.J., Addai-Mensah, J., Fornasiero, D., 2011. *Effect of pH, concentration and temperature on copper and zinc hydroxide formation/precipitation in solution.* Chemeca 2011: Engineering a Better World.

Athapaththu, S.M., 2013a. A comprehensive study of Cd(II) *Removal from Aqueous Solution via Adsorption and Solar Photocatalysis.* Master's thesis.

Avouris, P., 2010. *Graphene: Electronic and Photonic Properties and Devices.* Nano Lett. 10, 4285-4294.

Bamba, D., Atheba, P., Robert, D., Trokourey, A., Dongui, B., 2008. *Photocatalytic degradation of the diuron pesticide.* Environ Chem Lett. 6, 163-167.

Bhattacharya, A.K., Mandal, S.N., Das, S.K., 2006. *Adsorption of Zn(II) from aqueous solution by using different adsorbents.* Chem. Eng. J. 123, 43-51.

Boss, C.B., Fredeen, K.J., 1997. *Concepts, Instrumentation, and Techniques in Inductively Coupled Plasma Optical Emission Spectrometry.* Second edition. , 125.

Bouziane, L., Bendebane, F., Ismail, F., Delimi, R., 2012. *Removal of zinc and cadmium from an aqueous solution using sawdust as a low-cost adsorbent: application of Plackett–Burman design.* Desalination and Water Treatment. 49, 189-199.

Brix, K.V., Keithly, J., Santore, R.C., DeForest, D.K., Tobiason, S., 2010. *Ecological risk assessment of zinc from stormwater runoff to an aquatic ecosystem.* Sci. Total Environ. 408, 1824-1832.

Brownson, D.A.C., Banks, C.E., 2014. *The handbook of Graphene Electrochemistry*. springer London Heidelberg NY Dordecht. , 1-2-6,208.

Canterino, M., Di Somma, I., Marotta, R., Andreozzi, R., 2008. *Kinetic investigation of Cu(II) ions photoreduction in presence of titanium dioxide and formic acid*. Water Res. 42, 4498-4506.

Chan, S.H.S., Wu, T.Y., Juan, J.C., Teh, C.Y., 2011. *Recent developments of metal oxide semiconductors as photocatalysts in advanced oxidation processes (AOPs) for treatment of dye waste-water*. Journal of Chemical Technology and Biotechnology. 86, 1130-1158.

Chen, D., Sivakumar, M., Ray, A.K., 2000. *Heterogeneous Photocatalysis in Environmental Remediation*. Dev. Chem. Eng. Mineral Process. 8, 505-550.

Chen, C.C., Lu, C.S., Chung, Y.C., Jan, J.L., 2007. *UV light induced photodegradation of malachite green on TiO_2 nanoparticles*. J. Hazard. Mater. 141, 520-528.

Chen, D., Ray, A.K., 2001. *Removal of toxic metal ions from wastewater by semiconductor photocatalysis*. Chemical Engineering Science. 56, 1561-1570.

Chen, D., Ray, A.K., 1998. *Photodegradation kinetics of 4-nitrophenol in TiO_2 suspension*. Water Res. 32, 3223-3234.

Chenthamarakshan, C.R., Rajeshwar, K., 2000. *Photocatalytic reduction of divalent zinc and cadmium ions in aqueous TiO_2 suspensions: an interfacial induced adsorption–reduction pathway mediated by formate ions*. Electrochemistry Communications. 2, 527-530.

Chenthamarakshan, C.R., Yang, H., Savage, C.R., Rajeshwar, K., 1999. *Photocatalytic reactions of divalent lead ions in UV-irradiated titania suspensions*. Research on Chemical Intermediates. 25, 861-876.

Chenthamarakshan, C.R., Yang, H., Ming, Y., Rajeshwar, K., 2000. *Photocatalytic reactivity of zinc and cadmium ions in UV-irradiated titania suspensions*. J Electroanal Chem. 494, 79-86.

Chong, M.N., Jin, B., Chow, C.W.K., Saint, C., 2010a. *Recent developments in photocatalytic water treatment technology: A review*. Water Res. 44, 2997-3027.

Chowdhury, P., 2012. *Solar and visible light driven photocatalysis for sacrificial hydrogen generation and water detoxification with chemically modified TiO$_2$*. pHD Thesis.

Chowdhury, P., Elkamel, A., Ray, A.K., 2014. *Chapter 2 Photocatalytic Processes for the Removal of Toxic Metal Ions*. In: Anonymous, The Royal Society of Chemistry, pp. 25-43.

Chowdhury, P., Gomaa, H., Ray, A.K., 2013. *Dye-Sensitized Photocatalyst: A Breakthrough in Green Energy and Environmental Detoxification. In*: Anonymous American Chemical Society, pp. 231-266.

Clark, S.E., Pitt, R., 2012. *Targeting treatment technologies to address specific stormwater pollutants and numeric discharge limits*. Water Res. 46, 6715-6730.

Clark, S., Burian, S., Pitt, R., Field, R., 2005. *Urban wet-weather flows*. Water Environ. Res. 77, 826-981.

Delgado-Balderas, R., Hinojosa-Reyes, L., Guzman-Mar, J.L., Garza-Gonzalez, M.T., Lopez-Chuken, U.J., Hernandez-Ramirez, A., 2012. *Photocatalytic reduction of Cr(VI) from agricultural soil column leachates using zinc oxide under UV light irradiation*. Environ. Technol. 33, 2673-2680.

Deliyanni, E.A., Peleka, E.N., Matis, K.A., 2007. *Removal of zinc ion from water by sorption onto iron-based nanoadsorbent*. J. Hazard. Mater. 141, 176-184.

El Samrani, A.G., Lartiges, B.S., Villiéras, F., 2008. *Chemical coagulation of combined sewer overflow: Heavy metal removal and treatment optimizatio*n. Water Res. 42, 951-960.

EPA, 1992. U.S. Environmental Protection Agency. *EPA-738-F-92-007*, Washington, DC.

Farghali, A.A., Bahgat, M., Enaiet Allah, A., Khedr, M.H., 2013. *Adsorption of Pb(II) ions from aqueous solutions using copper oxide nanostructures*. Beni-Suef University Journal of Basic and Applied Sciences. 2, 61-71.

Field, R., 1982. An Overview of the United-States Environmental-Protection Agencys *Storm and Combined Sewer Program Collection System Research.* Water Res. 16, 859-870.

Field, R., Pitt, R., Brown, M., Oconnor, T., 1995. *Combined Sewer Overflow Control using Storage in Seawater*. Water Res. 29, 1505-1514.

Field, R., Pitt, R., Jager, D., Brown, M., 1994. *Combined Sewer Overflow Control through In-Receiving Water Storage - an Efficiency Evaluation*. Water Resour Bull. 30, 921-928.

Field, R., Sullivan, D., Tafuri, A., 2004. *Management of combined sewer overflows.* Lewis Publishers, Boca Raton, Fla.; London.

Flores-Rodriguez, J., Bussy, A.-. and Thevenot, D.R., 1994. *Toxic Metals in Urban Runoff*: Physico-Chemical Mobility Assessment Using Speciation Schemes. Water Sei. Technol. (G.B.), 29.

Foo, K.Y., Hameed, B.H., 2010. *Insights into the modeling of adsorption isotherm systems*. Chem. Eng. J. 156, 2-10.

Foster, N.S., Noble, R.D., Koval, C.A., 1993a. *In Photocatalytic Purification and Treatment of Water and Air*. Edited by D. F. Ollis, H. Al-Ekabi Amsterdam: Elsevier. , pp365-373.

Foster, N.S., Noble, R.D., Koval, C.A., 1993b. *In Photocatalytic Purification and Treatment of Water and Air* Edited by D. F. Ollis, H. Al-Ekabi. Amsterdam: Elsevier. , 365-373.

Fujishima, A., Rao, T.N., Tryk, D.A., 2000. *Titanium dioxide photocatalysis*. Journal of Photochemistry and Photobiology C: Photochemistry Reviews. 1, 1-21.

Fujishima, A., Zhang, X., Tryk, D.A., 2008. *TiO_2 photocatalysis and related surface phenomena*. Surface Science Reports. 63, 515-582.

Gaya, U.I., Abdullah, A.H., 2008. *Heterogeneous photocatalytic degradation of organic contaminants over titanium dioxide: A review of fundamentals, progress and problems*. Journal of Photochemistry and Photobiology C: Photochemistry Reviews. 9, 1-12.

Gu, Y., Xing, M., Zhang, J., 2014. *Synthesis and photocatalytic activity of graphene based doped TiO_2 nanocomposites*. Appl. Surf. Sci. 319, 8-15.

Herrmann, J., Disdier, J., Pichat, n., 1988. *Photocatalytic deposition of silver on powder titania: Consequences for the recovery of silver*. J. Catal. 113, 72.

Ho, Y., 2006. *Review of second-order models for adsorption systems*. J. Hazard. Mater. 136, 681-689.

Ho, Y., 2004. *Selection of optimum sorption isotherm.* Carbon. 42, 2113–2130.

Holeton, C., Chambers, P.A., Grace, L., 2011. *Wastewater release and its impacts on Canadian waters*. Can. J. Fish. Aquat. Sci. 68, 1836-1859.

Hummers, W.S., Offeman, R.E., 1958. *Preparation of graphitic oxide*. J. Am. Chem. Soc. 80, 1339.

Ibhadon A., O., Fitzpatrick, P., 2013. *Heterogeneous Photocatalysis: Recent Advances and Applications*. Catalysts. 3, 189-218.

Jeon, J.C., Kwon, K.H., Kim, L.H., Kim, J.H., Jung, Y.J., Min, K.S., 2013. *Application of coagulation process for the treatment of combined sewer overflows (CSOs).* Desalination and Water Treatment. 51, 4063-4071.

Jiang, G., Lin, Z., Chen, C., Zhu, L., Chang, Q., Wang, N., Wei, W., Tang, H., 2011. *TiO$_2$ nanoparticles assembled on graphene oxide nanosheets with high photocatalytic activity for removal of pollutants*. Carbon. 49, 2693-2701.

Kabra, K., Chaudhary, R., Sawhney, R.L., 2008. *Solar photocatalytic removal of Cu(II), Ni(II), Zn(II) and Pb(II): Speciation modeling of metal-citric acid complexes*. J. Hazard. Mater. 155, 424-432.

Kabra, K., Chaudhary, R., Sawhney, R.L., 2007. *Effect of pH on solar photocatalytic reduction and deposition of Cu(II), Ni(II), Pb(II) and Zn(II): Speciation modeling and reaction kinetics.* J. Hazard. Mater. 149, 680-685.

Kajitvichyanukul, P., Sungkaratana, T., 2006. *Photocatalytic Removal of Zinc (II) in UV - Irradiated Titania   Suspensions*. Asian Journal on Energy and Environment. 7, 256-265.

Kumar, S.G., Devi, L.G., 2011. *Review on Modified TiO2 Photocatalysis under UV/Visible Light: Selected Results and Related Mechanisms on Interfacial Charge Carrier Transfer Dynamics.* Journal of Physical Chemistry a. 115, 13211-13241.

Lee, Y., Yang, J., 2012. *Self-assembled flower-like TiO$_2$ on exfoliated graphite oxide for heavy metal removal.* Journal of Industrial and Engineering Chemistry. 18, 1178-1185.

Lennetech water treatment solutions, Accessed 9/15/2014. Online http://www.lenntech.com/processes/heavy/heavy-metals/heavy-metals.htm.

Li, K., Chen, T., Yan, L., Dai, Y., Huang, Z., Xiong, J., Song, D., Lv, Y., Zeng, Z., 2013. *Design of graphene and silica co-doped titania composites with ordered mesostructure and their simulated sunlight photocatalytic performance towards atrazine degradation*. Colloids Surf. Physicochem. Eng. Aspects. 422, 90-99.

Li, L., Jiang, F., Liu, J., Wan, H., Wan, Y., Zheng, S., 2012. *Enhanced photocatalytic reduction of aqueous Pb(II) over Ag loaded TiO2 with formic acid as hole scavenger*. Journal of Environmental Science and Health, Part A. 47, 327-336.

Litter, M.I., 1999. *Heterogeneous photocatalysis: Transition metal ions in photocatalytic systems*. Applied Catalysis B: Environmental. 23, 89-114.

Liu, Q., Li, Y., Zhang, J., Chi, Y., Ruan, X., Liu, J., Qian, G., 2011. *Effective removal of zinc from aqueous solution by hydrocalumite*. Chem. Eng. J. 175, 33-38.

Liu, S.X., Qu, Z.P., Han, X.W., Sun, C.L., 2004. *A mechanism for enhanced photocatalytic activity of silver-loaded titanium dioxide*. Catalysis Today. 93–95, 877-884.

Liu, X., Pan, L., Lv, T., Sun, Z., 2013. *Investigation of photocatalytic activities over ZnO–TiO$_2$–reduced graphene oxide composites synthesized via microwave-assisted reaction.* J. Colloid Interface Sci. 394, 441-444.

Li, W., Pan, G., Zhang, M., Zhao, D., Yang, Y., Chen, H., He, G., 2008. *EXAFS studies on adsorption irreversibility of Zn(II) on TiO2: Temperature dependence.* J. Colloid Interface Sci. 319, 385-391.

Low, K.S., Lee, C.K., Leo, A.C., 1995. *Removal of metals from electroplating wastes using banana pith*. Bioresour. Technol. 51, 227-231.

Lu, C., Chiu, H., 2006. *Adsorption of zinc(II) from water with purified carbon nanotubes. Chemical Engineering Science*. 61, 1138-1145.

Malandrino, M., Abollino, O., Giacomino, A., Aceto, M., Mentasti, E., 2006. *Adsorption of heavy metals on vermiculite: Influence of pH and organic ligands.* J. Colloid Interface Sci. 299, 537-546.

Malekshoar, G., Pal, K., He, Q., Yu, A., Ray, A.K., 2014. *Enhanced Solar Photocatalytic Degradation of Phenol with Coupled Graphene-Based Titanium Dioxide and Zinc Oxide*. Ind Eng Chem Res.

Marsalek, J., Rochfort, Q., 2004. *Urban wet-weather flows: Sources of fecal contamination impacting on recreational waters and threatening drinking-water sources*. Journal of Toxicology and Environmental Health-Part A-Current Issues. 67, 1765-1777.

Ming, Y., 2002. *Heterogeneous photocatalytic reduction of metal ions with very negative reduction potentials*. ProQuest Dissertations and Theses.

Ministry of Environment, *Determination of treatment requirements for municipal and private combined and partially separated sewer systems*. Procedure F-5-5.

Morales-Torres, S., Pastrana-Martínez, L.M., Figueiredo, J.L., Faria, J.L., Silva, A.M.T., 2013. *Graphene oxide-P25 photocatalysts for degradation of diphenhydramine pharmaceutical and methyl orange dye*. Appl. Surf. Sci. 275, 361-368.

Morales-Torres, S., Pastrana-Martínez, L., Figueiredo, J., Faria, J., Silva, A., 2012. *Design of graphene-based TiO2 photocatalysts—a review.* Environ Sci Pollut Res. 19, 3676-3687.

Moreno-Barbosa, J., López-Velandia, C., Maldonado, A., Giraldo, L., Moreno-Piraján, J., 2013. *Removal of lead (II) and zinc (II) ions from aqueous solutions by adsorption onto activated carbon synthesized from watermelon shell and walnut shell. Adsorption.* 19, 675-685.

Muliss, B., Revitt, D.M., and Shutes, R.B.E., 1996. *The Impact of Dis charges from Two Combined Sewer Overflows on the Water Quality of an Urban Watercourse. . 7th Int. Conf. Urban Storm Drain*, F. Sieker and H.-R. Verworn (Eds.), SuG, Hanover. 563.

Navío, J.A., Colón, G., Trillas, M., Peral, J., Domènech, X., Testa, J.J., Padrón, J., Rodríguez, D., Litter, M.I., 1998. *Heterogeneous photocatalytic reactions of nitrite oxidation and Cr(VI) reduction on iron-doped titania prepared by the wet impregnation method*. Applied Catalysis B: Environmental. 16, 187-196.

Nazeeruddin, K.M., Gratzel, M., Licht, S., 2002. *Encyclopedia of Electrochemistry.*

Nguyen, N.H., 2006. Photocatalytic Reduction of Cadmium and Selenium Ions and the Deposition of Cadmium Selenide. New South Wales: School of Chemical Engineering and Industrial Chemistry, University of New South Wales.

Ollis, D.F., 2000. *Photocatalytic purification and remediation of contaminated air and water.* Comptes Rendus de l'Académie des Sciences - Series IIC - Chemistry. 3, 405-411.

Park, Y., Singh, N.J., Kim, K.S., Tachikawa, T., Majima, T., Choi, W.Y., 2009. Chem. Eur. J. 15, 10843.

Pastrana-Martínez, L.M., Morales-Torres, S., Kontos, A.G., Moustakas, N.G., Faria, J.L., Doña-Rodríguez, J.M., Falaras, P., Silva, A.M.T., 2013. TiO_2, *surface modified TiO_2 and graphene oxide-TiO_2 photocatalysts for degradation of water pollutants under near-UV/Vis and visible light.* Chem. Eng. J. 224, 17-23.

Plum, V., Dahl, C.P., Bentsen, L., Petersen, C.R., Napstjert, L., Thomsen, N.B., 1998. *The Actiflo method.* Water Science and Technology. 37, 269-275.

Podolsky, L., MacDonald, E., Roberts, J., Lintner, 2008. *Using Green infrastructure to reduce combined sewer overflows.*

Pulido Melián, E., González Díaz, O., Doña Rodríguez, J.M., Colón, G., Navío, J.A., Macías, M., Pérez Peña, J., 2012. *Effect of deposition of silver on structural characteristics and photoactivity of TiO_2-based photocatalysts.* Applied Catalysis B: Environmental. 127, 112-120.

Ray, A.K., 1998. *A new photocatalytic reactor for destruction of toxic water pollutants by advanced oxidation process.* Catalysis Today. 44, 357-368.

Ray, A.K., Beenackers, A.A.C.M., 1998. *Development of a new photocatalytic reactor for water purification.* Catalysis Today. 40, 73-83.

Reemtsma, T., Gnirss, R., Jekel, M., 2000. *Infiltration of Combined Sewer Overflow and Tertiary Treated Municipal Wastewater:* An Integrated Laboratory and Field Study on Various Metals. Water Environ. Res. 72, 644-650.

Rincón, A., Pulgarin, C., 2004. *Effect of pH, inorganic ions, organic matter and H2O2 on E. coli K12 photocatalytic inactivation by TiO₂.* Applied Catalysis B: Environmental. 51, 283-302.

Salim, R., Al-Subu, M., Abu-Shqair, I., Braik, H., 2003. *Removal of Zinc from Aqueous Solutions by Dry Plant Leaves*. Process Saf. Environ. Prot. 81, 236-242.

Schroeter, H.O., 1997. *Toxic contaminant loadings from municipal sources in Ontario areas of concern.* Water Qual. Res. J. Can. 32, 7-22.

Sellappan, R., 2013. *Mechanisms of Enhanced Activity of Model TiO₂/Carbon and TiO₂/Metal Nanocomposite Photocatalysts.* PhD Thesis Chalmers University of Technology.

Serpone, N., Ah-You, Y.K., Tran, T.P., Harris, R., Pelizzetti, E., Hidaka, H., 1987. AM1 *simulated sunlight photoreduction and elimination of Hg(II) and CH3Hg(II) chloride salts from aqueous suspensions of titanium dioxide*. Solar Energy. 39, 491-498.

Sheela, T., Nayaka, Y.A., Viswanatha, R., Basavanna, S., Venkatesha, T.G., 2012. *Kinetics and thermodynamics studies on the adsorption of Zn(II), Cd(II) and Hg(II) from aqueous solution using zinc oxide nanoparticles.* Powder Technol. 217, 163-170.

Singh, C., Chaudhary, R., 2013a. *Removal of metal ion by means of solar oxidation processes based on pH TiO₂ and Oxidants*. Desalination and water treatment. 52, 1263-1271.

Singh, C., Chaudhary, R., 2013b. *Visible light induced photocatalytic reduction of metals (Cr, Cu, Ni, Zn) and its synergism with different pH, TiO$_2$ and H$_2$O$_2$ doses in simulated wastewater.* Journal of Renewable and sustainable Energy. 5, 1-13.

Tan, T., Beydoun, D., Amal, R., 2003. *Effects of organic hole scavengers on the photocatalytic reduction of selenium anions*. J. Photochem. Photobiol. A. 159, 273-280.

Tanaka, K., Harada, K., Murata, S., 1986. *Photocatalytic deposition of metal ions onto TiO$_2$ powder.* Solar Energy. 36, 159-161.

Tchobanoglous, G., Burton, F.L., Stensel, H.D., Metcalf & Eddy, 2003. W*astewater engineering: treatment and reuse*, 4th ed. McGraw-Hill, Boston.

Turan, N.G., Elevli, S., Mesci, B., 2011. *Adsorption of copper and zinc ions on illite: Determination of the optimal conditions by the statistical design of experiments.* Applied Clay Science. 52, 392-399.

U.S. Environmental Protection Agency, 2001. *Report to Congress: Implementation and Enforcement of the CSO Control Policy*. EPA 833-R-01-003. U.S. Environmental Protection Agency, Washington, DC.

Upadhyay, R.K., Soin, N., Roy, S.S., 2013. *Role of graphene/metal oxide composites as photocatalysts, adsorbents and disinfectants in water treatment: a review*. - RSC Adv., - 3823.

US Environmental Protection Agency, 2014. *Greening CSO Plans- Planning and Modeling Green Infrastructure for Combined Sewer Overflow (CSO) Control.* Technical resource. 832-R-14-001.

US Environmental Protection Agency, 1994. C*ombined Sewer Overflow (CSO) Control Policy Notice.* Federal register. 75, 7.

Veli, S., Alyüz, B., 2007. *Adsorption of copper and zinc from aqueous solutions by using natural clay.* J. Hazard. Mater. 149, 226-233.

Wang, H., Yuan, X., Wu, Y., Huang, H., Zeng, G., Liu, Y., Wang, X., Lin, N., Qi, Y., 2013. *Adsorption characteristics and behaviors of graphene oxide for Zn (II) removal from aqueous solution.* Appl. Surf. Sci. 279, 432-440.

Wang, N., Zhu, L., Deng, K., She, Y., Yu, Y., Tang, H., 2010. *Visible light photocatalytic reduction of Cr(VI) on TiO_2 in situ modified with small molecular weight organic acids.* Applied Catalysis B: Environmental. 95, 400-407.

Ward, M.D., White, J.R., Bard, A.J., 1983. *Electrochemical investigation of the energetics of particulate titanium dioxide photocatalysts. The methyl viologen-acetate system.* J. Am. Chem. Soc. 105, 27-31.

Yang, Y., Chen, H., Pan, G., 2007. *Particle concentration effect in adsorption/desorption of Zn(II) on anatase type nano TiO_2.* Journal of Environmental Sciences. 19, 1442-1445.

Yeber, M.C., Soto, C., Riveros, R., Navarrete, J., Vidal, G., 2009a. *Optimization by factorial design of copper (II) and toxicity removal using a photocatalytic process with TiO$_2$ as semiconductor.* Chem. Eng. J. 152, 14-19.

Yeber, M.C., Soto, C., Riveros, R., Navarrete, J., Vidal, G., 2009b. *Optimization by factorial design of copper (II) and toxicity removal using a photocatalytic process with TiO$_2$ as semiconductor.* Chem. Eng. J. 152, 14-19.

Zhang, H., Lv, X., Li, Y., Wang, Y., Li, J., 2010a. *P25-Graphene Composite as a High Performance Photocatalyst.* ACS Nano. 4, 380-386.

Zhang, K., Kemp, K.C., Chandra, V., 2012. *Homogeneous anchoring of TiO$_2$ nanoparticles on graphene sheets for waste water treatment*. Mater Lett. 81, 127-130.

Zhang, X., Li, H., Cui, X., Lin, Y., 2010b. *Graphene/TiO$_2$ nanocomposites: synthesis, characterization and application in hydrogen evolution from water photocatalytic splitting*. J. Mater. Chem. 20, 2801-2806.

Zhou, S., 2001. *Kinetic Study for the photocatalytic degradation of Eosin B*. PhD Thesis National University of Singapore.

Zukovs, G., 2005. *CSO regulations in great lakes region of Canada and the United States a comparative evaluation.* , American Society of Civil Engineers Environmental and water Resources Institute.
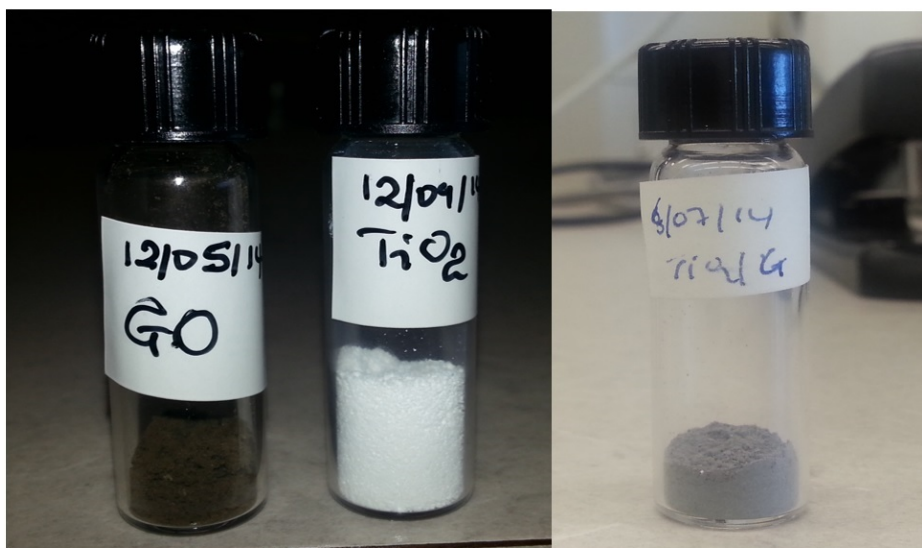
APPENDIX 1

Figure A.1 Graphite Oxide, TiO_2 and TiO_2-G composite catalyst.

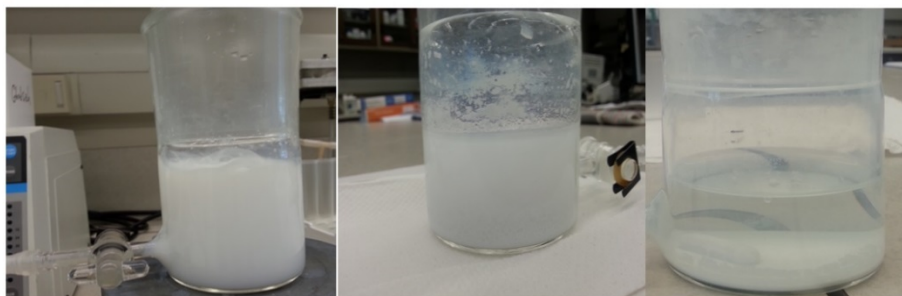Figure A.2 Reaction before and after solar irradiation using TiO_2

CURRICULUM VITAE

K U M O R D Z I   G L O R I A

EDUCATION

The University of Western Ontario   Jan. 2013 – Apr. 2015

MESc. Chemical Engineering.

Research Topic: solar photocatalytic reduction of Zn^{2+} using graphene-based TiO_2 composite catalyst for application to CSO treatment

Kwame Nkrumah University of Science and Technology, Kumasi, Ghana
          Aug.2006 – Jun. 2010

BSc. Chemical Engineering

Plant design project topic: Production of Alum from Bauxite

Tema Senior High School, Tema, Ghana   Oct. 2002 – Aug.2005

WORK EXPERIENCE

Internship

Ashbridges Bay Treatment Plant, Toronto, ON   Oct. 2013 – Mar. 2014

Research and Teaching Assistant

The University of Western Ontario   Jan. 2013- Apr. 2015

Engineer-In-Training   Nov.2010–Aug2011

Volta River Authority, Team Thermal Complex, Team, Ghana

Internship

Nestlé Ghana Limited, Tema, Ghana   Jul. 2008 – Aug. 2008

OTHER TEAM AND LEADERSHIP WORK

Graduate seminar planning committee member- Western University

 Jul. 2013- Apr. 2014

Financial secretary (KNUST Chemical Eng. Students' Association)

Aug. 2007 - Apr. 200